TECHNISCHE UNIVERSITÄT MÜNCHEN

FAKULTÄT FÜR CHEMIE

LEHRSTUHL FÜR ORGANISCHE CHEMIE II

VIRULENCE ATTENUATION THROUGH CHEMICAL AND GENETIC MANIPULATION OF THE *STAPHYLOCOCCUS AUREUS* CLPXP PROTEASE

DISSERTATION ZUR ERLANGUNG DES AKADEMISCHEN GRADES EINES DOKTORS

DER NATURWISSENSCHAFTEN VON

CHRISTIAN FETZER

MÜNCHEN 2018

TECHNISCHE UNIVERSITÄT MÜNCHEN

FAKULTÄT FÜR CHEMIE

LEHRSTUHL FÜR ORGANISCHE CHEMIE II

Virulence Attenuation through Chemical and Genetic Manipulation of the *Staphylococcus aureus* ClpXP Protease

Christian Fetzer

Vollständiger Abdruck der von der Fakultät für Chemie der Technischen Universität München zur Erlangung des akademischen Grades eines

DOKTORS DER NATURWISSENSCHAFTEN (Dr. rer. nat.)

genehmigten Dissertation.

Vorsitzender: Prof. Dr. Michael Groll

Prüfer der Dissertation: 1. Prof. Dr. Stephan A. Sieber

2. Prof. Dr. Matthias Feige

Die Dissertation wurde am 07.11.2017 bei der Technischen Universität München eingereicht und durch die Fakultät für Chemie am 06.12.2017 angenommen.

"… I am still confused - but on a higher level."

Enrico Fermi

Danksagung

Table of Contents

Summary

For the past 30 years, no new antibiotic classes have been discovered. The emergence of antimicrobial resistance of bacterial isolates, e.g. *Staphylococcus aureus*, poses a major health threat for the future. Today, certain multidrug resistant bacteria cause infections that can no longer be treated with existing antibiotics. This troubling circumstance calls for the development of new therapeutic strategies in order to keep humanity from falling back into the pre-antibiotic era. Antivirulence strategies present one new possible approach to tackle this problem. In contrast to classical antibiotics, these compounds aim to disarm bacteria instead of killing them. Hence, direct selective pressure on bacteria is reduced, potentially resulting in no or slower resistance development.

The caseinolytic protease complex ClpXP of *S. aureus* is a major regulator of virulence. A high-throughput screen (HTS) with > 40,000 compounds was conducted to find small molecule inhibitors of the ClpXP complex. Two compounds, sharing the same structure class were identified to inhibit ClpXP by disruption of its oligomeric state. Moreover, both compounds disrupted the hexameric complex of ClpX, thus representing the first confirmed small molecule inhibitors of this chaperone. Synthesis of several derivatives revealed a tight structure-activity relationship (SAR) and potential positions for modifications. Synthesis of probes for activity-based protein profiling and affinity pull-down experiments only showed limited usability. Treatment of *S. aureus* with the compounds globally reduced expression of virulence factors. Data obtained by transcriptome analysis, whole-proteome and secretome studies partially matched the pattern of *clpX* deletion cells (*ΔclpX*). However, treatment of *ΔclpX* cells with compounds revealed further toxin depletion, thus leading to the perspective that additional virulence pathways are addressed by the compounds.

The same HTS revealed a second compound class exhibiting inhibition of ClpXP. It inhibited neither ClpP nor ClpX alone suggesting an intriguing mode of action. Thermal-shift assays revealed strong stabilization of ClpP, therefore proposing binding to the ClpP complex. A small library of compound derivatives gave insight into SAR and initiated separation of enantiomers. Subsequent ClpXP assays displayed potent inhibition of only one enantiomer. *S. aureus* was treated with the compounds and expression of

hemolysins was determined. While only one enantiomer showed a slight reduction of hemolysin expression, it was surprisingly not the one inhibiting ClpXP. Considering this discrepancy, the compound remains interesting for the elucidation of the mode of action, albeit not for further development as a potential pharmacological compound.

The effect of genetic modifications of *clpP* on its activity was determined. Two point mutations, already characterized in *in vitro* studies, were inserted into the genome of *S. aureus*. Additionally, a markerless deletion mutant of *clpP* was generated. Deletion of *clpP* or mutations in the active site resulted in strongly attenuated hemolysin expression, whereas a point mutation outside of the active site had only a minor influence. Whole-proteome analysis corroborated these results, showing strong down-regulation of several virulence factors in the deletion and active site mutant. These results set the foundation for potential future studies, such as the influence of ClpP on bacterial metabolism.

Zusammenfassung

In den letzten 30 Jahren wurden keine neuen Antibiotikaklassen entdeckt. Das Auftreten von antibiotikaresistenten bakteriellen Isolaten, z.B. *Staphylococcus aureus*, stellt künftig eine große gesundheitliche Bedrohung dar. Bereits heute sind manche Infektionen mit multiresistenten Bakterien mit vorhandenen Antibiotika nicht mehr behandelbar. Um einen Rückfall in die präantibiotische Ära zu verhindern, werden deshalb dringend neue Behandlungsstrategien benötigt. Antivirulenz-Verbindungen stellen hierbei eine mögliche Herangehensweise dar, um diesem Problem entgegen zu wirken. Im Gegensatz zu klassischen Antibiotika, zielen Antivirulenz-Verbindungen auf die Entwaffnung der Bakterien ab, anstatt sie zu töten. Dadurch reduziert sich der direkte Selektionsdruck, was möglicherweise zu keiner, oder nur niedriger Resistenzbildung führen könnte.

Der caseinolytische Proteasekomplex ClpXP von *S. aureus* ist ein Hauptregulator der Virulenz. Ein Hochdurchsatzscreen (HTS) mit > 40.000 Substanzen wurde durchgeführt, um niedermolekulare Inhibitoren des ClpXP-Komplexes zu finden. Zwei strukturell ähnliche Verbindungen wurden identifiziert, welche ClpXP durch die Zerstörung der oligomeren Struktur inhibieren. Weiterhin beeinträchtigen beide Verbindungen die hexamere Struktur von ClpX und stellen dadurch die ersten bestätigten niedermolekularen Inhibitoren des Chaperons ClpX dar. Die Synthese mehrerer Derivate offenbarte eine enge Struktur-Aktivitäts-Beziehung (SAR) und potentielle Positionen zur Modifikation. Sonden, die für affinitätsbasiertes Protein-Profiling und Affinitäts-Anreicherungs-Experimente synthetisiert wurden, zeigten jedoch nur eine eingeschränkte Verwendbarkeit in den genannten Experimenten. Die Behandlung von *S. aureus* mit den Verbindungen reduzierte die globale Expression von Virulenzfaktoren. Die durch Transkriptomanalyse, Gesamtproteom- und Sekretom-Studien erhaltenen Daten stimmten teilweise mit dem Muster von *clpX* Deletionsmutanten (*ΔclpX*) überein, jedoch führte die Behandlung von *ΔclpX* Zellen mit der Verbindung zu einer weiteren Verringerung der Toxin-Produktion. Somit ergibt sich die Möglichkeit, dass weitere Virulenzpfade durch die Verbindungen adressiert werden.

Derselbe HTS offenbarte eine weitere Verbindungsklasse, welche eine Inhibition von ClpXP zeigt. Interessanterweise inhibierten diese Moleküle weder ClpP, noch ClpX

alleine, was auf einen außergewöhnlichen Wirkmechanismus hindeutet. Thermal-Shift-Experimente wiesen auf eine starke Stabilisierung von ClpP hin und weisen so auf eine Bindung an ClpP hin. Eine kleine Substanzbibliothek gab Einblicke in die SAR und initiierte die Trennung der Stereoisomere. Anschließende ClpXP-Assays zeigten die starke Inhibition durch nur ein Enantiomer. *S. aureus* wurde mit beiden Verbindungen behandelt, um die Hämolysin-Expression zu untersuchen. Zwar zeigte ein Enantiomer eine leichte Reduktion der Hämolysin-Expression, überraschenderweise aber nicht das Enantiomer, welches ClpXP inhibiert. Diese Diskrepanz führt dazu, dass die Verbindung für die Bestimmung des Wirkmechanismus sehr interessant bleibt, jedoch nicht für die weitere Entwicklung eines potentiellen pharmakologischen Wirkstoffes.

Zusätzlich zur Wirkung niedermolekularer Verbindungen auf die ClpXP-Aktivität wurde der Effekt von genetischen *clpP* Modifikationen bestimmt. Zwei mittels *in vitro* Studien zuvor charakterisierte Punktmutationen wurden in das Genom von *S. aureus* eingebracht. Zusätzlich wurde eine markierungsfreie Deletionsmutante von *clpP* generiert. Sowohl die Deletion von *clpP*, als auch die entsprechende Mutation des aktiven Zentrums resultierten in einer stark verringerten Hämolysin-Expression, wohingegen eine Punktmutation außerhalb des aktiven Zentrums nur einen geringen Einfluss hatte. Eine Gesamtproteom-Analyse bekräftigte diese Ergebnisse und zeigte eine starke Herabregulation diverser Virulenzfaktoren bei der Deletionsmutante und der Mutante, mit Mutation im aktiven Zentrum. Diese Ergebnisse legen den Grundstein für zukünftige Studien, um z.B. den Einfluss von ClpP auf den bakteriellen Metabolismus zu untersuchen.

Introductory Remarks

This dissertation was completed between October 2013 and September 2017 under the supervision of Prof. Dr. Stephan A. Sieber at the Chair of Organic Chemistry II at the Technical University of Munich.

Parts of this thesis have been published in:

C. Fetzer, V. S. Korotkov, R. Thänert, K. M. Lee, M. Neuenschwander, J. P. von Kries, E. Medina, S. A. Sieber, "A Chemical Disruptor of the ClpX Chaperone Complex Attenuates the Virulence of Multidrug-Resistant Staphylococcus aureus", *Angew. Chem. Int. Ed.* **2017**, *56*, 15746–15750.

Publications not highlighted in this thesis:

M. H. Wright, C. Fetzer, S. A. Sieber, "Chemical Probes Unravel an Antimicrobial Defense Response Triggered by Binding of the Human Opioid Dynorphin to a Bacterial Sensor Kinase", *J. Am. Chem. Soc.* **2017**, *139*, 6152–6159.

J. Krysiak, M. Stahl, J. Vomacka, C. Fetzer, M. Lakemeyer, A. Fux, S. A. Sieber, "Quantitative Map of β-Lactone-Induced Virulence Regulation", *J. Proteome Res.* **2017**, *16*, 1180–1192.

F. A. Mandl, V. C. Kirsch, I. Ugur, E. Kunold, J. Vomacka, C. Fetzer, S. Schneider, K. Richter, T. M. Fuchs, I. Antes, S. A. Sieber, "Natural-Product-Inspired Aminoepoxybenzoquinones Kill Members of the Gram-Negative Pathogen Salmonella by Attenuating Cellular Stress Response", *Angew. Chem. Int. Ed.* **2016**, *55*, 14852–14857.

A. Pahl, M. Lakemeyer, M.-T. Vielberg, M. W. Hackl, J. Vomacka, V. S. Korotkov, M. L. Stein, C. Fetzer, K. Lorenz-Baath, K. Richter, H. Waldmann, M. Groll, S. A. Sieber, "Reversible Inhibitors Arrest ClpP in a Defined Conformational State that Can Be Revoked by ClpX Association", *Angew. Chem. Int. Ed.* **2015**, *54*, 15892–15896.

Introduction

1. The Antibiotic Crisis

In September 1928, almost 90 years ago, the Scottish scientist Alexander Fleming made one of the most important discoveries in modern medicine. Mold on staphylococci culture plates induced clear areas without any bacterial growth. Fleming investigated this effect and named the responsible substance penicillin, after the producer fungi *Penicillium*.[1] It took more than ten years before Howard Florey, Ernst Chain and Norman Heatly transformed this discovery into a practical drug, saving millions of lives.[2] Only a few years later, in 1945, Fleming, Chain and Florey received the Nobel Prize in Physiology or Medicine *"for the discovery of penicillin and its curative effect in various infectious diseases"*.[3]
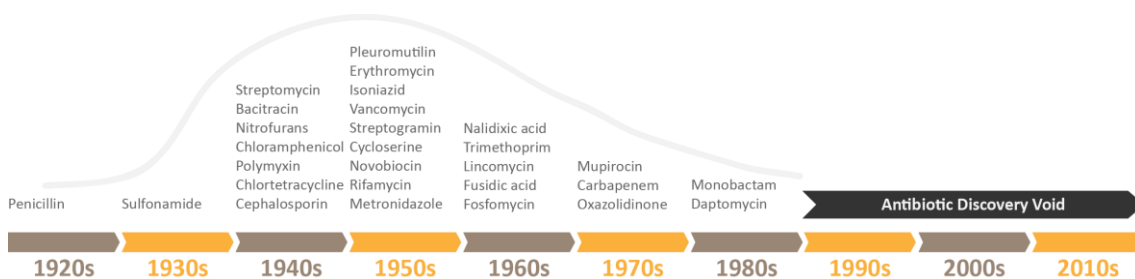
Figure 1 Discovery of new antibiotics in the past century:[4] the "golden era" in the middle of the 19th century followed by a "discovery void".

The discovery and production of penicillin led to the golden antibiotic era resulting in a plethora of new antibiotic classes between the mid-1940s and the 1970s (Figure 1).

There are six main bacterial pathways addressed by today's antibacterial compounds (Table 1). Construction of the bacterial cell wall is blocked by β-lactams through inhibition of peptidoglycan synthesis.[5–7] The glycopeptide vancomycin also inhibits cell wall synthesis of gram-positive bacteria, but unlike β-lactams, this is achieved by the prevention of cross-linking of the cell membrane.[4,8] Daptomycin causes calcium dependent formation of pores in the cell membrane of gram-positive bacteria and leads to depolarization followed by cell death.[9–11] Cationic polymyxins show high affinity for the lipid moiety of lipopolysaccharide and disrupt gram-negative membranes in a detergent-like manner.[12,13] Protein synthesis is a second pathway targeted by antibacterial compounds. Aminoglycosides and tetracyclines address the 30S subunit of

the ribosome, while macrolides, chloramphenicol, clindamycin (lincosamides) and oxazolidinones interfere with the 50S ribosomal subunit (Table 1).[4,14–20]

Table 1 Bacterial targets of several antibiotic classes.[4,14]

Bacterial Target/Pathway	Antibiotics
Cell wall/membrane	Penicillins
	Cephalosporins
	Glycopeptides
	Carbapenems
	Monobactams
	Daptomycin
	Polymyxins
Protein synthesis	Aminoglycosides^a
	Tetracyclines^a
	Macrolides^b
	Chloramphenicol^b
	Clindamycin^b
	Oxazolidinone^b
RNA synthesis	Rifampicin
DNA replication	Metronidazole
	Quinolones
Mycolic acid synthesis	Isoniazid
Folic acid synthesis	Sulfonamides
	Trimethoprim

a) inhibit 30S ribosomal subunit; b) inhibit(s) 50S ribosomal subunit

Rifampicin inhibits RNA synthesis by blocking the DNA-dependent RNA polymerase.[21] DNA replication displays another pathway for tackling bacterial survival. Nitroimidazole compounds, e.g. metronidazole, oxidize DNA and cause strand breaks leading to cell death.[22,23] As this mechanism is not dependent on selective enzymes, nitroimidazole antibiotics are potent in gram-negative and gram-positive bacteria as well as protozoa.[22] Quinolones target DNA replication by inhibition of bacterial DNA gyrase and topoisomerase IV.[24] Mycolic acid and folic acid synthesis represent two other pathways targeted by antibiotics. Isoniazid enters the cells as a prodrug and is converted to target enoyl reductase InhA.[25] Additionally, nitric oxide originating from the conversion of the prodrug enhances the antibacterial effect.[26] Sulfonamides and trimethoprim block folic acid synthesis by competitive inhibition of dihydropteroate synthase and dihydrofolate reductase, respectively.[27,28]

As depicted in the timeline in Figure 1, all successful discoveries were made before 1990.[4] Although resistance against antibiotics was already first observed in 1940, only few years after the discovery of penicillin, in the past 30 years, advances were only made through modification and improvement of already existing antibiotics.[29–31] Now, increasing numbers of resistant bacterial strains call for novel classes of antibacterials. Resulting from numerous naturally occurring antibiotics (e.g. penicillin), bacteria have developed a multitude of mechanisms to survive. Resistance to small molecules is mainly mediated by five mechanisms (Figure 2). Bacterial cells can either overexpress the target to overwrite the antibiotic effect or change the target binding site of the antibacterial compound by mutation of single residues.[32] Alternatively, affected pathways can be bypassed and replaced by surrogate pathways.
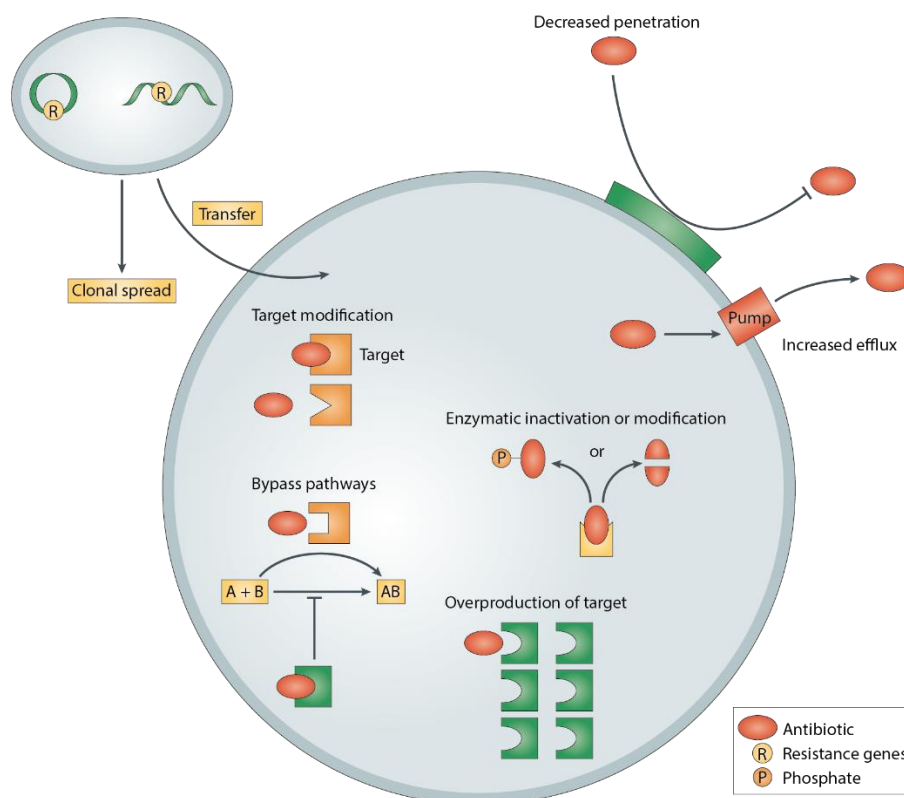
Figure 2 Bacteria have developed five main mechanisms to mediate resistance against antibacterial compounds.[14,32] i) Target modification: Mutations in the binding site prevent antibiotic from binding. ii) Bypass pathways: Alternative pathways are used by the organism. iii) Overproduction of target: Overexpression of the target reduces antibacterial effect. iv) Enzymatic inactivation or modification: Antibacterial compounds are modified by enzymes resulting in loss of activity. v) Decreased penetration: Reduction of intracellular antibiotic concentration by reducing membrane permeability or active efflux. Figure is reproduced with permission from the Nature Publishing Group (license number 4197130393499 and 4197121438392).

Another mechanism is the production of antibiotic modifying/inactivating enzymes, for example β-lactamases, which hydrolase the β-lactam ring of penicillins.[29,33] Finally, the reduction of intracellular antibiotic concentration by either reducing membrane

penetration or active efflux of the antibacterial compounds represents the fifth resistance mechanism.[34,35]

Despite the fact that the occurrence of bacterial resistance against antibiotics is in itself a natural process, the misuse of antibiotic drugs by their excessive use in unnecessary cases renders antibiotic resistance to a global threat for human health. A recent report from the World Health Organization (WHO) revealed that in 43% of the European countries antimicrobial drugs are available without prescription.[36] Antibiotic drugs are extensively and irresponsibly administered to animals in the agricultural industry and veterinary sectors, facilitating resistance development.[37] Together with the widespread belief that viral infections can be treated with antibiotics, this unfortunate phenomenon acts as a catalyst for rapid resistance development.[36] Increased global travel spreads locally generated resistances around the world.[37] In a 2016 study from the National Healthcare Safety Network of the United States, high levels of resistance in several gram-negative and gram-positive bacteria were reported during 2011 and 2014.[37] Vancomycin resistance was observed in more than 80% of *Enterococcus faecium* isolates.[38] More than 43% of *Acinetobacter baumannii* isolates showed either resistance to carbapenem antibiotics or even multidrug resistance, while resistance to methicillin, oxacillin and cefoxitin was detected in over 50% of *Staphylococcus aureus* isolates.[38]

According to the WHO, the current development programs are "*insufficient to mitigate the threat of antimicrobial resistance*", consequently calling for governmental and non-governmental organizations to work together in the development of innovative alternative approaches to fight this threat.[39,40] Alternative strategies for future development, in addition to the development of new antibiotic classes, could be the targeting of resistance mechanisms (e.g. inhibitors of metallo-β-lactamases and efflux pumps), repurposing of already known drugs for the use against bacterial infections and antivirulence approaches.[41–47] The WHO has compiled a "Priority Pathogen List" ranking three categories of pathogens for which new antibiotics are desperately needed. *Acinetobacter baumannii*, *Pseudomonas aeruginosa* and *Enterobacteriaceae* represent the pathogens with the highest, "critical priority".[37] The pathogen group with second highest priority ("high priority") is formed by six bacterial species, among them,

Enterococcus faecium, *Salmonella spp.* and *Staphylococcus aureus*.[37]

The focus of this thesis is set on virulence and its inhibition of *S. aureus*.

2. *Staphylococcus aureus*

At the end of the 19th century, Alexander Ogston was searching for the cause of blood poisoning. The pus of surgical wounds revealed microorganisms which Ogston first identified as micrococci.[48,49] In order to distinguish the often co-occurring "chain formed" streptococci from the "grouped" micrococci, he named them staphylococci, according to the Greek *staphylē* – a bunch of grapes.[49,50] Friedrich Julius Rosenbach further differentiated staphylococci strains and named them according to their color – *Staphylococcus aureus*, forming yellow colonies, and *Staphylococcus albus*, forming white colonies.[49,51]

The golden color of gram-positive *S. aureus* arises from the pigment staphyloxanthin and depicts the most visible virulence factor. Staphyloxanthin acts as an antioxidant, protecting the cell from reactive oxygen species, consequently preventing killing by neutrophils.[52,53] *S. aureus* utilizes an arsenal of these virulence factors to evade the human immune system and to establish an infection.[54] Staphylococcal virulence factors can be divided into two groups: secreted factors or toxins and non-secreted or cell-surface-associated factors.[55,56] A diverse set of toxins is released by *S. aureus* to directly damage host membranes through pore formation. Examples are α-hemolysin, bi-component leukotoxins (panton-valentine leukocidin, leukotoxins and γ-hemolysin) which act in a receptor-mediated manner and several phenol-soluble modulins which have a receptor-independent mode of action.[56] Enterotoxins and toxic shock syndrome toxin belong to the group of superantigens and both trigger non-specific T cell activation or release of IL-1, IL-2 and TNF-α cytokines.[56–58] Proteases, such as aureolysin, glutamyl endopeptidase, staphopain, exfoliative toxins and several others represent another important group of secreted toxins. They interfere with and degrade host proteins, such as the human defensing peptide cathelicidin, insulin and cadherins, and complement factors, thus facilitating evasion of bacterial killing.[55,56,59,60] Staphylokinase activates and interacts with plasminogen, enabling evasion of an important part of the innate immune system and leading to successful dissemination in the host organism.[55,61]

Coagulases (staphylocoagulase and the von Willebrand factor) allow *S. aureus* to trigger the formation of fibrin from fibrinogen.[56,62] In the bloodstream, this leads to clotting on the cell surface with subsequent inhibition of phagocytosis and abscess formation.[62,63] In addition, several lipases and nucleases complete the set of extracellular toxins, nevertheless, the exact functions of these enzymes are not fully understood.[56]

The two most important cell-surface-associated virulence factors are protein A and clumping factor A. Protein A binds to the heavy chain in the F_C region of IgG antibodies, coating the bacterial cell with IgG in incorrect position for opsonization and as a result, prevents phagocytosis.[55,64,65] Clumping factor A (ClfA) binds to fibrinogen and can either lead to coating with fibrinogen or cell clumping (at high cell concentrations), resulting in an antiphagocytic effect.[55,66,67]

With this elaborate arsenal of virulence factors *S. aureus* is very successful in causing a variety of healthcare and community-associated diseases. 30-50% of all humans are colonized with this commensal and opportunistic pathogen.[68] As soon as the immune system is weakened, *S. aureus* can cause devastating infections, such as bacteremia, endocarditis, skin and soft tissue infections, osteoarticular infections, pleuropulmonary infections, epidural abscesses, meningitis, urinary tract infections and toxic shock syndrome.[69,70] Especially bacteremia (15-50%) and infective endocarditis (22-66%) show relatively high overall mortality rates, corroborating the severity of these infections.[69,71] Its ability to form biofilms renders *S. aureus* an important pathogen, often leading to prosthetic device related infections.[69,72] Other common origins for infections are cardiac devices, intravascular catheters, breast implants, ventricular shunts and penile implants.[69] Due to the intrinsic insensitivity of *S. aureus* in biofilms to any treatment, surgery regularly remains the only option.[69,72,73]

Even though, in the present day, treatment of staphylococcal infections with antibiotics has drastically decreased mortality rates compared to the pre-antibiotic era, antibiotic resistance of *S. aureus* aggravates successful treatment nonetheless.[69,71] A study in Turkey showed that from 2009 to 2014 all tested *S. aureus* isolates were resistant against penicillin G, the drug responsible for the beginning of the antibiotic era.[74] In Europe, the overall numbers of methicillin resistance (MRSA) have decreased slightly from 2012 (18.8%) to 2015 (16.8%), however, 85.2% of MRSA strains also showed resistance against fluoroquinolones.[75] Resistance to the last resort antibiotic linezolid

was only observed in 0.1% of the tested isolates.[75] As infections with MRSA or multidrug resistant *S. aureus* are most commonly treated using vancomycin, daptomycin and linezolid, the rising appearance of resistances to all of these antibiotics leads into an uncertain future.[76–78]

This unfortunate phenomenon calls for new strategies in the fight against multidrug resistant *S. aureus*, either through the development of new antibiotic classes or alternative approaches. One strategy, the so-called antivirulence approach, focuses on tackling the broad arsenal of virulence factors expressed by *S. aureus* thus protecting human cells by supporting the immune system.

3. Antivirulence

The emergence of antimicrobial resistance and the scarce numbers of new antibiotics require new thinking and unconventional strategies in order not to turn treatment of bacterial infections into a futile endeavor. Bacteria utilize various virulence factors to evade the human immune system and establish infections. Antivirulence approaches focus on these factors by either inhibiting their production or directly blocking them. The main difference to conventional antibiotics is that they do not interfere with the pathogens' survival but rather disarm the bacteria, therefore supporting the immune system.[46,79,80] Hence, the direct selective pressure on the bacteria caused by antibiotics is reduced or eliminated, hopefully resulting in slower rates of resistance development.[46,80,81] Additionally, a major problem of classical antibiotics, namely the killing of beneficial, commensal bacteria of the human microbiota, could be completely avoided.[46] The general idea of treating toxins instead of bacteria is already 125 years old. At the end of the 19th century, Emil von Behring proposed the targeting of toxins of diphtheria and tetanus bacteria instead of the bacteria itself.[82] He treated children with antiserum against diphtheria toxin, thence receiving the first Nobel Prize in Medicine or Physiology in 1901.[46] Unfortunately, the introduction of antibiotics led to the disappearance of antivirulence research.

Due to the antibacterial discovery void, antivirulence research has once more become attractive in recent years. Five promising drug candidates are currently in development for the treatment of *S. aureus* infections (Table 2).[46] The monoclonal antibodies MEDI4893 and AR-301 both target α-hemolysin (Hla), one of the most important virulence factors of *S. aureus*.[46,83] Binding of MEDI4893 to Hla inhibits its oligomerization, as well as the interaction with the corresponding receptor on the host cell, showing efficacy in various animal models.[46] Both anti-Hla-antibodies (MEDI4893 and AR-301) have entered phase II clinical trials.[46] ASN-100 represents another monoclonal antibody, that targets not only Hla but also an additional set of four leukotoxins.[84,85] This antibody showed efficacy in pneumonia and sepsis animal models and is in clinical phase II.[46] The transpeptidase sortase A (SrtA) is essential for anchoring cell surface proteins in the membrane, with mutants having been shown incapable of causing bacteremia in mouse models.[86,87] Screening for small molecule inhibitors of

SrtA and structural optimization resulted in compound **6e** successfully protecting mice from lethal bacteremia.[88]

Table 2 Antivirulence compounds currently in development for the treatment of *S. aureus* infections.[46]

Compound	Molecule Type	Cellular Target	Development Stage
MEDI4893	Antibody, human, mAb IgG1	α-hemolysin	Phase II
AR-301	Antibody, human, mAb IgG1	α-hemolysin	Phase II
ASN-100	Antibody, human, mAb IgG1	α-hemolysin, panton-valentine leukocidin, leukocidins LukED, LukGH and γ-hemolysin	Phase II
6e	3,6-Disubstituted triazolo-thiadiazole compounds	Sortase A (SrtA)	Preclinical
Savirin	3-(4-Propan-2-ylphenyl) sulfonyl-1H-triazolo [1,5-a] quinazolin-5-one	Accessory gene regulator protein A (AgrA)	Preclinical

Development of the small molecule savirin as an antivirulence agent followed a different principle. Savirin inhibits the accessory gene regulator protein A (AgrA), a key regulator of staphylococcal virulence.[46,89,90] Targeting a regulator prevents expression of many virulence factors simultaneously instead of blocking individual proteins. While Agr-regulated toxin expression was efficiently inhibited by savirin, skin abscess models in mice also displayed a protective effect against *S. aureus*.[46,91]

Similarly, the staphylococcal caseinolytic protease complex ClpXP exhibits a global impact on the regulation of virulence factor expression.[92–94] The protease machinery consists of a tetradecameric barrel-shaped ClpP proteolytic core which associates with hexameric chaperone complexes such as ClpX. Chemical inhibition as well as genetic deletion of *clpP* showed dramatic changes in virulence factor expression.[93–97] Murine skin abscess models displayed requirement of both ClpP and ClpX for virulence.[93] A look at the aforementioned research as a whole leads one to the conclusion that the ClpXP protease complex represents a promising target for manipulation of staphylococcal virulence and the development of antivirulence agents.

4. The ClpXP Protease of *Staphylococcus aureus*

When proteins reach the end of their lifetime, are misfolded or aggregate, they are no longer able to fulfill their cellular function. In order to maintain proteostasis, cells express proteases which degrade and recycle those proteins. *S. aureus* partly controls proteostasis by expressing the caseinolytic protease complex ClpXP. While ClpP's function is hydrolysis of peptide bonds, substrate specificity and unfolding are determined through association with chaperones such as ClpC or ClpX.[98] Several studies revealed the impact of ClpXP on virulence regulation.[92–94,96] Deletion of either ClpX or ClpP resulted in drastic reduction of *S. aureus* virulence in mouse models.[93]

The barrel-shaped structure of ClpP is built up by two rings, each consisting of seven ClpP monomers (Figure 3A and B). The heptameric rings are stacked face-to-face and enclose a cavity surrounded by fourteen active sites. Single monomers contain N-terminal, core and E-helix domains. The N-terminal regions form narrow axial pores at the top and bottom part of the barrel, thus preventing uncontrolled proteolysis. The core domain contains the active site serine S98, forming a catalytic triad with histidine H123 and aspartate D172 (Figure 3C).
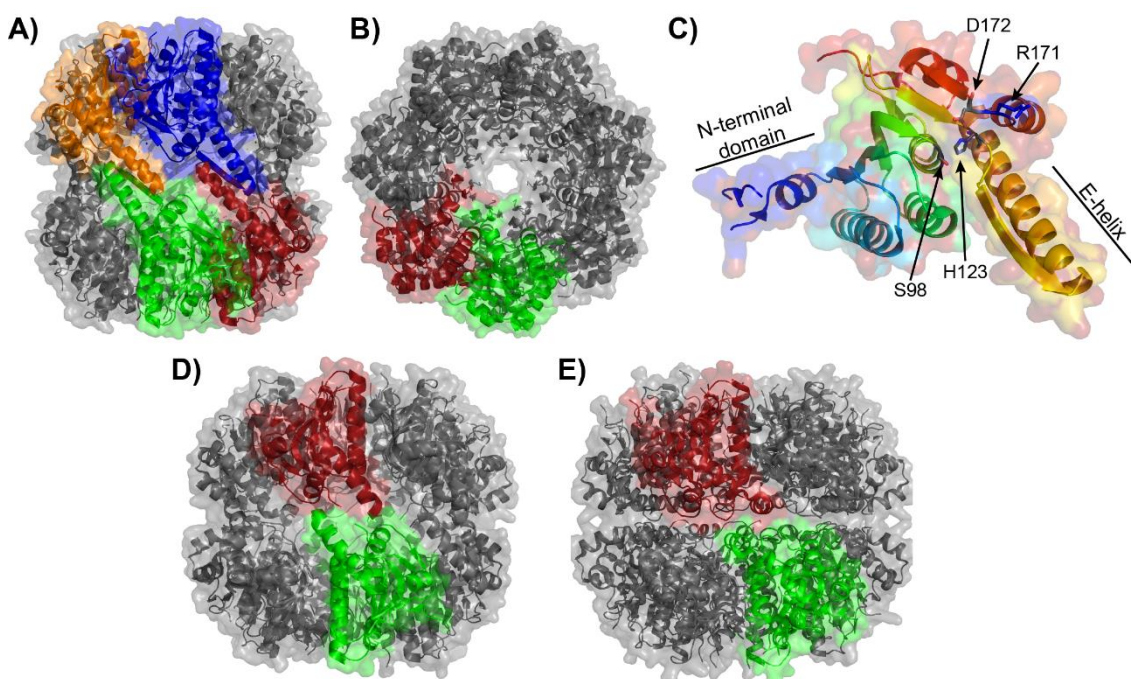
Figure 3 Crystal structures of *S. aureus* ClpP. Single monomers in A), B), D) and E) are highlighted in green, red, blue and orange. A) Extended, active conformation of ClpP; side view (PDB: 3V5E).[99] B) top view of A). C) Monomer structure of ClpP in active conformation. Highlighted are amino acids of the catalytic triad (S98, H123 and D172) and the sensor region (R171). D) Compact, inactive conformation of ClpP (PDB: 4EMM).[100] E) Compressed, inactive conformation of ClpP (PDB: 3ST9).[101]

The E-helix domain interacts with its counterpart in the other heptameric ring, accordingly aligning the catalytic triad and establishing proteolytic activity. Crystallographic X-ray experiments revealed that arginine R171 acts as a sensor responsible for the formation of the tetradecamer complex and correct alignment of the catalytic triad.[99] Mutation of the arginine to alanine or lysine resulted in inactive heptameric ClpP species.[99] Crystallography and NMR-studies showed that the tetradecameric ClpP complex is a highly dynamic system as several conformations were observed.[99,102–104] Only the extended conformation (Figure 3A) exhibits correct positioning of the E-helix and thus, full activity. The compressed as well as compact ClpP conformation both show misaligned catalytic triads and therefore no activity (Figure 3D and E).[100,101,104] Several potential substrate proteins were identified using an S98A active site mutant of ClpP.[105]

The chaperone ClpX is a member of the AAA+ family (ATPases associated with diverse cellular activities). Structure and function of *Escherichia coli* ClpX (85% sequence similarity to *S. aureus* ClpP) have been extensively studied. Six monomers of ClpX form the hexameric ring-superstructure (Figure 4A and B). The monomers each contain small and large domains and have Walker A and B motives for nucleotide hydrolysis and binding (Figure 4C). This allows for triggered conformational changes within the hexamer.[106] Mutation of glutamate E185 in the Walker B motif to alanine blocks ATP hydrolysis leading to stable ATP binding and reduced conformational dynamics.[107]
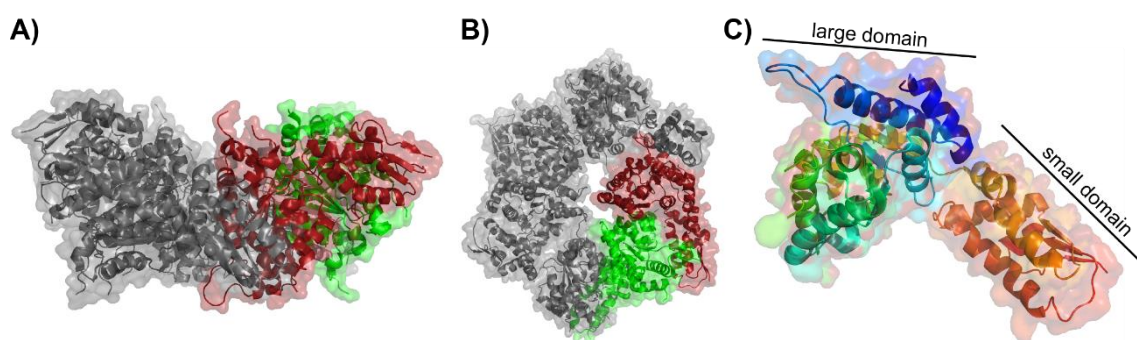
Figure 4 Crystal structure of nucleotide-bound *E. coli* ClpX (PDB: 3HWS).[106] Single monomers in A) and B) are highlighted in green and red. A) Side view of ClpX hexamer. B) Top view of ClpX hexamer. C) ClpX monomer in nucleotide-bound state.

The N-terminal domain of ClpX directly recognizes and binds substrates such as FtsZ and MuA, as well as adaptor proteins such as RssB and SspB.[108–111] However, the N domain is not required for recognition of the SsrA-tag which marks ribosomal stalled proteins for degradation by ClpXP.[112–115] After successful substrate recognition, proteins are

unfolded under ATP consumption and translocated into the ClpP barrel. Highly conserved YVG loops (tyrosine-valine-glycine; residues 153-155) grip substrate proteins and apply mechanical force (power strokes).[116] These strokes are mediated by conformational changes of single ClpX monomers caused by hydrolysis of ATP.[116]

Both *E. coli* and *S. aureus* ClpXP complex formation is established by binding of the tripeptidic IGF loop of ClpX (isoleucine-glycine-phenylalanine; residues 267-269 in *S. aureus* ClpX) into hydrophobic clefts on the axial face of ClpP.[114,117] Mutations in the IGF loop of just one monomer in the ClpX hexamer resulted in a 50-fold reduced ClpP affinity.[118] To this day, no molecular structures have been obtained to explain the intriguing symmetry mismatch of ClpX hexamers and ClpP heptamers upon complex formation.

Owing to the importance of ClpXP in virulence regulation, chemical manipulation has been the focus of extensive research in recent years. However, to date little is known about inhibition of ClpX with small molecules.[119,120] In contrast, several small molecules were published as modulators of ClpP activity (Figure 5). Circular acyldepsipeptides (ADEPs) were identified as potent activators of ClpP.[121] Binding of ADEPs into the hydrophobic clefts of ClpP mimics ClpX binding, followed by pore opening, uncontrolled proteolysis and finally cell death.[121–124]

Several classes of covalent ClpP inhibitors have been studied. The substrate mimic **Z-LY-CMK** binds to the active site and covalently links the catalytic histidine (H123) via the chloromethyl ketone (CMK) moiety.[125,126] β-sultam inhibitors exhibit an intriguing mechanism of action: Nucleophilic attack of the active site serine S98 opens the sultam ring followed by subsequent elimination and formation of dehydroalanine.[126] The most extensively studied inhibitor class of ClpP are β-lactones. These are opened by S98 and form an ester bond which results in ClpP inhibition. Several studies revealed the impact of β-lactone induced ClpP inhibition on *S. aureus* virulence.[95–97,127–130] Phenyl esters are another class of potent ClpP inhibitors. Similar to lactones, they form esters with S98, subsequently leading to inhibition of ClpP.[131] However, the labile ester bond formed by lactone and phenyl ester inhibitors can be hydrolyzed over time. Oxazole compounds represent the latest generation of ClpP inhibitors with an unprecedented mode of action. The compounds bind non-covalently near to the active site and lock ClpP in an inactive conformational state.[132] However, this effect on ClpP activity is overwritten by

ClpX binding.[132] Ergo, stable inhibition of ClpP strongly depends on the compounds' capabilities to inhibit ClpXP.
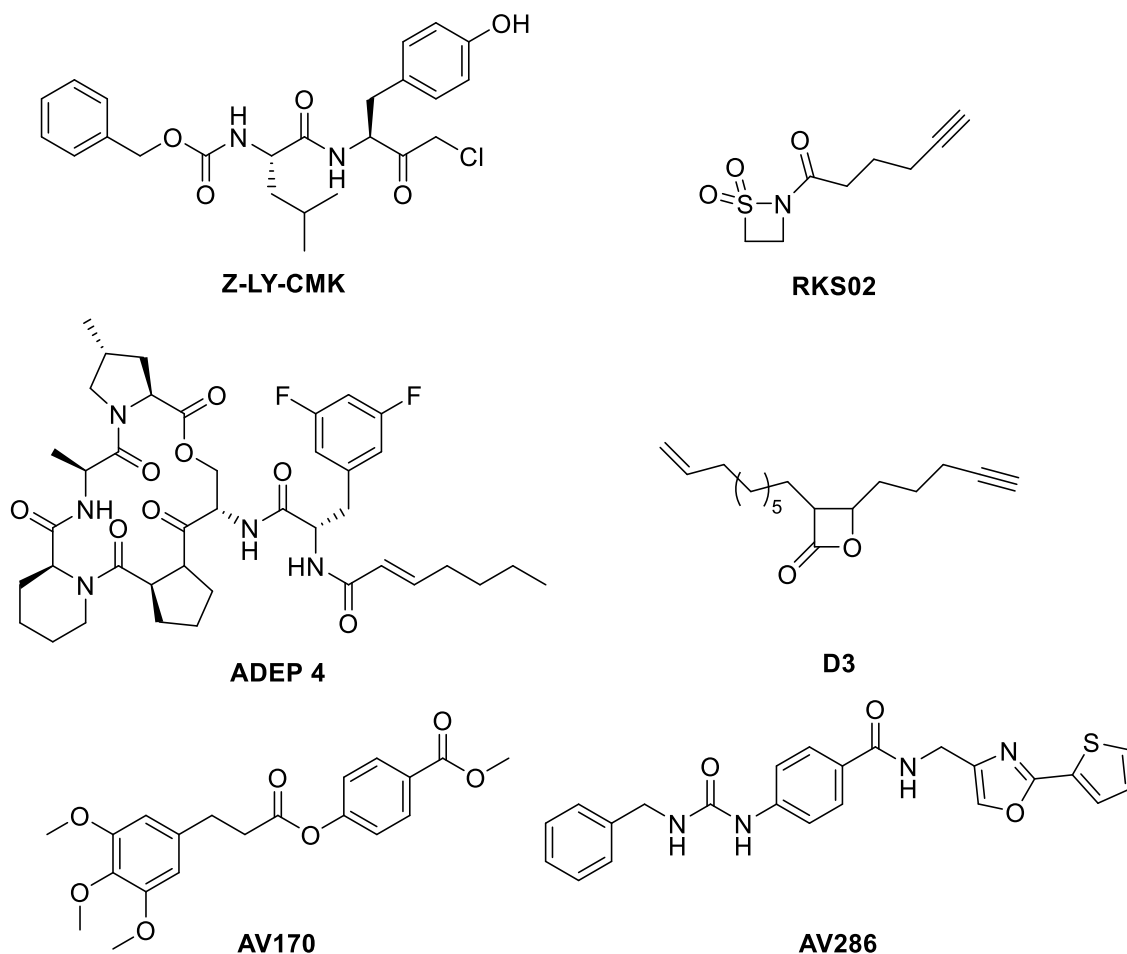
Figure 5 Structures of molecules for chemical manipulation of ClpP. ClpP activator **ADEP 4**,[121] covalent inhibitors **Z-LY-CMK**,[125] **RKS02**,[126] **D3**[97] and **AV170**[131] and non-covalent inhibitor **AV286**[132].

The motivation of this thesis is: i) the search for more stable and potent inhibitors of the *S. aureus* ClpXP protease for the potential use in future pharmacological applications and ii) the investigation of the global impact of genetic clpP modifications on *S. aureus*.

Chapter I – A Chemical Disruptor of the ClpX Chaperone Complex Attenuates the Virulence of Multidrug-Resistant *Staphylococcus aureus*

This chapter is based on the following publication:

1. Introduction

A recent high-throughput screen (HTS) of 140.000 compounds against ClpP revealed oxazoles as novel inhibitor scaffolds with enhanced stability and potency.[132] Conversely, these reversible binders were rapidly ejected from the ClpP active site upon chaperone binding via conformational selection. Hence, a HTS against the whole ClpXP complex was performed and one potent hit molecule identified that inhibits proteolysis by dissociation of ClpXP protein interactions and globally reduces virulence of *S. aureus* and MRSA.

2. Results and Discussion

2.1. High-Throughput Screen

For the identification of novel potent inhibitors of the ClpXP protease a high-throughput screen (HTS) against the whole ClpXP complex was performed. For the HTS an established assay based on the degradation of green fluorescent protein (GFP) equipped with an SsrA peptide-tag was used (Figure 6A).[133] This native peptide sequence, usually appended to ribosome-stalled proteins, is recognized by ClpX, which unfolds the tagged GFP under ATP consumption. Subsequently, the linear peptide chain is digested within the proteolytic ClpP barrel resulting in a loss of fluorescence signal. Multiple turnover is achieved by ATP regeneration with creatine kinase.[134] Putative inhibitors of proteolysis can either target ClpP, ClpX, the interaction between these two components or the kinase, requiring careful validation of hits in secondary assays.
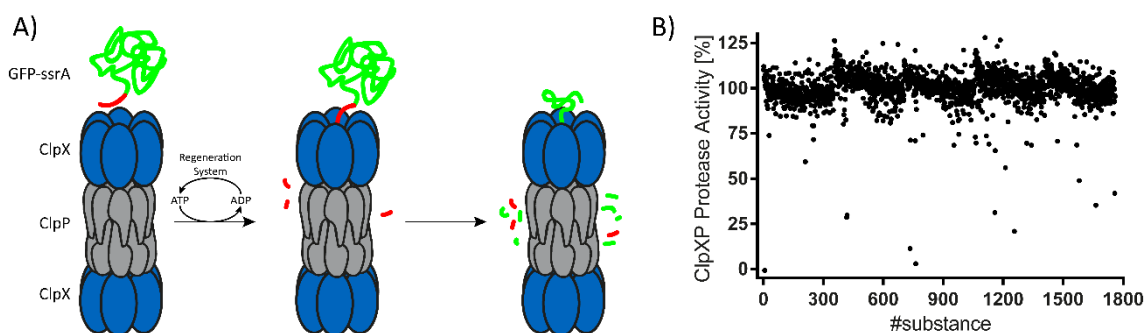
Figure 6 GFP degradation assay for monitoring ClpXP activity. A) GFP is tagged to a SsrA peptide-tag which is recognized by ClpX. ATP-dependent unfolding by ClpX and degradation by ClpP leads to loss of fluorescence signal. ADP is transformed back to ATP by the regeneration system containing creatine kinase. B) Pre-screen of 1760 compounds using the established 384-well format ClpXP assay (10 µM final compound concentration).

The fluorescence assay was adapted for the needs of HTS in a 384-well format and a kinetic measurement time of 20 min. After reaching an acceptable dynamic range between positive and negative controls an initial (pre-) screen of 1760 compounds was conducted (Figure 6B). A Z-factor of > 0.6 indicated sufficient reliability and a full screen with a total of 40480 compounds from the FMP library was performed (overall Z-factor of 0.69 ± 0.09; Figure 7A).

The 332 best inhibiting and the 20 best activating molecules were identified as primary hits deviating from the normal distribution by three standard deviations (z-score > 3) for inhibitors or four standard deviations (z-score < -4) for activators, respectively. To select the most potent compounds and exclude inhibitors of the ATP regenerating system, IC_{50} values were determined (validation) and molecules assayed against creatine kinase in a secondary screen (Figure 7B and C). 158 molecules were identified as sole ClpXP inhibitors with a relative activity difference of > 70% and thereof six compounds with IC_{50} values ranging between 0.6 and 3.1 µM were selected for a closer inspection of their mode of action after conducting another validation step in a 96-well format (Figure 7B and D).
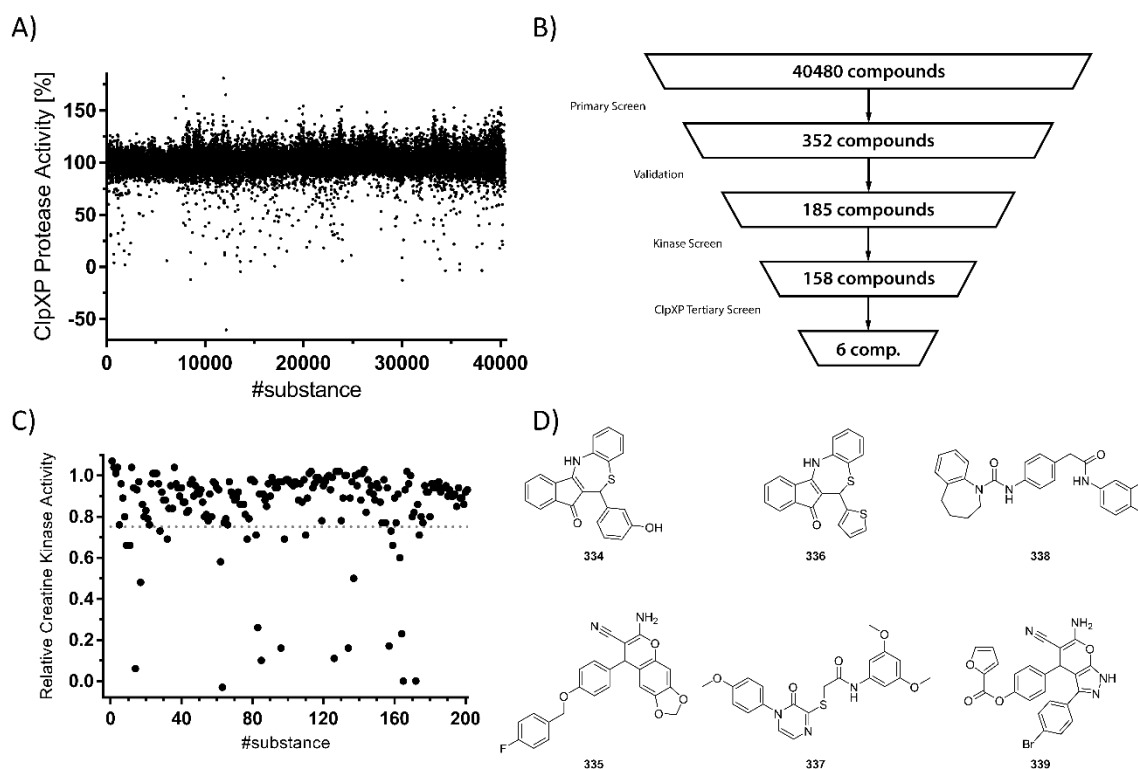
Figure 7 HTS of 40480 compounds revealed potent inhibitors of ClpX and ClpXP. A) Initial screen with 10 µM compound concentration yielded 352 compounds for further validation. B) After validation of 352 compounds only 185 showed a sufficient dose-dependent behavior and were tested for creatine kinase inhibition. Compounds showing < 75% inhibition (at 50 µM) were again validated in a 96-well format. C) All validated primary active hits were counter-screened against inhibition of creatine kinase (50 µM final concentration) which is required for ATP

regeneration in the ClpXP assay. D) Chemical structures of the six most potent compounds with IC$_{50}$ values ranging between 0.6 and 3.1 µM.

2.2. *In vitro* Characterization

To elucidate the mode of action of the six ClpXP inhibiting compounds several assays, focusing on either ClpP, ClpX or the ClpXP complex were performed. Interestingly, none of the six hit compounds inhibited ClpP peptidase activity up to a concentration of 25 µM (25-fold excess), suggesting that these molecules exhibit a novel inhibitory mechanism (Figure 8A). Compounds **334** and **336**, which encompass a similar structural core motif (Figure 7D), blocked ClpX ATPase activity with an IC$_{50}$ of 0.8 and 1.8 µM, respectively, while all other compounds were largely inactive (Figure 8B). Inhibition of chaperone activity is an intriguing finding since specific ClpX inhibitors have not been reported so far and previous molecules targeting ClpC, a related chaperone, even stimulated its activity.[135,136] Both hits did not alter ClpCP proteolysis demonstrating selectivity solely for ClpX (Figure 8C).
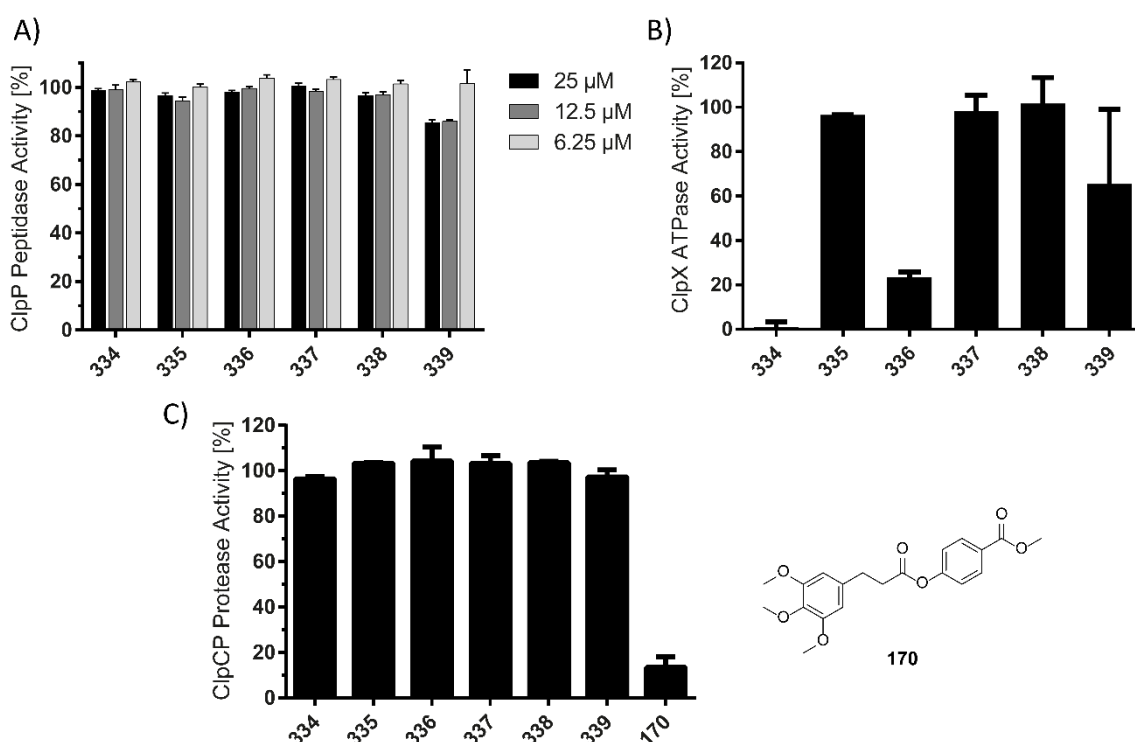
Figure 8 Influence of the six hit compounds on ClpP, ClpX and ClpCP activity. A) None of the identified ClpXP inhibitors alters ClpP peptidase activity in a fluorescent assay (1 µM ClpP; mean ± standard error). B) ClpX ATPase activity assay with the hit compounds (100 µM final compound concentration; mean ± standard deviation). C) ClpCP (MecA as adaptor) activity is not inhibited by the six compounds at 100 µM concentration. The covalent ClpP inhibitor **170** was used as a positive control (mean ± standard deviation).[131]

The main focus was set on compound **334** as the most potent ClpX inhibitor and to further analyze its mechanism of action. The structure of **334** does not exhibit any obvious reactive electrophilic moieties and accordingly no covalent modification of ClpX was obtained by intact-protein mass spectrometry (Figure 9A). ClpX hexamer stability was evaluated in presence and absence of **334** via analytical size-exclusion
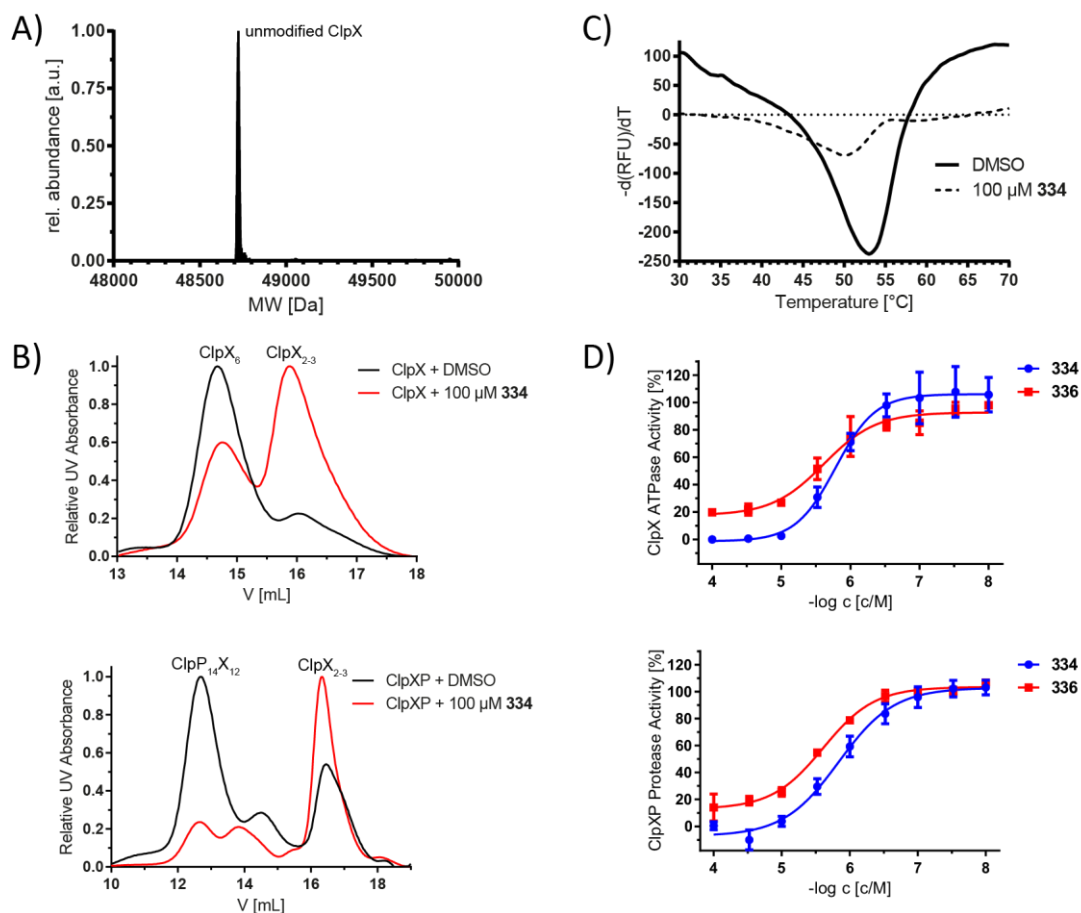
Figure 9 Compounds **334** and **336** reversibly inhibit ClpXP through disruption of ClpX hexamer and ClpXP complex. A) No covalent modifications of ClpX are detectable upon treatment with **334** at 100 µM (33-fold excess). B) Size-exclusion chromatography experiments show the disruption of ClpX-hexamer and ClpXP-complex upon treatment with 100 µM **334**. C) Thermal-shift assay performed with 10 µM ClpX and 100 µM **334** reveals a destabilization of ca. 2.8 K compared to DMSO-treated ClpX. D) **334** and **336** are potent inhibitors of both ClpX ATPase activity and ClpXP protease activity (mean ± standard deviation, n ≥ 3).

chromatography (Figure 9B). Importantly, a dramatic disruption of the oligomeric state to dimeric/trimeric species was observed upon compound addition and even the whole ClpXP proteolytic complex collapsed in response to **334** binding (Figure 9B). The **334**-induced deoligomerization of ClpX was associated with a decrease in the melting temperature of 2.8 K as obtained in thermal-shift assays indicating destabilization of the hexameric complex (Figure 9C). The less pronounced peak in the **334** treated sample possibly arises from quenching of fluorescence signal by **334**. The similar IC$_{50}$ values and curve shapes of **334** (and **336**) determined in dose-dependent ClpX ATPase and ClpXP

protease assays corroborate the inhibition of the ClpXP complex through specific inhibition of ClpX (Figure 9D).

For prospective *in vivo* experiments, the stability of **334** was examined in mouse plasma. The compound shows no significant decrease over five hours of incubation in plasma (Figure 10) indicating potential for further use in *in vivo* experiments.
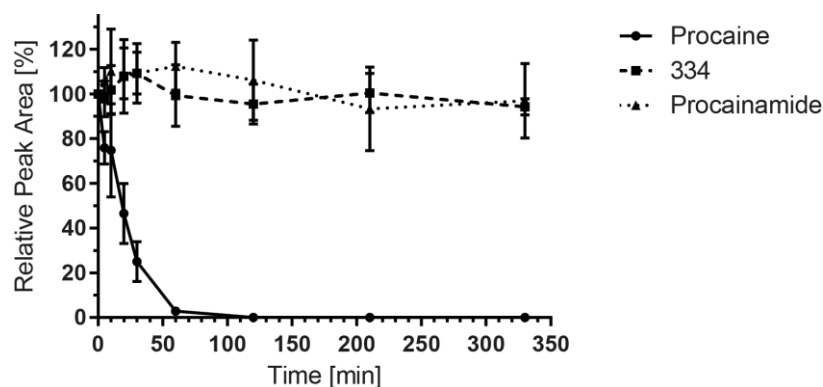
Figure 10 Compound 334 (100 µM) is stable in mouse plasma for ≥ 5.5 h. Procaine (100 µM) and procainamide (100 µM) are used as positive and negative controls, respectively (mean ± standard deviation, n = 3).

2.3.   Structure-Activity Relationship Studies

To dissect the molecular prerequisites for **334** inhibitory activity 31 derivatives were prepared, varying in their aromatic ring substitutions. The synthetic strategy was initiated by condensation of indan-1,3-dione with the corresponding benzaldehydes. The desired dihydrothiazepines were obtained by the reaction of 2-benzylideneindan-1,3-diones with 2-aminothiophenol. In most cases, this reaction proceeded smoothly in ethanol at r.t. except for compound **343** that exhibits a strong donor substituent in para-position. This reaction was thus performed under acidic conditions (Scheme 1).
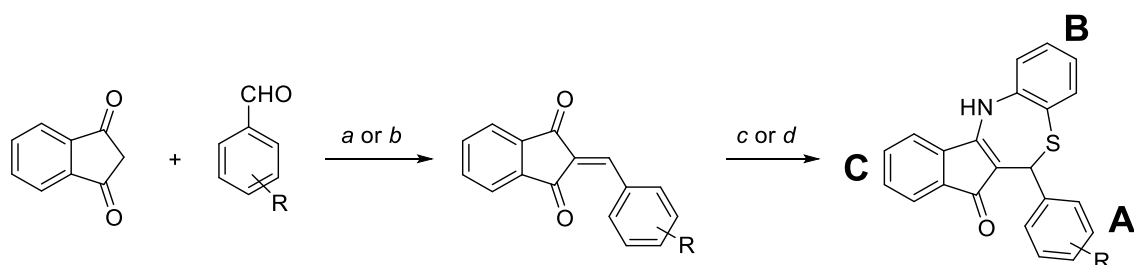
Scheme 1 Synthesis of dihydrothiazepines. Reagents and conditions: *a)* HOAc, NaOAc, reflux, 3 h; *b)* *L*-proline, MeOH, r. t., 16 h; *c)* 2-aminothiophenol, EtOH, r. t., 18 h; *d)* 2-aminothiophenol, *i*PrOH/HOAc, r. t., 18 h.

Introduction of a methoxy substituent at 5 position in the upper B-benzene ring (**345**) almost completely abolished inhibition of ClpXP suggesting that this site is less suited for

structural modifications (Figure 11A). An exchange of the lower phenol ring A by thiophene (**336**) retained potency while a replacement by pyridine (**352**) resulted in a significantly increased IC_{50} value. Interestingly, the phenol ring turned out to be amenable for the introduction of additional hydroxy- (**347**), bromo- (**358**) or methoxy- (**344**) groups. However, positioning of the phenolic hydroxy-group in *meta* (parent **334**) and *para* (**343**) was crucial for activity while *ortho* (**351**) resulted in a significant drop of potency. Other substituents at meta-position including fluorine (**348**), methoxy (**341**), amino (**359**) and hydroxymethyl (**367**) showed reduced activity similar to the unsubstituted benzene (**340**). Together with the observation that bulky substituents (**365**, **350**) were not tolerated, it can be concluded, that the A-benzene ring is, like the B-ring, crucial for enzyme binding. A certain degree of structural flexibility was observed for the C-ring where chlorine (**366**) and alkynyl (**356**) substituents were tolerated. Oxidation of the thioether to a sulfone (e.g. **355**) resulted in a tenfold drop of potency. Of note, some compounds, although exhibiting comparable IC_{50} values, largely varied in the extent of maximum inhibition, ranging from 100% (e.g. **334**) to 8% (e.g. **375**) (Figure 11B).
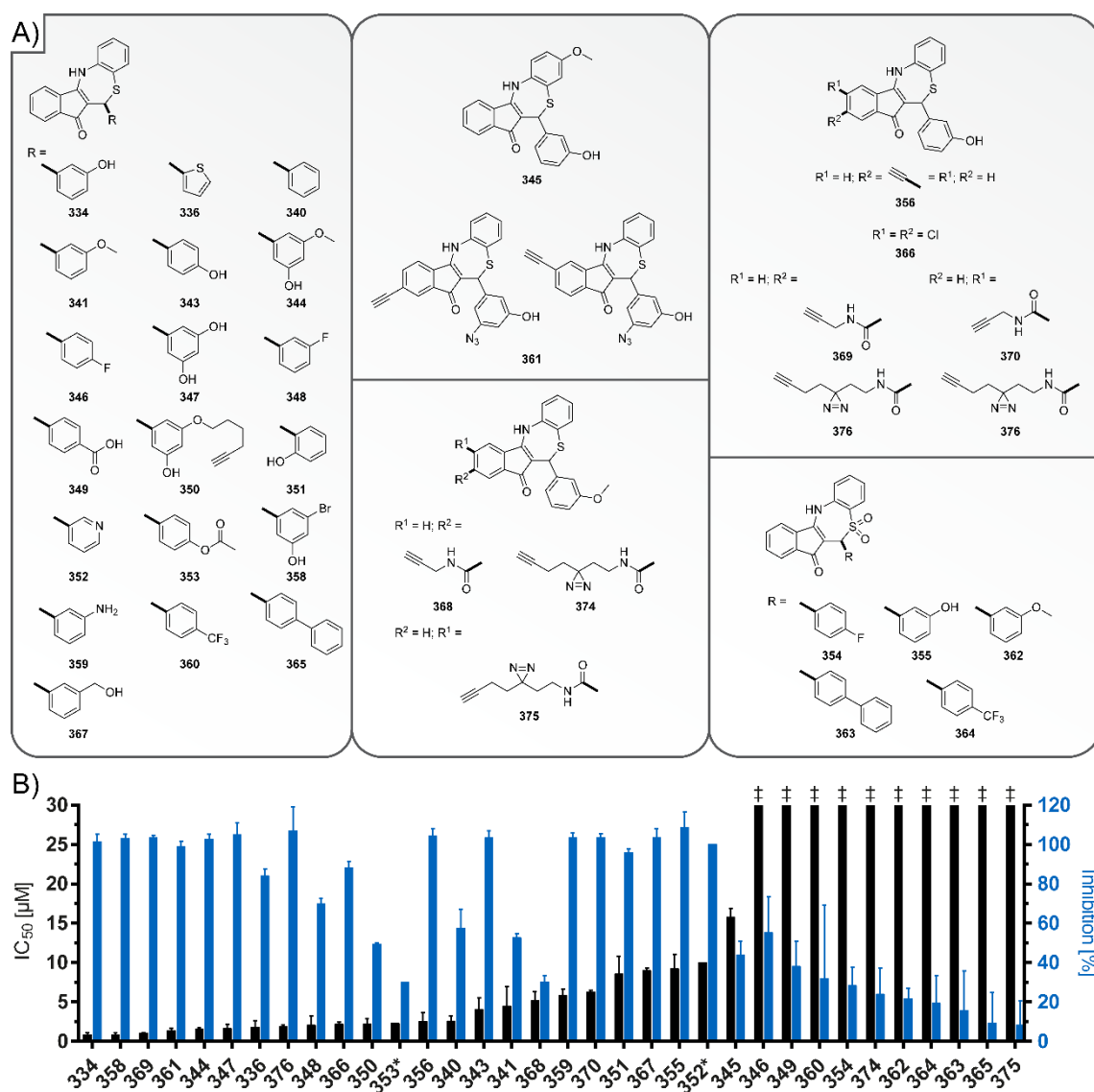
Figure 11 Structure-activity relationship studies of **334** analogues in ClpXP-protease assay. A) Synthesized derivatives of compound **334**. B) Inhibition data of all compounds in the ClpXP-assay. Shown are IC$_{50}$ values (black bars) and the degree of inhibition (blue bars). Compounds marked with * only tested in the HTS validation, compounds marked with ‡ exhibited an IC$_{50}$ > 50 µM. Presented data result from at least three independent experiments and are shown in mean ± standard deviation.

2.4. Efforts for *in vivo/in vitro* Target Validation

2.4.1. *Affinity-Based Protein Profiling*

The initial structure-activity relationship (SAR) studies revealed flexibility for compound functionalization and guided the design of probes for *in situ* target validation via affinity-based protein profiling (AfBPP).[137–139] For this methodology, the compound needs to be equipped with a photoreactive moiety and an alkyne tag for irreversible target binding and identification via tandem mass-spectrometry (LC-MS/MS), respectively.

First, a probe that was equipped with an alkyne handle in the flexible C-ring and an azide substituent incorporated in the A-ring next to the crucial hydroxy group (**361**) was designed (Scheme 2). Synthesis using asymmetric starting materials resulted in the formation of two region isomers (products in Scheme 2).
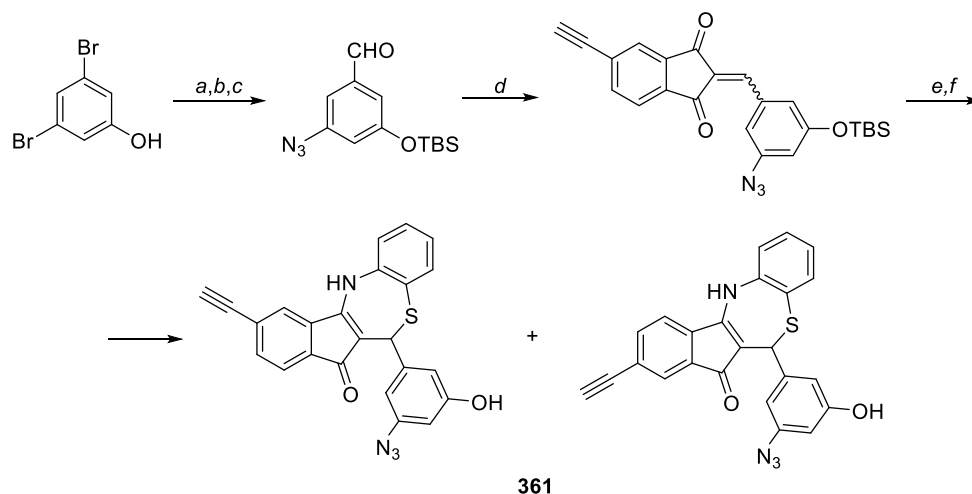
Scheme 2 Synthesis of arylazide probe **361**. Reagents and conditions: *a)* 1) BuLi (2 eq.), THF, −78 °C, 30 min, 2) DMF, −78 °C to r. t., 2 h, 50%; *b)* NaN$_3$, sodium ascorbate, CuI, *trans*-N,N'-dimethylcyclohexane-1,2-diamine, EtOH/H$_2$O/DMF, reflux, 3 h, 27%; *c)* TBSCl, imidazole, CH$_2$Cl$_2$, 18 h, r. t., 79%; *d)* 5-ethynyl-indan-1,3-dione, *L*-proline, MeOH, r. t., 16 h, 66%; *e)* 2-aminothiophenol, EtOH, r. t., 18 h, 64%; *f)* Bu$_4$NF·3H$_2$O, THF/H$_2$O, r. t., 2 h, 10%.

While the probe retained activity (IC$_{50}$ = 1.1 µM), it rapidly decomposed under UV-irradiation leading to fragments that presumably did not link the alkyne to the protein. The same UV-lability was observed for the parent molecule (**334**) rendering a separation of alkyne and photoreactive group unfeasible (Figure 12).
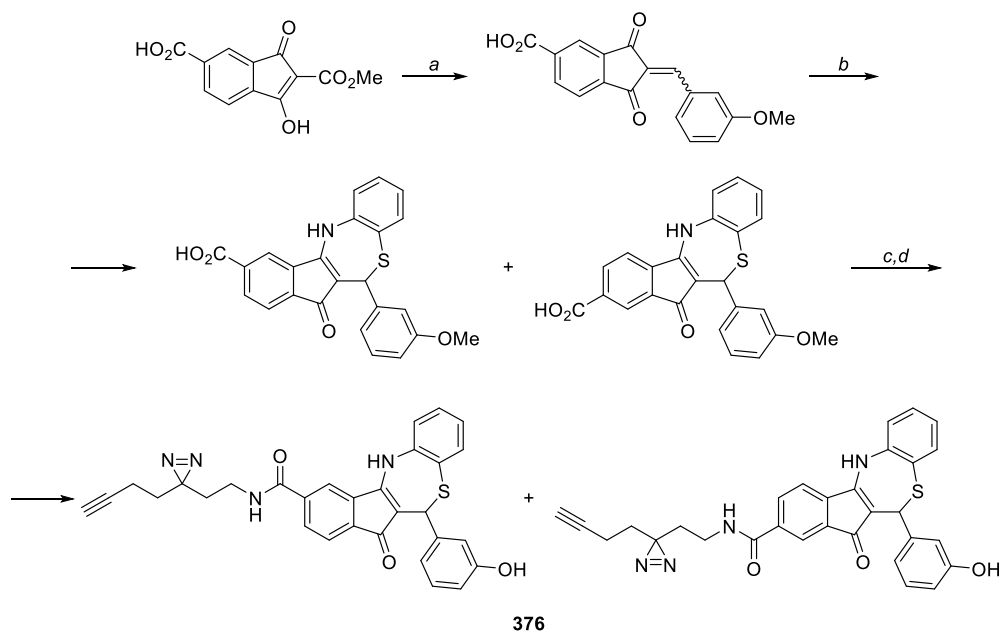
Scheme 3 Synthesis of diazirine photoprobe **376**. Reagents and conditions. *a)* 3-methoxybenzaldehyde, HOAc, 100 °C, 2 h, 33%; *b*) 2-aminothiophenol, EtOH, r. t., 24 h, 99%; *c)* BBr₃, CH₂Cl₂, 3 h, r.t.; *d*) 2-(3-(but-3-inyl)-3*H*-diazirin-3-yl)ethylamine, HCTU, DIPEA, CH₂Cl₂, 48 h, 7% over 2 steps.
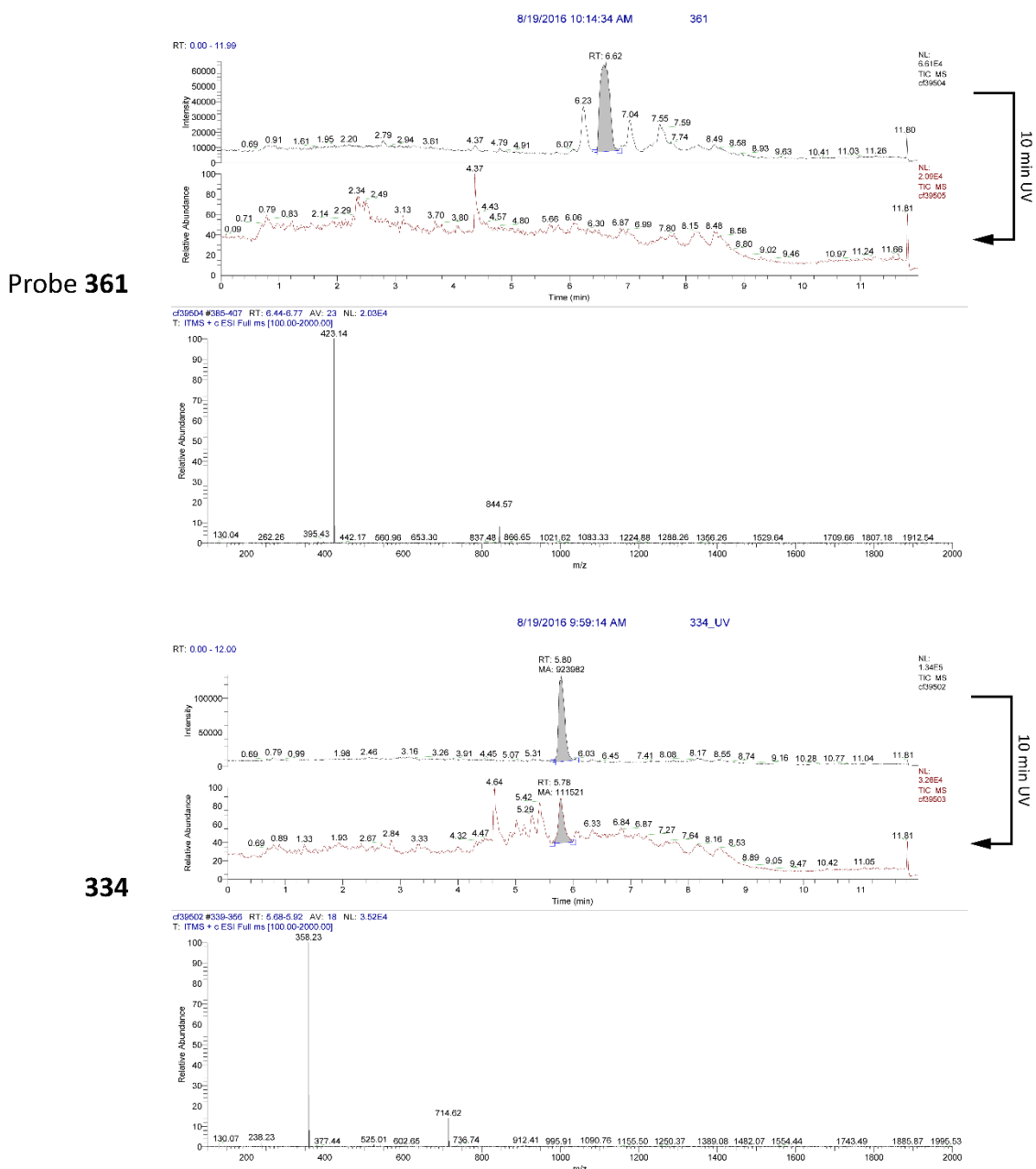
Figure 12 LC-MS data show decrease in intensity of photoprobe **361** after 10 min of UV-irradiation, however, compound **334** also shows a strong decrease of intensity suggesting UV instability (MS spectra of the respective parent compound).

In a second strategy, the focus was set on the flexible C-ring which is tolerant for alkyne introduction via amide linkage (**369**, **370**) and incorporation of a minimal diazirine-alkyne tag (**376**, Scheme 3) was performed.[140] This strategy ensures linkage of the alkyne with the target protein upon binding and irradiation regardless of decomposition. The probe again retained activity with an IC$_{50}$ of 2 μM, but no specific labeling of either ClpX or ClpXP was observed in gel-based analytical AfBPP experiments using recombinantly expressed proteins (Figure 13). For this, photoprobe **376** was incubated with either ClpP, ClpX, BSA (bovine serum albumin) or a combination of these in two

25

different buffer systems. BSA was used as background to account for (and visualize) unspecific binding. After incubation, samples were irradiated, "clicked"[141–143] to rhodamine azide and analyzed on polyacrylamide gels (SDS-PAGE). The selective **321**[132] oxazole photoprobe for ClpP was used as a positive control. In accordance to literature, **321** shows labeling when incubating it with ClpP alone but labeling vanishes upon complex formation of ClpP with chaperone ClpX.[132] Labeling of ClpP by **376** vanishes after addition of BSA indicating unspecific labeling.
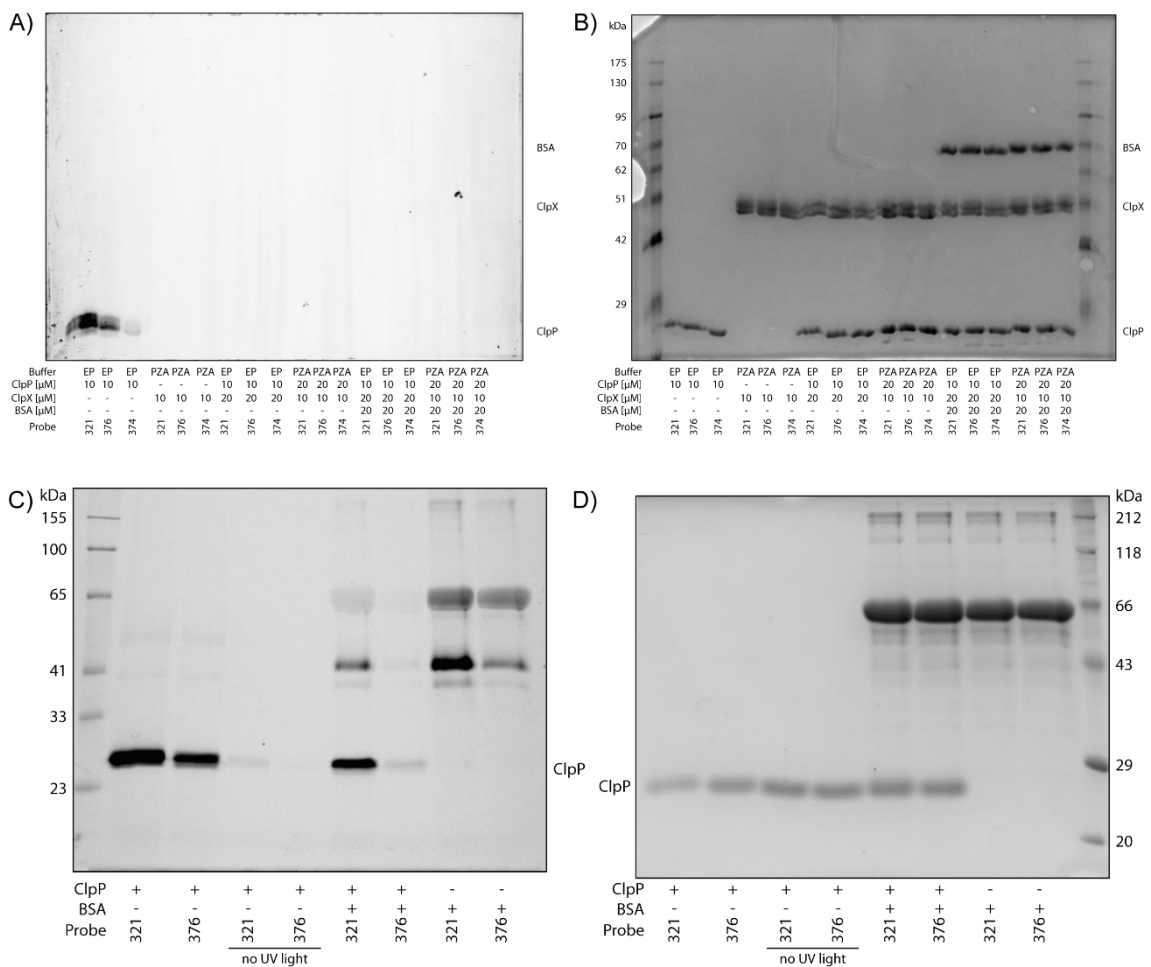
Figure 13 Analytical affinity-based protein profiling (AfBPP) labeling experiments of recombinantly expressed ClpP, ClpX and BSA using diazirine probes **374** and **376** and ClpP-specific oxazol photoprobe **321** (10 µM final concentration).[132] A) Fluorescence SDS-PAGE of labeling experiments performed in either EP buffer (100 mM Hepes, pH 7.0, 100 mM NaCl) or PZA buffer (25 mM Hepes, pH 7.6, 200 mM KCl, 5 mM MgCl$_2$, 1 mM DTT, 10% (v/v) glycerol, 4 mM ATP). B) Coomassie stained gel A. C) Fluorescence SDS-PAGE of labeling experiments performed in EP-buffer using 10 µM ClpP/BSA and 10 µM probe concentration. **376** labels ClpP unspecifically as the band vanishes upon addition of BSA. Specific labeling of ClpP by **321** remains even after addition of BSA. D) Coomassie stained gel C.

To rule out any differences in *in vitro* and *in situ* experiments, quantitative AfBPP experiments with photoprobe **376** in *S. aureus* NCTC 8325 were performed. Cells were treated: a) with either 3 µM **376** or DMSO (enrichment), b) with either 3 µM **376** or 30 µM **334** followed by 3 µM **376** (competition). Following incubation, the cells were

irradiated, lysed, "clicked" to trifunctional linker (rhodamine and biotin coupled to an azide linker) and enriched on avidin beads. Before preparation for LC-MS/MS measurement the samples were split and treated for label-free quantification or dimethyl labeling, respectively. The volcano plots of the enrichment experiments (probe vs. DMSO) show several enriched proteins with high ratios (Figure 14A and C). This is a quite common phenomenon due to unspecific binding especially when using probes with photocrosslinkers.[144] To overcome this effect a competition experiment was conducted using the parent compound **334** as the competitor. The volcano plots show a reduced amount of enriched proteins and only one protein (phosphate acyltransferase PlsX; Uniprot ID: Q2FZ55) showed enrichment in both experiments (Figure 14B and D). As expected from the *in vitro* results, neither ClpX nor ClpP were enriched in these experiments.
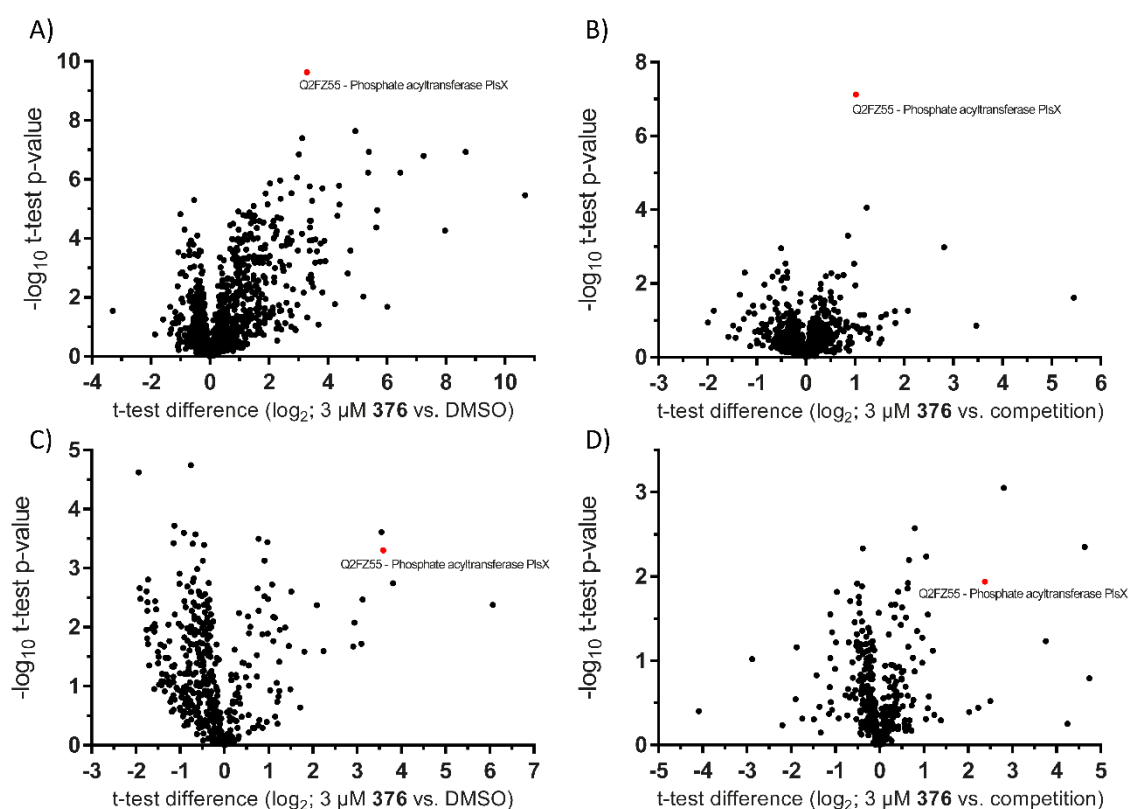
Figure 14 Volcano plot depictions of quantitative AfBPP experiments with photoprobe **376** in *S. aureus* NCTC 8325. X-axis shows log_2 enrichment and y-axis the p-value of the two sample t-test (A and B) or one sample t-test (C and D), respectively. Phosphate acyltransferase PlsX (Uniprot ID: Q2FZ55) was the only protein found both enriched in enrichment and competition experiments. All data result from four experiments. A) Cells were treated with either 3 μM **376** or DMSO. Proteins ratios were determined by label-free quantification (LFQ). B) Competition experiment (LFQ). Cells were treated with either 3 μM **376** or 30 μM **334** followed by 3 μM **376**. C) Cells were treated with either 3 μM **376** or DMSO. Proteins ratios were determined by dimethyl labeling (DML). D) Competition experiment (DML). Cells were treated with either 3 μM **376** or 30 μM **334** followed by 3 μM **376**.

Given the restrictions in rings A and B (Scheme 1) for modifications it can be hypothesized, that these are embedded in a defined binding pocket while ring C points at least partially out into bulk solvent and is thus incapable of making protein contacts with the photocrosslinker. This is supported by SAR data showing that even large substituents are well tolerated in this position. Based on the lability of the core structure, it can be concluded that development of a functional probe is, despite massive synthetic efforts, not feasible.

2.4.2. Affinity Pull-Down

As a complementary method for target validation, affinity pull-down experiments were considered. In general, the (small) molecule of interest has to be coupled to beads and incubated with cell lysate. After specific binding of the target protein all other proteins can be washed off the beads and the target protein can be eluted and further analyzed. Using this technique, several target proteins of small molecules (and proteins) were unraveled.[145–147]

Other amino acid residues often surround the binding pockets of proteins and therefore it is necessary to insert a linker between the small molecule and the beads to facilitate protein-molecule interactions. Hence, the alkyne bearing compound **369** was coupled by "click reaction" to a modified biotin-PEG8-azide linker (Scheme 4) allowing strong (non-covalent) coupling to avidin agarose beads. The resulting biotinylated compound **371** (IC_{50} = 27 µM; 78% inhibition) showed a significant drop in potency against the ClpXP protease when compared to the parent compound **369** (IC_{50} = 1 µM; 100% inhibition).
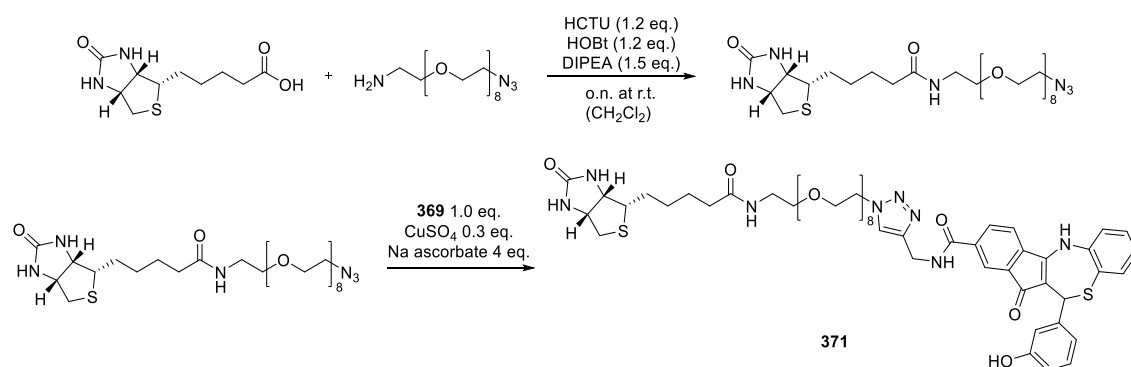
Scheme 4 Synthesis of probe **371** for affinity pull-down experiments.

To account for unspecific protein binding to the beads (and linker) a competitive experimental approach was implemented. Lysates of *S. aureus* NCTC 8325 were

incubated with avidin beads, 10 µM (or 30 µM) **371** and either DMSO or 100 µM **334**. After incubation, beads were washed with PBS and proteins either eluted in Laemmli buffer (for SDS-PAGE) or directly processed for quantitative LC-MS/MS measurements by dimethyl labeling. Gel-based analysis showed no differences between **371** and competition samples (Figure 15A). Quantitative analysis resulted in few enriched proteins, however, due to the low number of replicates only limited information can be obtained (Figure 15B). In this experiment, neither ClpX nor ClpP could be identified.

For affinity pull-down experiments, the chances of success strongly depend on the mechanism of action of **334**. Binding of this molecule leads to the disruption of ClpX hexamer to dimeric/trimeric species. However, nothing is known about the affinity of **334** to hexameric or smaller species, respectively. If the affinity of **334** to smaller ClpX species is reduced, affinity pull-down experiments are not feasible as high affinities are essential.
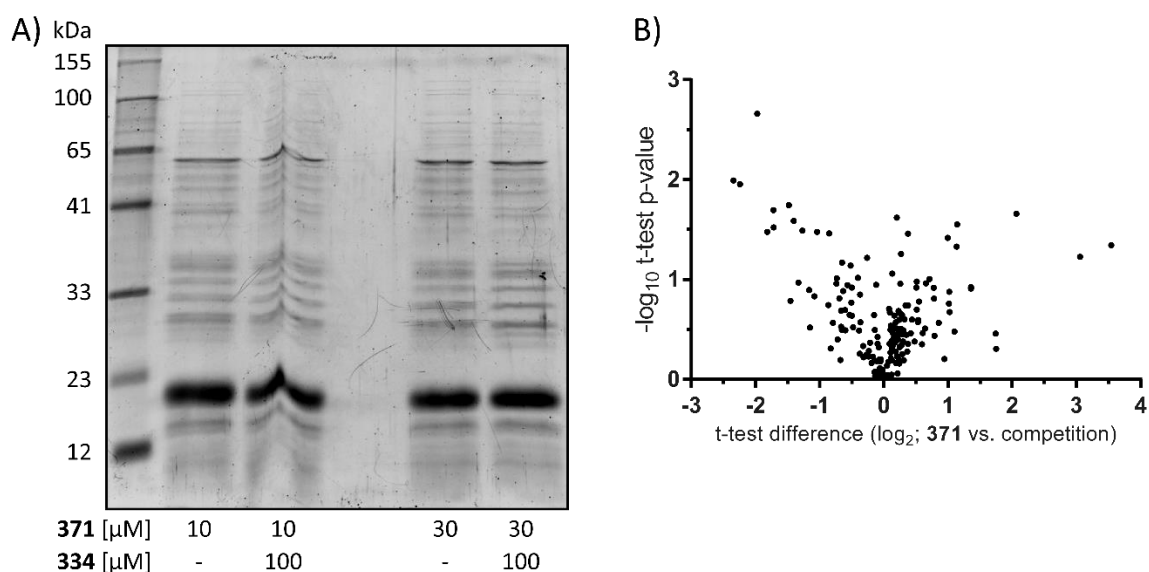
Figure 15 Affinity pull-down experiments with biotinylated compound **371** in *S. aureus* NCTC 8325 lysate. A) Gel-based analysis of two sets of experiments. Lysate with 10 µM (or 30 µM) **371** were incubated with either DMSO or 100 µM **334** as a competitor. Beads were washed, proteins eluted in Laemmli buffer, analyzed by SDS-PAGE and stained with coomassie. B) Initial quantitative pull-down experiment (DML). Combined analysis of 10 µM and 30 µM **371** versus the respective competition (100 µM **334**) experiment (2 replicates each). X-axis shows $\log_2$ enrichment and y-axis the p-value of the one sample t-test.

2.5.   Phenotypic Effects

Seminal studies by Frees *et al.* already demonstrated a global reduction of toxin secretion in a *S. aureus clpX* knockout strain.[93] One predominant trait of *S. aureus*

virulence is the secretion of hemolysins. Thus, *S. aureus* was treated with various concentrations of **334** overnight and the bacterial supernatants were sterile filtered and applied to agar plates containing sheep erythrocytes to assess the level of hemolysin production. As expected, a concentration dependent reduction of hemolysis activity with an IC_{50} of approximately 3 μM was observed (Figure 17A). Alternatively, *S. aureus* was grown in presence of different amounts of **334** directly on sheep-blood agar (Figure 17A). Moreover, overall proteolysis, an additional hallmark of staphylococcal virulence, was significantly reduced when growing *S. aureus* in presence of **334** on agar plates containing skimmed milk (Figure 16).

| 300 nmol | 90 nmol | 30 nmol | 9 nmol | 3 nmol | DMSO |
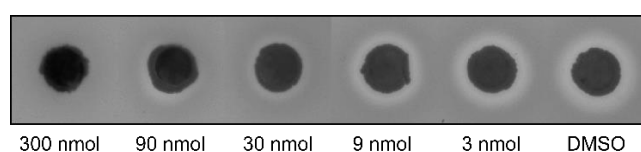
Figure 16 Inhibition of extracellular proteolysis activity after treatment of *S. aureus* NCTC 8325 with different amounts of **334**. Diluted cells (3 μL) and different concentrations of **334** (3 μL) were pipetted on small paper filters on LB agar plates containing skimmed milk.

To globally monitor the expression of virulence proteins that are affected by **334**, a MS-based whole secretome analysis platform was established. *S. aureus* NCTC 8325 as well as MRSA strain USA300 were incubated overnight in the presence of 10 μM **334** or DMSO. The bacterial supernatant was collected, proteins precipitated, tryptically digested and peptides modified by dimethyl labeling for quantitative analysis. Importantly, the visualization of **334**/DMSO protein ratios of NCTC 8325 and MRSA in the respective volcano plots shows a dramatic and global down-regulation of major virulence factors including toxins (hemolysins alpha and gamma, leukotoxin) and diverse proteases (serine proteases A-F, staphopain) upon compound treatment (Figure 17B). In addition, the novel MS-based virulence assay allowed the individual determination of IC_{50} values for each detected toxin. For this purpose, LC-MS/MS analysis was performed via label-free quantification (LFQ)[148] at various **334** concentrations and the corresponding toxin secretion was determined. All IC_{50} values are in the low μM range corroborating the results of the hemolysis assay (Figure 17C).

To gain more detailed insights into the inhibitory activity of **334,** changes in global gene expression of *S. aureus* induced by treatment with **334** were analyzed using RNA-Seq. Strikingly, the reduced expression of genes encoding toxins (*hla*, *hlgA/B/C*, *hld*, *lukS*) and the proteases (*aur*) matched the secretome data (Figure 17D) and are in accordance

with previous studies reporting reduced extracellular virulence factor expression in absence of ClpX.[93] Notably, **334** treatment had a remarkable impact on the expression of important regulatory systems such as RNAIII, Sae, and TRAP, which control the expression of a large number of virulence factors including several toxins and adhesins (Figure 17D). The secretome and transcriptome data demonstrate the significant impact of **334** on *S. aureus* expression and production of virulence factors.
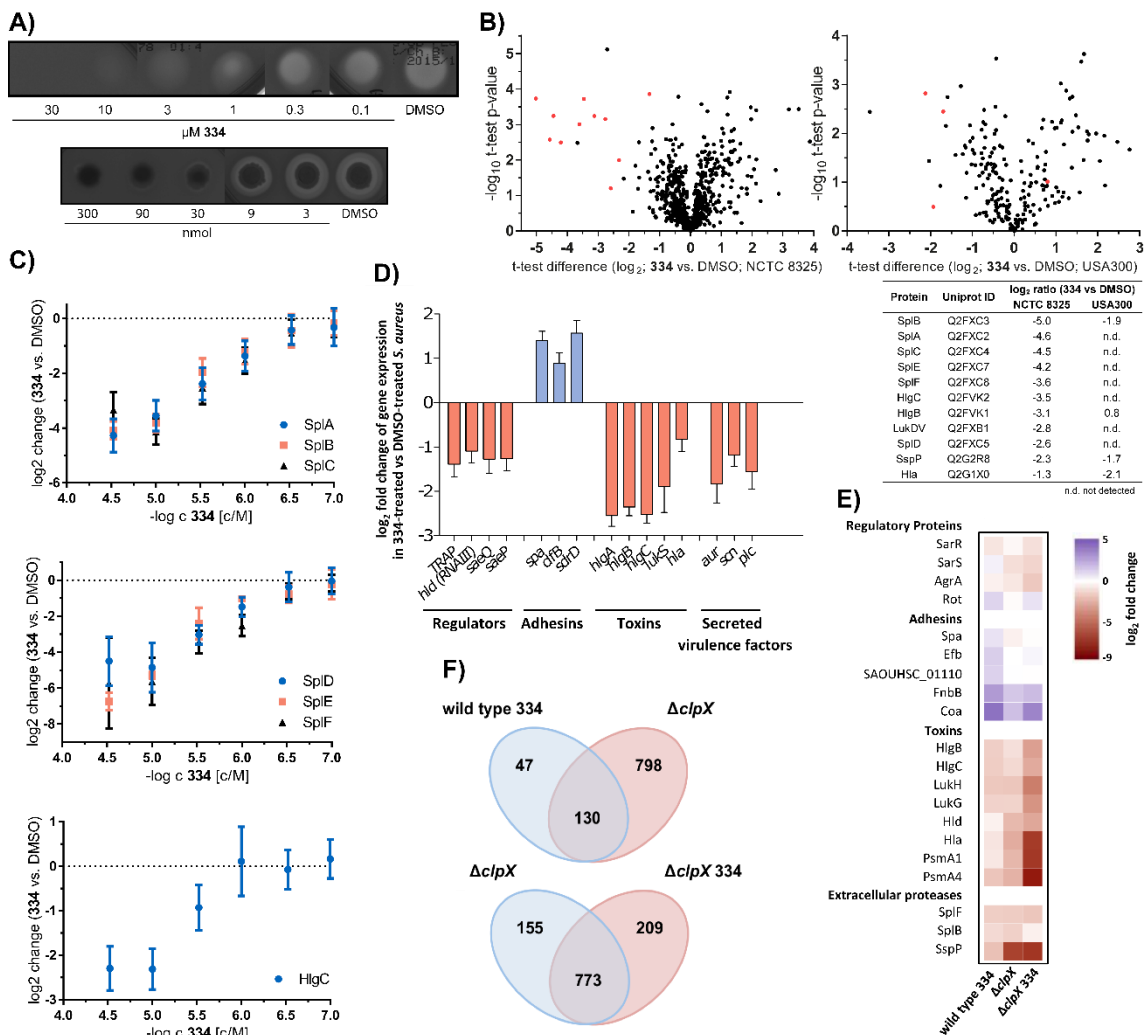
Figure 17 Treatment with **334** reduces the transcription and synthesis of toxins and proteases by *S. aureus*. A) Supernatants of *S. aureus* treated with different concentrations of **334** show reduced hemolysis on sheep-blood agar (top). *S. aureus* treated and grown with different amounts of **334** show dose-depenent hemolysis on sheep-blood agar (bottom). B) Secretome analysis of **334** (10 µM) treated *S. aureus* NCTC 8325 and USA300 reveals lower levels of secreted toxins in comparison to DMSO-treated cells. Red dots in volcano plots represent toxins listed in table. C) Titration of **334** in MS experiments leads to concentration dependent LFQ detection of toxin abundances in NCTC 8325. Data resulted from three experiments (mean ± standard deviation). D) Changes in the expression levels of selected genes encoding virulence factors or regulators by *S. aureus* wild-type strain in response to **334** treatment. Presented data result from three independent experiments and are shown as mean value ± standard error. E) Heatmap showing the changes in protein abundance induced by **334** treatment in wild-type *S. aureus* in comparison with DMSO control (left lane), Δ*clpX* in comparison with *S. aureus* in DMSO control (middle lane) and **334**-treated Δ*clpX* compared to *S. aureus* in DMSO control (right lane). A red-blue color scale depicts protein expression levels (blue: high, red: low). F) Venn diagram showing the numbers of proteins with changes in abundance that are shared or unique between **334**-treated *S. aureus* wild-type and *S. aureus* Δ*clpX*, or between DMSO-treated *S. aureus* Δ*clpX* and **334**-treated *S. aureus* Δ*clpX*.

To determine, if this effect was mediated by the **334**-targeting of ClpX, whole proteome analysis was performed on *S. aureus* wild-type strain after treatment with **334** or DMSO as well as on a *S. aureus* ClpX knock out (Δ*clpX*)[93] after incubation with **334** or DMSO. Treatment of wild-type *S. aureus* with **334** resulted in reduced expression of extracellular toxins and proteases and in an increased production of adhesins (Figure 17E). The effect of **334** on the level of virulence factor expression was largely comparable to that observed after genetic deletion of ClpX (Figure 17E). Therefore, the significant overlap of 130 proteins with changes in overall abundance (of which 84 are regulated in the same direction) induced by **334** with those induced by the genetic deletion of ClpX suggested, at least in part, an inhibitory effect on ClpX (Figure 17). Interestingly, **334** also significantly affected the expression of virulence factors and other proteins in the Δ*clpX* mutant strain (Figure 17E and F). These findings indicate that **334** could address additional targets that further enhance the inhibitory effect on the production of extracellular virulence factors by ClpX.

3. Summary and Outlook

In this work, a high-throughput screen against the *Staphylococcus aureus* ClpXP protease revealed a set of six potent small molecule inhibitors. Intriguingly, none of these compounds inhibited ClpP peptidase indicating a novel mechanism of action. Two compounds were shown to exhibit activity against the chaperone ClpX, which is unprecedented in literature. Experiments showed that this non-covalent inhibition is specific for the ClpX chaperone and is caused by disruption of the hexameric super-structure. Structure-activity relationship studies with various synthesized compounds point to specific embedment of two aromatic core moieties into protein binding pockets, however, some flexibility on the third aromatic moiety was identified. Probes for affinity pull-down experiments as well as photo-AfBPP experiments were designed. However, SAR restrictions and the potential binding mode rendered these experiments unsuccessful.

Global transcriptome and proteome analysis indicated targeting of ClpXP also in living cells. Accordingly, a reduction of virulence expression was detected via classical assays and more comprehensively with a mass spectrometry platform allowing reliable *in situ*

toxin monitoring. Given the susceptibility of the Δ*clpX* mutant strain towards **334** it is very likely that other cellular virulence pathways may be directly or indirectly addressed. This opens an intriguing perspective of a multifaceted virulence reduction effective also for MRSA strains.

Due to the restrictions of **334** and its corresponding derivatives for application in chemical proteomics, assessing the direct effect of the compound on key regulators within the agr system will constitute the most straightforward way for the identification of these putative targets in future studies.

Chapter II – Small Molecule Inhibition of the *Staphylococcus aureus* ClpXP Complex

1. Introduction

In Chapter I, an HTS against the complete ClpXP protease complex of *S. aureus* was conducted. While the screen identified dihydrothiazepines as potent inhibitors of ClpXP through unprecedented inhibition of chaperone ClpX, it also revealed a second compound class with a new mode of action. Even though this compound class inhibited the whole ClpXP complex, it inhibited neither ClpP peptidase activity, nor ClpX ATPase activity, alone.

2. Results and Discussion

Realization of the HTS described in Chapter I commenced with an establishment phase. The utilized fluorescence assay monitoring the degradation of a SsrA-tagged GFP substrate by ClpXP had to be optimized for the use of 384-well plates and a total measurement time of 20 min. After successful validation (Z-factor) a pre-screen with 1760 compounds (on five 384-well plates) was conducted to corroborate robust assay conditions. This pre-screen revealed one compound (**320**) leading to a complete inhibition of the ClpXP system at a concentration of 10 µM. This compound was chosen for further investigation prior to implementation of the entire HTS (Figure 18).
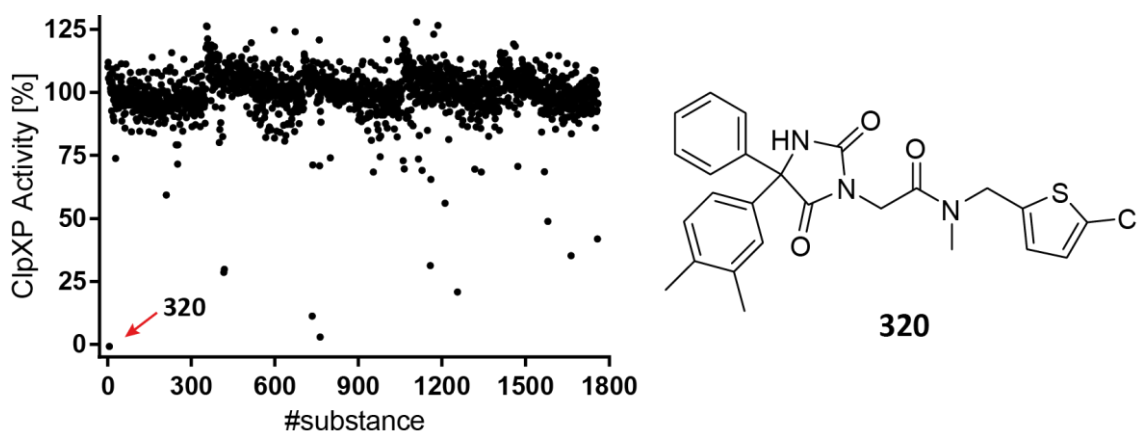
Figure 18 Pre-screen of 1760 compounds using the established 384-well format ClpXP assay (10 µM final compound concentration) reveals **320** as a potent inhibitor.

2.1. *In vitro* Characterization

Ahead of any further investigation of the mode of action of this compound class, compound **320** was tested in a secondary assay against creatine kinase. This kinase is

required in the GFP degradation assay to retransform ADP into ATP, enabling constant substrate degradation by ClpXP. Creatine kinase activity was measured using the commercially available Kinase-Glo® Luminescent Kinase kit (Promega), in the presence or absence of 30 µM **320** and an enzyme concentration similar to the screening conditions. No significant difference was observed between the **320** and DMSO-treated samples, indicating actual inhibition of ClpXP (Figure 19A).
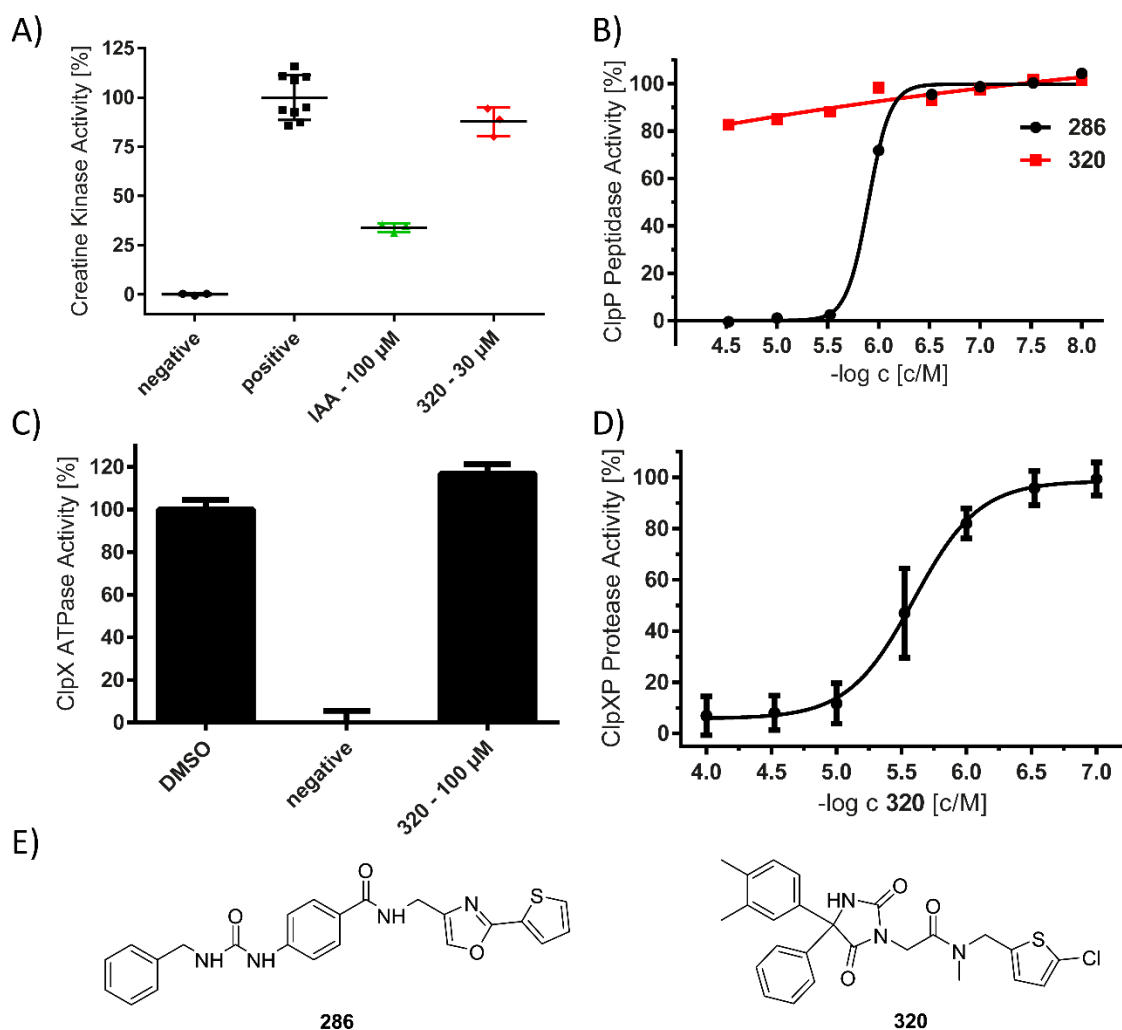
Figure 19 Influence of compound **320** on creatine kinase, ClpP, ClpX and ClpXP activity. A) Creatine kinase activity remains unchanged after addition of **320**. Iodoacetamide (IAA) was used as a positive control for inhibition (mean ± standard deviation). B) **320** does not alter ClpP peptidase activity in a fluorescent assay (1 µM ClpP; mean ± standard error). The non-covalent ClpP inhibitor **286** was used as a positive control.[132] C) ClpX ATPase activity assay is not inhibited by **320** (100 µM final compound concentration; mean ± standard deviation). D) **320** shows a dose-dependent inhibition of the ClpXP protease. (mean ± standard error). E) Chemical structures of ClpP inhibitor **286** and ClpXP inhibitor **320**.

Furthermore, ClpP peptidase activity was not significantly altered up to a concentration of 30 µM (Figure 19B). What's more, **320** did not inhibit ClpX ATPase activity up to 100 µM compound concentration (Figure 19C). Interestingly, repetition of the ClpXP protease assay under non-HTS conditions revealed very potent inhibition by **320** with an

IC_{50} of 2.5 µM (Figure 19D). This is an unexpected result as the majority of known ClpXP modulating compounds either 1) target ClpP, either at the active site or in case of ADEPs at the axial pores, or 2) target the corresponding chaperone ClpX as introduced in Chapter I.[97,122,128,131,132,124] Although similar behavior was observed for small cyclic peptides, it was not yet possible to completely unravel the exact mechanism of action.[119]

Thermal-shift assays with 10 µM ClpX in either the presence or absence of 60 µM **320** did not reveal any striking differences in melting temperatures. Intriguingly, when ClpP
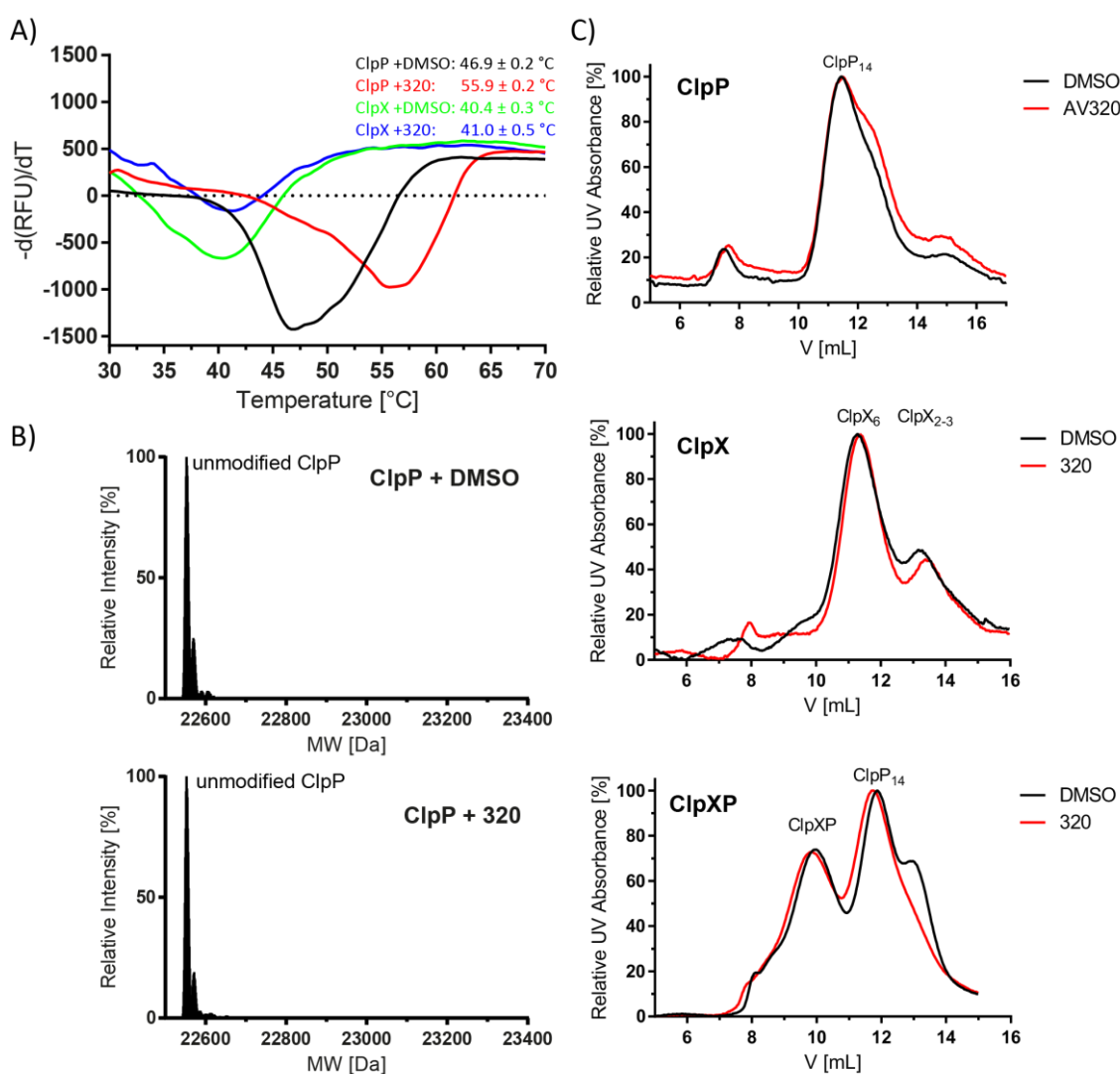
Figure 20 Interaction of **320** with ClpP and ClpX. A) Thermal-shift assay depicts strong 9 K stabilization of ClpP while the melting point of ClpX remains unaltered. Experiments were conducted with 10 µM enzyme concentration in PBS buffer and DMSO or 60 µM of **320**. B) No covalent modifications of ClpX are detectable by intact-protein mass spectrometry upon treatment with **320** at 100 µM (100-fold excess). C) Size-exclusion chromatography experiments show no substantial change of ClpP-tetradecamer, ClpX-hexamer and ClpXP-complex upon treatment with 100 µM **320**.

(10 µM) was examined either with or without **320** (60 µM) in thermal-shift assays, a strong stabilization indicated by a shift in melting temperature of 9 K (Figure 20A) was

observed. Despite the fact that this finding generally points towards binding to ClpP, no covalent modifications of ClpP by **320** were observed in intact-protein mass spectrometry experiments (Figure 20B). As the compound does not contain any obvious electrophilic positions, this supports a non-covalent inhibition mode. Analytical size-exclusion chromatography experiments in either the absence or presence of **320** revealed a disruption of neither the ClpP-tetradecamer, nor the ClpX-hexamer (Figure 20C). Likewise, when the ClpXP complex was incubated with **320**, no significant changes were observed in comparison with DMSO-treated samples (Figure 20C).

The information gained by the aforementioned findings suggests that inhibition of the ClpXP protease is induced by binding of **320** to ClpP, yet not into the active site as ClpP activity is still preserved. The exact mechanism of action remains unknown and calls for further studies to completely understand these intriguing discoveries.

2.2. Structure-Activity Relationship Studies

In order to gain insight into the basic structure-activity relationship, a small library of nine compounds was established. Compounds were either commercially available or synthesized. Chemical variations in all three moieties (Scheme 5) of **320** were examined.
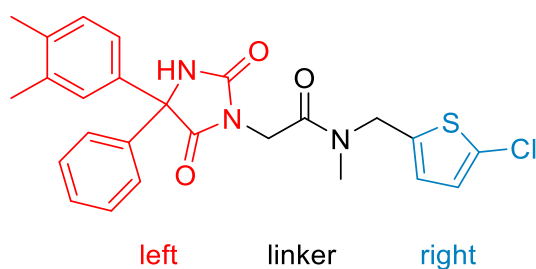
Scheme 5 Chemical structure of the **320** compound class.

Changing the right section of the molecule from a 2-chlorothiophene substituent to a phenyl group (**329**) resulted in a tenfold lower IC_{50} value in the ClpXP protease assay. Propylation (**333**) instead of methylation (**330**) of the nitrogen located in the linker almost completely prevented inhibition. However, shortening of the linker and removal of the nitrogen (**332**) still retained some activity, although only incomplete inhibition was obtained. Substitution of a phenyl group by a methyl substituent left of the core structure (**327**) resulted in a 40-fold drop in potency. This suggests that sterically demanding groups are necessary for potent inhibition. Hence, the role of additional

methyl substituted phenyl groups was further elucidated. Disubstituted compound **320** showed the highest potency with an IC$_{50}$ of 1.9 µM. Compound **331**, bearing two equally methyl substituted phenyl moieties, showed complete loss of activity. This result substantiates the suspicion that only one enantiomer of **320** is binding to ClpP. Consequently, enantiomers were separated by chiral high-performance liquid chromatography and individually tested in the ClpXP protease assay. As expected, only one enantiomer (**320**-E1) showed inhibition, while the other enantiomer (**320**-E2) was completely inactive (Figure 21B). Unfortunately, the absolute configuration could not be determined.
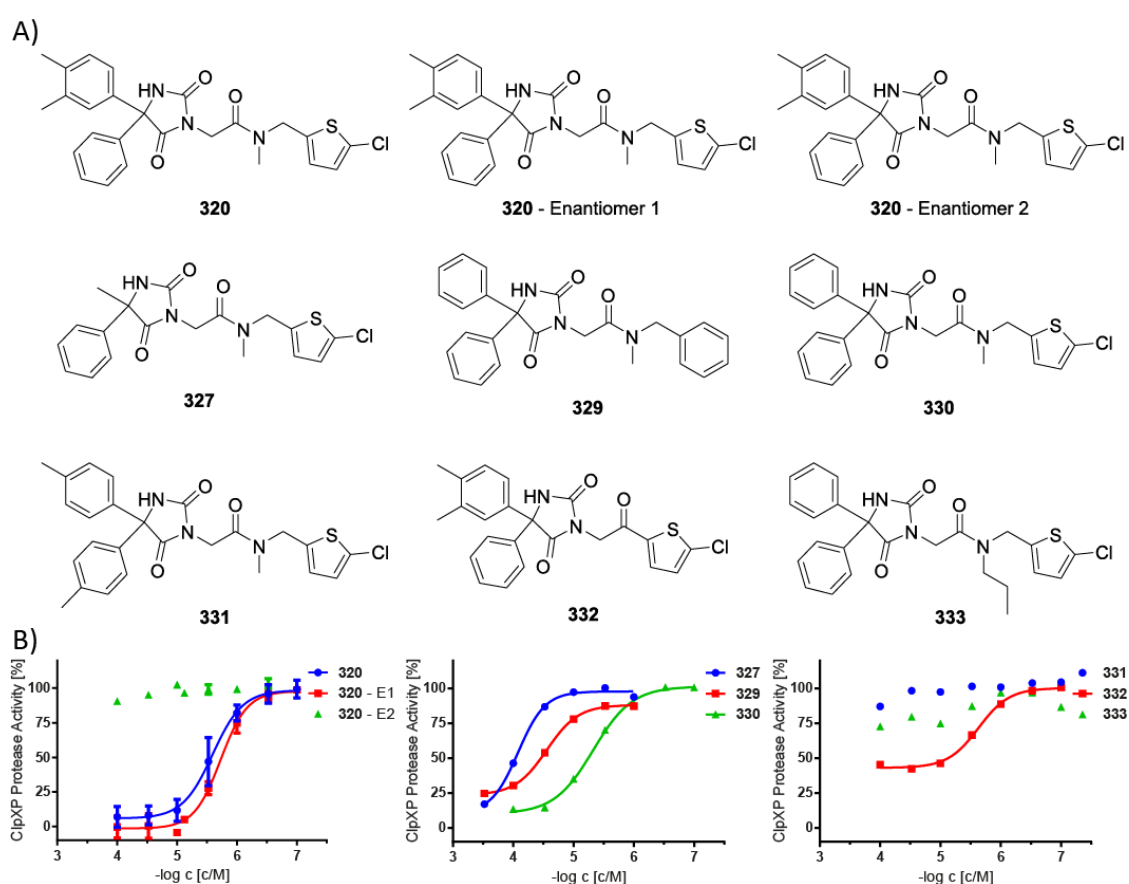
Figure 21 Structure-activity relationship studies of **320** analogues in ClpXP-protease assay. A) Chemical structures of **320** analogues. Enantiomers **320**-E1 and **320**-E2 were separated from the racemic mixture by chiral high-performance liquid chromatography using a Daicel Chiralpak AD-H (250 × 4.6 mm) column. The absolute configuration is unknown. B) Inhibition data of all compounds in the ClpXP protease assay.

2.3. Effects on Production of α-Hemolysin

The pore forming toxin α-hemolysin (Hla) is a highly important virulence factor of *S. aureus.* In order to determine whether **320** has an effect on the production of this toxin,

a hemolysis assay was performed. Accordingly, *S. aureus* NCTC 8325 was grown with different concentrations of **320** for 20 h. After incubation, the supernatants were removed, mixed with a sheep erythrocyte suspension and absorbance was measured using a multiplate reader. DMSO-treated samples showed rapid lysis of red blood cells, whereas **320** treated samples exhibited a dose-dependent inhibition of lysis (Figure 22). However, the magnitude of this effect strongly depended on the time point of the measurement. With increasing time (over approx. 30 min), the inhibition plateau decreased to 0% (depicted in Figure 22). This effect presumably arises from incomplete inhibition of hemolysins and therefore slower lysis kinetics.
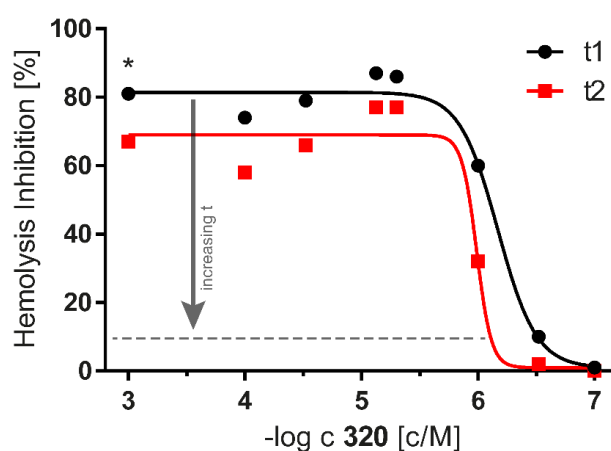
Figure 22 Hemolysis assay using *S. aureus* NCTC 8325 supernatants with sheep erythrocytes after incubation with **320** overnight. Graph shows measurement of erythrocyte integrity at two different time points t1 and t2. With increasing time the inhibition plateau decreases. * concentration at which growth reduction of *S. aureus* cells was observed.

In order to further validate hemolysis reduction, western blot analysis was performed. Cultures of *S. aureus* NCTC 8325 were grown in presence or absence of **320** for 20 h. Supernatants were collected and analyzed by SDS-PAGE and subsequently, western blot analysis with an anti-Hla antibody was conducted (Figure 23). The experiment brought to light a slightly dose-dependent reduction of Hla with increasing **320** concentrations. No complete inhibition of Hla production was observed. Testing of **320**-E1 and **320**-E2 in the same setup exhibited enantiomer-specific reduction of Hla by **320**-E2 (Figure 23). This result distinctly contradicts the enantiomer-specific inhibition of the recombinant ClpXP protease by the opposite enantiomer (Figure 21B). Consequently, the observed reduction of Hla does not seem to be mediated by ClpXP in this case, but rather by another unknown target. Further studies are necessary in order to ascertain 1) whether

320-E1 is able to inhibit ClpXP *in vivo* and 2) which other targets are addressed by **320**-E2.
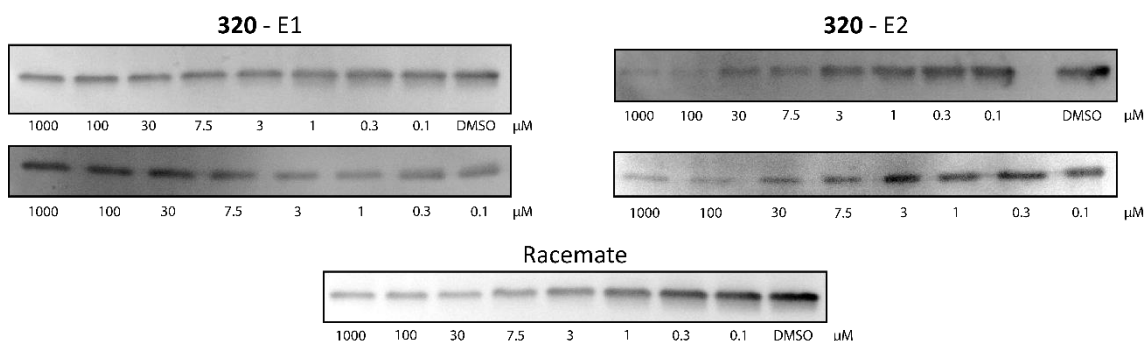
Figure 23 Western blot of α-hemolysin in supernatants of *S. aureus* NCTC 8325 grown in presence or absence of **320** racemate or the single enantiomers **320**-E1 and **320**-E2 (two replicates).

3. Summary and Outlook

In preparation for a complete HTS against the *S. aureus* ClpXP protease machinery, a pre-screen with a subset of 1760 compounds was performed. This small screen revealed compound **320** as a potent inhibitor. Impressively, **320** inhibited neither the sole ClpP peptidase, nor the ClpX ATPase activity, nor the creatine kinase required for the ClpXP protease assay. Thermal-shift assays showed a strong stabilization of ClpP upon incubation with **320** resulting from a non-covalent interaction. Size-exclusion chromatography experiments showed no significant changes compared to DMSO-treated samples, indicating no substantial effect on protein-protein interactions.

Initial SAR studies pointed towards the need for sterically demanding groups on the left of the molecular scaffold. Variations in the aromatic substitution pattern indicated the preference of a single enantiomer for ClpXP inhibition. Separation of the racemate by chiral high-performance liquid chromatography and applying single enantiomers in the ClpXP protease assay confirmed this assumption.

Treating *S. aureus* with **320** led to slightly reduced Hla abundance in supernatants. The equivalent setup with single enantiomers disclosed the fact that only one enantiomer inhibited Hla expression, albeit not the one inhibiting ClpXP protease activity.

Considering this discrepancy, **320** is not suitable for further development as a ClpXP based anti-virulence agent. Regardless, the intriguing mode of action of these molecules renders this compound class attractive for mechanistic studies and target identification.

Chapter III – Genetic Modifications of the *clpP* Gene in *Staphylococcus aureus*

1. Introduction

The aim of this work was to examine the influence of two chromosomal point mutations S98A and R171A on living *S. aureus* cells. The S98A active site mutant mimics a *clpP* deletion mutant but protein-protein interactions of ClpP to other proteins still remain possible. In order to investigate the influence of heptameric ClpP on *S. aureus*, the R171A mutation was selected for this study. Furthermore, the construction of a markerless *clpP* deletion mutant enabled direct comparison to the generated point mutants, eliminating possible secondary effects of selective antibiotics on *S. aureus*.

Allelic replacement of the modified *clpP* gene was achieved using the shuttle plasmid pMAD derived from pE194[ts]::pBR322 and initially constructed by Arnaud *et al.*[149] The 9666 bp pMAD plasmid contains the thermosensitive pE194 replication origin, *bla* and *ermC* resistance genes, allowing for selection with either ampicillin or erythromycin and the β-galactosidase encoding gene *bgaB*, enabling convenient blue/white screen of colonies. DNA can be introduced at the multiple cloning site by classical cloning. The pMAD shuttle vector has been extensively used for many years for the introduction of markerless deletion mutants, such as *ΔsarA* and *Δagr*, or very recently for the development of CRISPR/Cas9 antimicrobials.[149–151]

2. Results and Discussion

2.1. Cloning of *clpP*-Shuttle Vectors

At the project's initiation, a strategy for the construction of point mutations in the *clpP* gene and the corresponding deletion thereof was mapped out. The two plasmids pIMAY and pMAD developed by Monk *et al.* and Arnaud *et al.*, respectively, were chosen for allelic replacement in gram-positive *S. aureus*.[149,152,153] Initial cloning was performed in the pIMAY vector. For the following procedures, the system was then changed to pMAD, as this plasmid allowed for convenient blue-white screening mediated by β-galactosidase (BgaB).

Construction of a vector bearing point mutations of clpP

Prior to the generation of point mutations, the wt *clpP* gene of *S. aureus* NCTC 8325 was cloned into the pIMAY vector (Figure 24). Primers were designed to yield a PCR product with the *clpP* gene and around 900 bp of each up and downstream region. The PCR

product was digested at the introduced *SmaI* and *SacI* restriction sites, dephosphorylated and ligated with empty pIMAY vector linearized with the same restriction enzymes. The ligated product was subsequently transformed into *E.coli* TOP10 cells and the right insert confirmed by analytical restriction digest and sequencing. The point mutations S98A and R171A were inserted using site-directed mutagenesis and the pIMAY clpP wt vector as a template in the PCR. Template DNA was digested with DpnI and the remaining DNA transformed into *E. coli* XL1Blue cells. Plasmids were extracted and the correct mutations confirmed by sequencing. In order to change from the pIMAY system to the pMAD vector, another PCR was performed with pIMAY vectors as templates and primers bearing *BamHI* restriction sites. The product was dephosphorylated and ligated into linearized pMAD (cut with BamHI). This allowed insertion of the PCR product in two different directions, allowing for maximum flexibility for the following cloning steps. The resulting, confirmed pMAD clpP S98A/R171A plasmids were finally transformed into *E. coli* SA08B[154] and ready for electroporation into *S. aureus*.
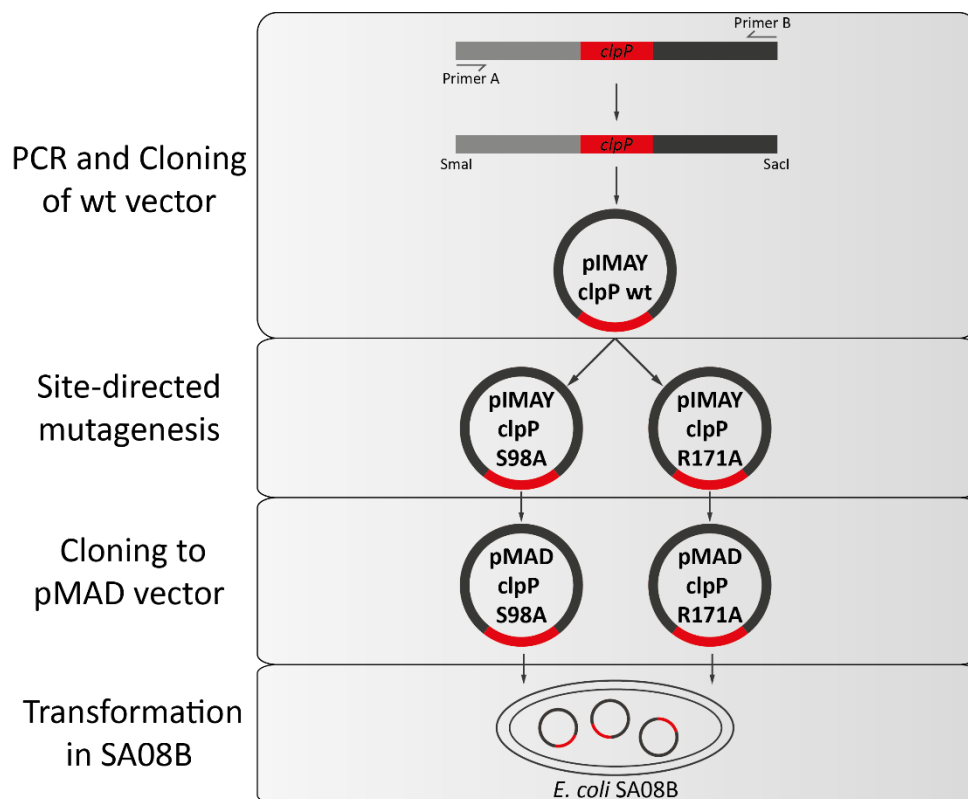
Figure 24 Cloning strategy for the generation of shuttle vectors bearing point mutations in the *clpP* gene. A pIMAY *clpP* wt vector was constructed by PCR and subsequent ligation. After insertion of the desired point mutations via site-directed mutagenesis, the insert was transferred into the pMAD vector and finally transformed into *E. coli* SA08B.

Construction of a vector for clpP deletion

For the generation of a *clpP* deletion vector, overlap extension PCR (OE-PCR)[155] was utilized as the key step (Figure 25). Four primers A-D were designed to obtain an upstream-downstream fusion product (approx. 2000 bp) in which only the fused start/stop codon (ATGTAA) of the *clpP* gene remained. Primers A (upstream) and D (downstream) contained *KpnI* and *SacI* restriction sites, respectively, for subsequent ligation of the final PCR product. Primers B and C were located either at the beginning or the end of *clpP* and contained either the start or stop codon, respectively. Additionally, primer C contained the reverse complement sequence of primer B allowing for fusion by OE-PCR. In a primary PCR, AB and CD fragments were generated, cleaned and used as templates in the following PCR. The second PCR was split into two parts: 1) 15 cycles of the PCR were conducted with fragments AB and CD but without any primers. This step ensured formation of complete ABCD fragments. 2) Primers A and D were added and the PCR was continued for 24 cycles. This step facilitated amplification of ABCD fragments. After clean-up, the product was digested with KpnI and SacI, dephosphorylated and ligated into pIMAY cut with the same restriction enzymes. The ligation product was subsequently transformed into *E. coli* TOP10 cells. The correct insertion was confirmed by analytical restriction digest and sequencing. In order to transfer the *clpP* deletion into the pMAD vector, the pIMAY *ΔclpP* construct was used as a template in a PCR reaction with primers encompassing the 2000 bp insert. As both primers were containing *BamHI* restriction sites, the PCR product was digested, dephosphorylated and ligated into linearized pMAD (also BamHI treated). After transformation into *E. coli* SA08B correct pMAD *ΔclpP* constructs were confirmed by analytical restriction digest and sequencing.
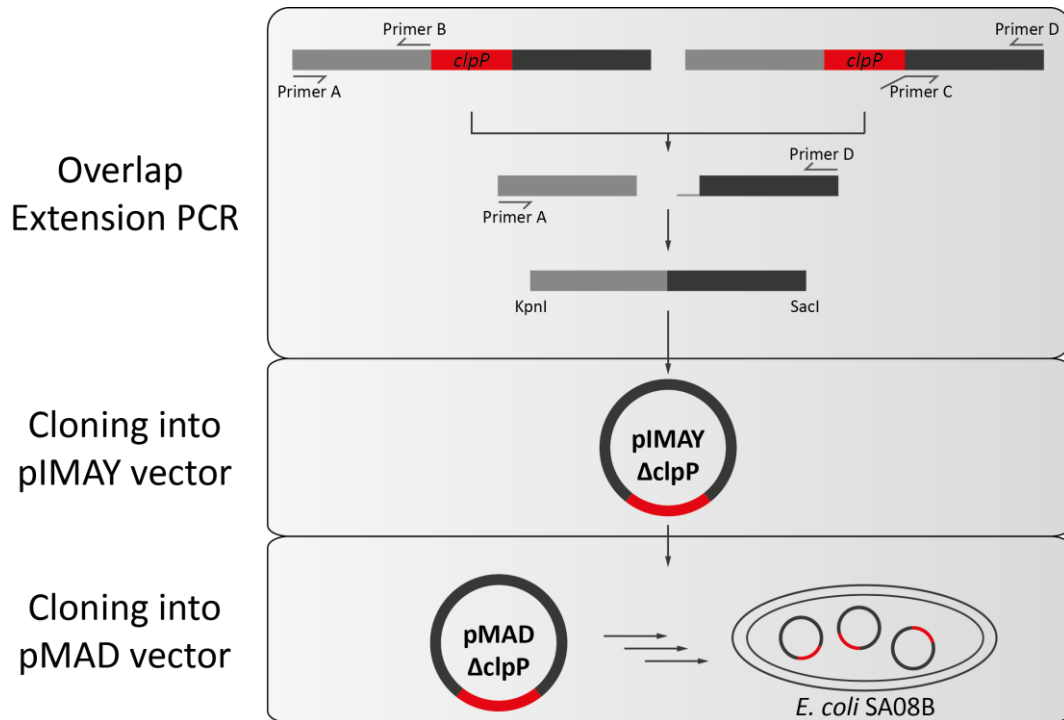
Figure 25 Cloning strategy for the generation of a shuttle vector without the *clpP* gene. *ClpP* was removed in two steps using overlap extension PCR (OE-PCR) and cloned into pIMAY. Insertion into pMAD was achieved by another PCR reaction using pIMAY *ΔclpP* as a template, following digestion, ligation and transformation into *E. coli* SA08B.

2.2. Generation and Selection of Genetically Modified *S. aureus*

Staphylococcus aureus possesses diverse restriction barriers which often prevent direct transformation of exogenous DNA, especially when originating from *E. coli*.[152,156,157] As a result, *S. aureus* strain RN4220, lacking most of these restriction mechanisms, is often used as an intermediate host.[158]

As high DNA concentrations are crucial for satisfactory transformation efficiencies, sufficient amounts of pMAD plasmid (*ΔclpP*, S98A and R171A) were extracted from *E. coli* SA08B and, if necessary, further concentrated. Electrocompetent *S. aureus* RN4220 was briefly incubated with 1000-5000 ng of plasmid, transferred into electroporation cuvettes and quickly electroporated. After incubation in freshly added rich medium, cells were streaked onto agar plates containing antibiotic and X-gal, then subsequently incubated until colonies formed. Blue colonies, indicating presence of pMAD, were grown for subsequent plasmid extraction using a modified protocol for gram-positive bacteria. The electroporation protocol was repeated using plasmid from RN4220 and electrocompetent *S. aureus* NCTC 8325 cells. Blue colonies were isolated and subjected to an elaborate selection protocol (Figure 26; details in experimental section).
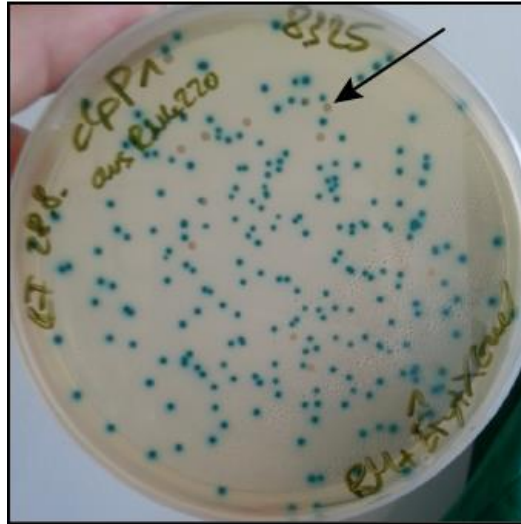
Figure 26 Cleavage of X-gal by β-galactosidase leads to formation of a blue product. X-gal is incorporated into agar and is cleaved if colonies contain pMAD carrying the *bgaB* gene. White colonies (black arrow) imply unsuccessful transformation.

Firstly, integration of the plasmid into the genome was achieved by incubation at different temperatures and the presence or absence of antibiotic. Secondly, after selection of colonies with single crossovers, another selection step with varying temperatures was performed. The resulting white colonies (plasmid loss) were subsequently screened for loss of antibiotic resistance and presence of the desired mutation (Figure 27A).

The first step of the validation screen was based on colony PCR with subsequent analytical restriction digest experiments. For *clpP* deletion mutants, a 588 bp loss pointed towards a successful removal of the *clpP* gene (Figure 27B). As the point mutations S98A and R171A did not differ in sequence length from the wt gene, an alternative approach was used. Luckily, the introduction of S98A and R171A created *BsrDI* and *AlwNI* restriction sites, respectively (Figure 27C-E). The distinctive restriction patterns revealed possible positive clones, which were further assessed by sequencing for presence of the desired mutations.
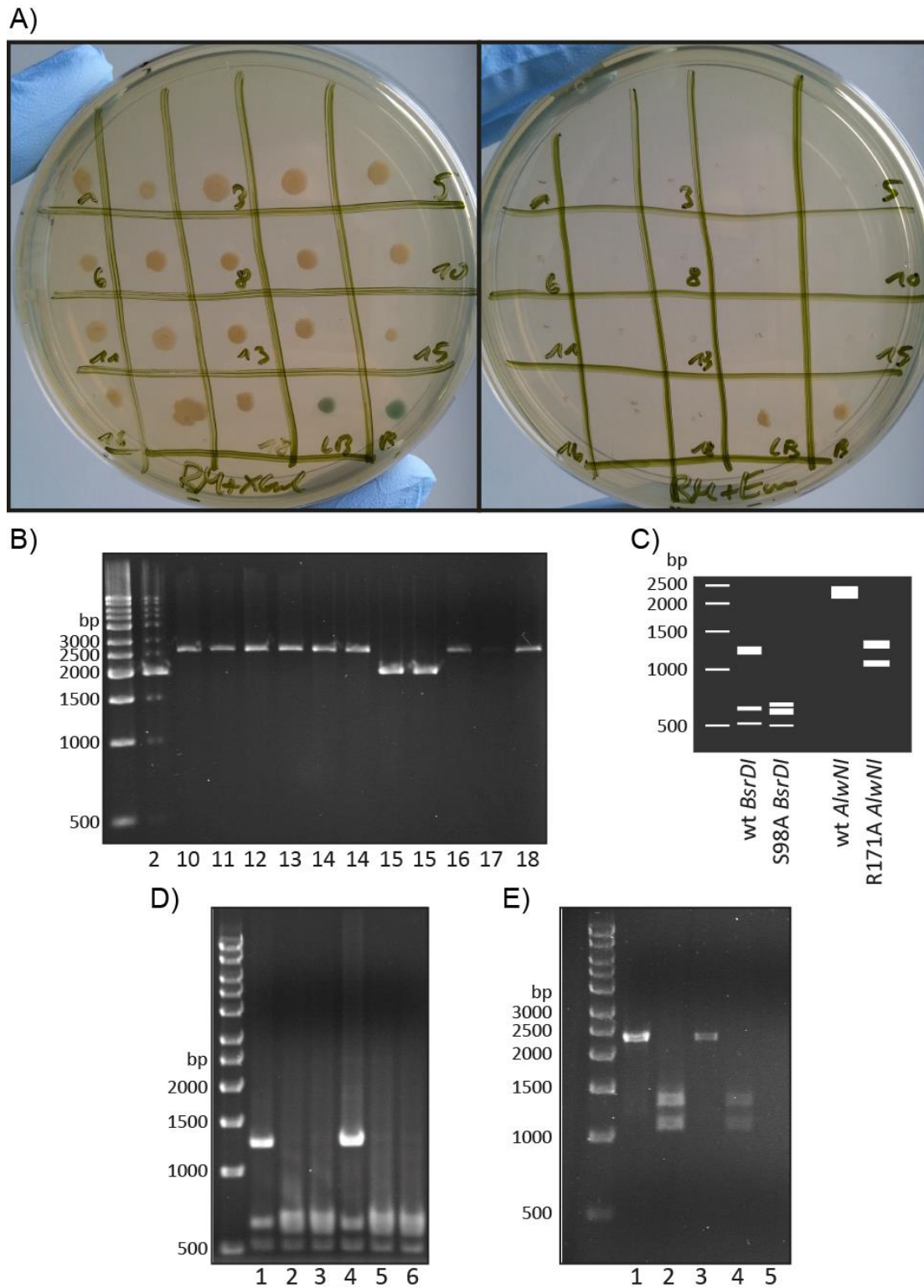
Figure 27 Selection and validation of *clpP* mutations in *S. aureus* NCTC 8325. A) Screening of single colonies for loss of pMAD plasmid on agar plates containing X-gal in absence or presence of erythromycin. Colonies without pMAD show no blue coloration and do not grow on plates containing antibiotic. B) Analytical restriction digest confirms deletion of *clpP* in colonies 2 and 15 whereas all remaining colonies correspond to wt *clpP*. C) Simulated agarose gel of wt *clpP* and the point mutants S98A and R171A digested with BsrDI and AlwNI, respectively. D) Screening of single colonies for S98A point mutations. Colonies 1 and 4 show wt while all remaining colonies indicate successful S98A mutation. E) Screening of single colonies for R171A point mutations. Colonies 1 and 3 show wt while colonies 2 and 4 indicate successful R171A mutation.

2.3.   Phenotypic Studies

2.3.1. Growth Characteristics

After the generation of genetic modifications in the endogenous *clpP* locus of *S. aureus,* several single colonies were isolated and their mutations validated. In order to elucidate possible substantial differences compared to the wt NCTC 8325 strain, growth of wt, S98A and *ΔclpP* strains was monitored. Overnight cultures of the respective strains were prepared, diluted and monitored using two different methods. Aliquots of diluted *S. aureus* were transferred into 96-well plates and subsequently incubated. Absorbance was measured using a microplate reader (Figure 28A). As longer incubation at 37 °C may lead to evaporation of medium this approach was only used to obtain an initial insight. While the measured growth curves showed no extensive differences in growth rate, mutations in or loss of *clpP* did on the other hand lead to slightly delayed increase in density (1 to 1.5 h). Strikingly, wt NCTC 8325 reached the stationary phase significantly earlier and with lower optical density than *clpP* mutants.

The same observations were made when incubating the bacterial cultures in Erlenmeyer flasks and measuring the optical density with cuvettes (Figure 28B). The growth rate was once again comparable between all strains. At mid-exponential phase, a delay of approx. 1.3 h between wt and *ΔclpP* was also detected. Both strains with mutations in *clpP* exhibited higher optical densities when reaching stationary phase significantly later than the wt strain. These results suggest that ClpP might be involved in growth phase transition.
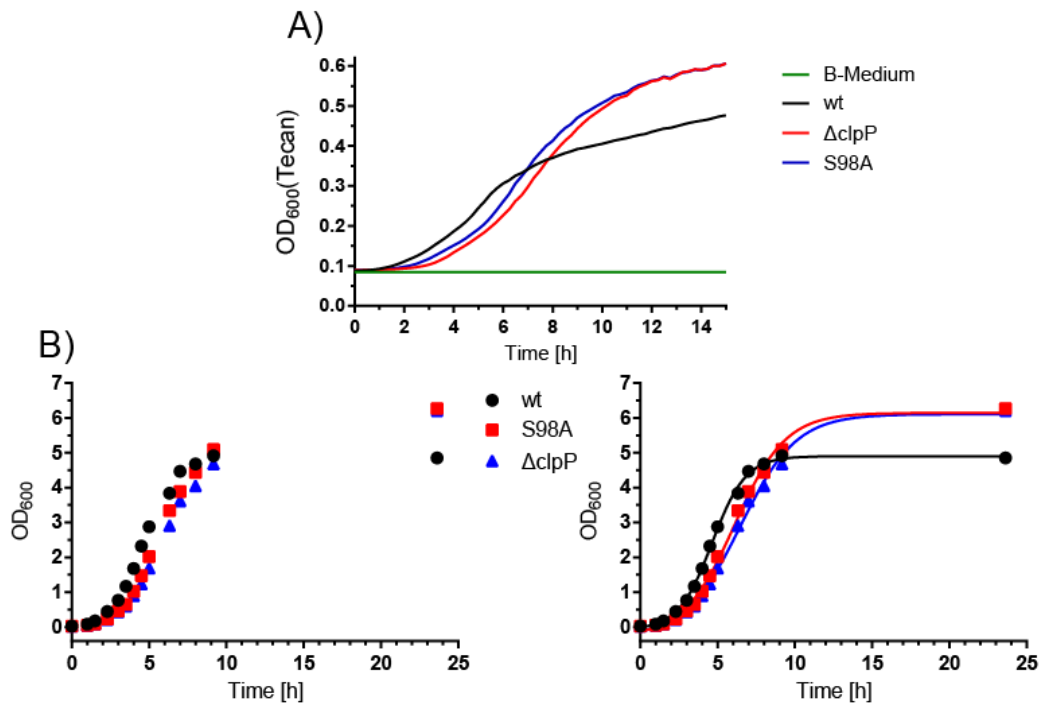
Figure 28 Growth curves of *S. aureus* NCTC 8325 wt, *ΔclpP* and S98A strains. A) Growth curves measured in a 96-well format using a Tecan M200Pro multiplate reader. B) Growth curves measured in Erlenmeyer flasks using standard cuvettes and photometer. Left: raw data; right: interpolated growth curve.

2.3.2. Hemolysis

Previous studies have shown reduced virulence of *S. aureus clpP* deletion strains.[92–94] Furthermore, chemical manipulation of the active site serine S98 with β-lactones also led to reduced hemolytic activity.[97,128–130] In order to determine if the hemolytic activity of the newly generated mutations behaved as expected, two different hemolysis assay variants were carried out. Growth experiments on sheep-blood agar plates revealed complete absence of blood lysis for the *clpP* deletion mutant. The S98A mutants showed significantly reduced hemolytic areas, whereas the R171A mutants only showed very little hemolysis reduction (Figure 29A). The shift from tetradecameric to heptameric ClpP induced by R171A[100,124] and the loss of proteolytic activity observed *in vitro* seemed to have only a minor effect *in vivo*.
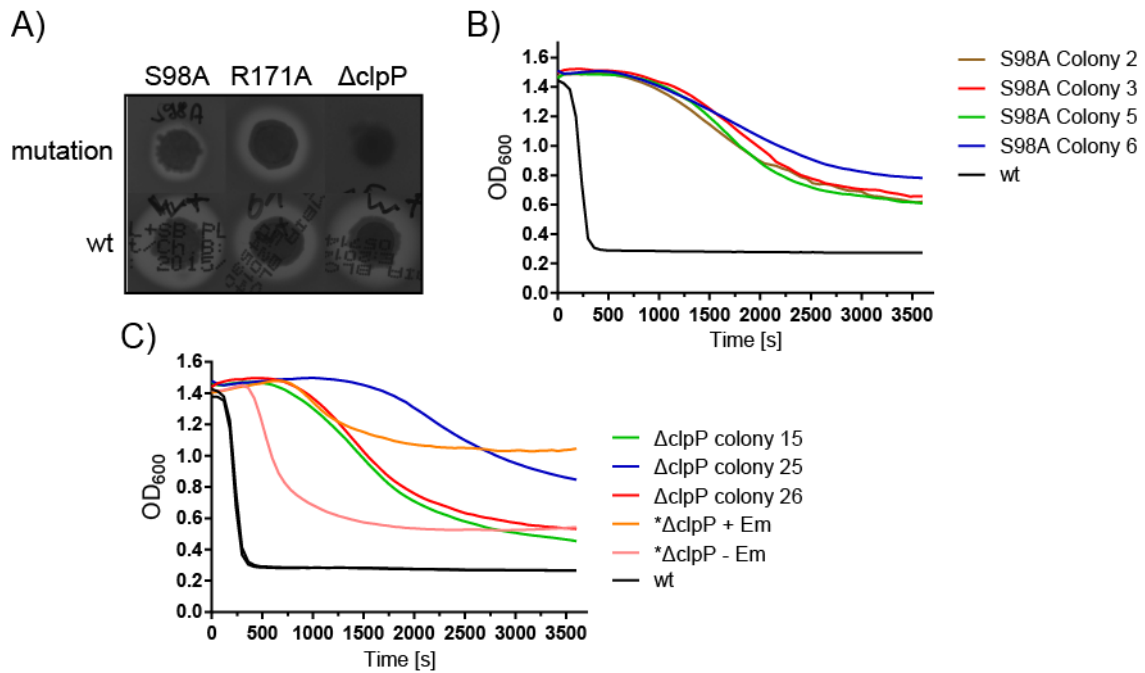
Figure 29 Hemolytic activity of *S. aureus clpP* mutants. A) Plate hemolysis assay with *S. aureus* wt (bottom row), *ΔclpP*, S98A and R171A mutant strains (top row). White areas represent lysed erythrocytes. B) Hemolytic activity of *S. aureus* supernatants. NCTC 8325 wt and four S98A colonies were tested. C) Hemolytic activity of *S. aureus* supernatants. NCTC 8325 wt, three *ΔclpP* colonies, and a previously published *ΔclpP* strain were tested. * previously published *ΔclpP* strain, carrying an antibiotic resistance cassette[94] was tested in presence and absence of erythromycin.

ΔclpP and S98A strains were tested in an alternative hemolysis assay. For this experiment, cultures were grown to OD = 0.4 to 0.6, subsequently diluted and aliquots transferred to plastic culture tubes. After incubation for 20 h supernatants were removed and incubated with sheep blood. Lysis of erythrocytes was monitored in a microplate reader. Different colonies of S98A were tested, all showing significantly slower lysis kinetics (Figure 29B). Even though the same phenomenon was observed with *ΔclpP* colonies, a higher variance between single colonies was obtained in this case (Figure 29C). A previously published *clpP* deletion mutant[94] containing an antibiotic resistance cassette was used as a benchmark. Impressively, the presence or absence of antibiotic had a strong effect on hemolysis levels, corroborating the need for markerless mutations for detailed phenotypic analyses.

2.3.3. Whole-Proteome Analysis

In order to obtain a complete picture of changes induced by genetic manipulation of the *clpP* locus, a whole-proteome analysis was implemented. Overnight cultures of *S. aureus* NCTC 8325 wt, S98A and *ΔclpP* were diluted and grown to stationary phase. Cells were washed, lysed and the total protein amount adjusted by BCA assay. Proteins were

digested and modified by dimethyl labeling for quantitative LC-MS/MS measurements. Experiments comparing the protein abundances of the *clpP* deletion mutant and the S98A point mutant showed only minor differences between both strains (Figure 30A). Granted the majority of proteins have similar abundances, a slight shift of the proteins in the volcano plot to the left indicates stronger regulation by *ΔclpP*. Only few proteins were significantly different between these two strains (Figure 30B). As expected, ClpP was found to be strongly depleted in the *ΔclpP* strain due to the quantification method used in MaxQuant analysis.

Comparison of *ΔclpP* and S98A to NCTC 8325 wt strain revealed major differences in protein abundances (Figure 31A and B): 62% (28 proteins) of the up-regulated proteins are shared by both (*ΔclpP* and S98A) strains (Figure 31C and F). Remarkably, two clp
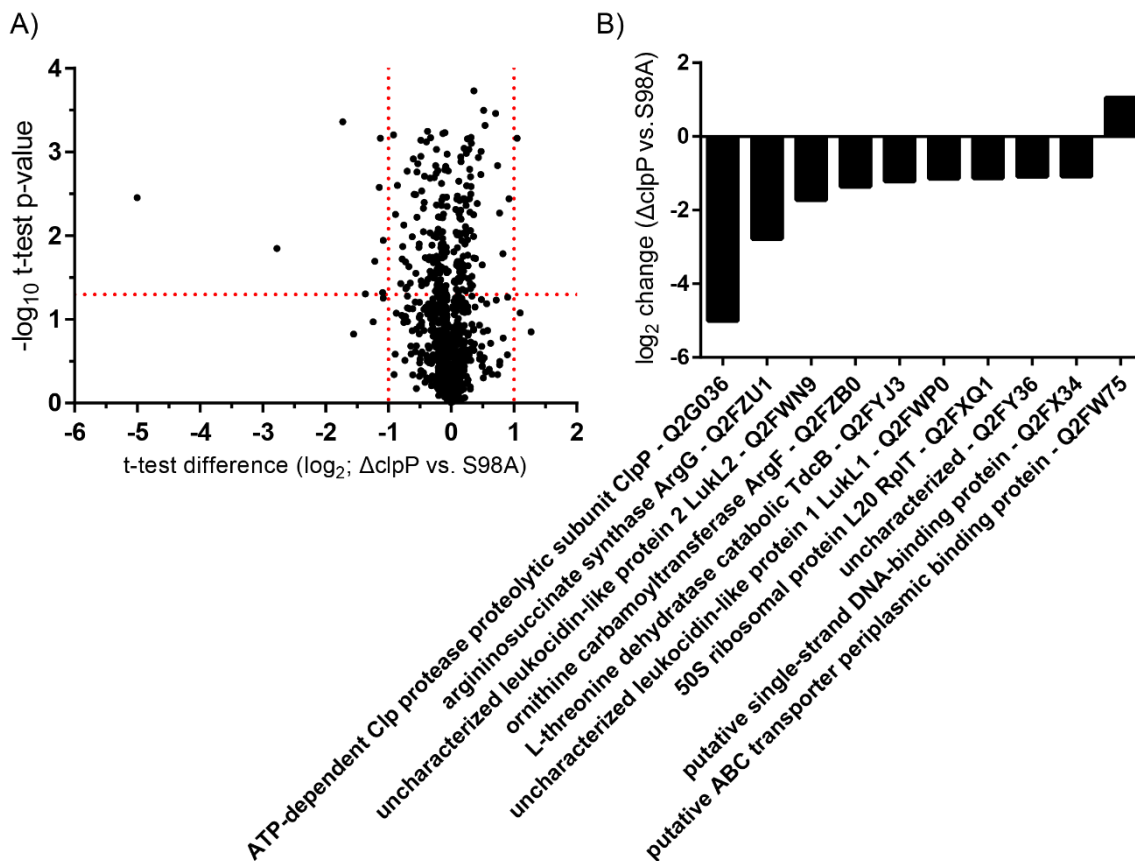
Figure 30 Whole-proteome analysis of *S. aureus* NCTC 8325 *ΔclpP* and S98A. A) Volcano plot showing different protein abundances of *ΔclpP* versus S98A. Data results from four experiments. B) Differently expressed proteins in *ΔclpP* compared to S98A. Shown are proteins with enrichment > 1 or depletion < -1 and a p-value < 0.05 (depicted by red dotted lines in A)).

related proteins ClpB and ClpC, as well as four previously described substrate proteins of ClpP (MecA, McsB, Ctsr and Spx) were found to be up-regulated in both strains.[105,159–161] Functional clustering using the DAVID[162,163] tool revealed a stress response cluster

containing ClpC, protein arginine kinase (Q2G0P6) and the transcriptional regulator CtsR (Q2G0P8).

A similar number of proteins was obtained regarding the depleted proteins. 64% (32 proteins) of the depleted proteins were shared by *ΔclpP* and S98A (Figure 31D and E). DAVID analysis resulted in the identification of two enriched clusters: 1) ribosomal proteins, containing 30S subunit S18 (RpsR), 50S subunit L24 (RplX) and 50S subunit L33 (RpmG1) and 2) pathogenesis and signal related proteins, containing nucleotidase (Q2G170), MHC class II protein (Q2FWW1), α-hemolysin (Hly), γ-hemolysin components A-C and subunit B, desuccinylase (Q2FWN9), extracellular matrix protein (Q2G012) and uncharacterized protein (Q2G2G0). Particularly the depletion of a high number of virulence associated proteins reflected previously published attenuation of virulence in a *clpP* deletion mutant.[93]

These initial proteomic experiments constitute the basis for future, more detailed investigations of the influences of genetic modification of *clpP* on *S. aureus*.
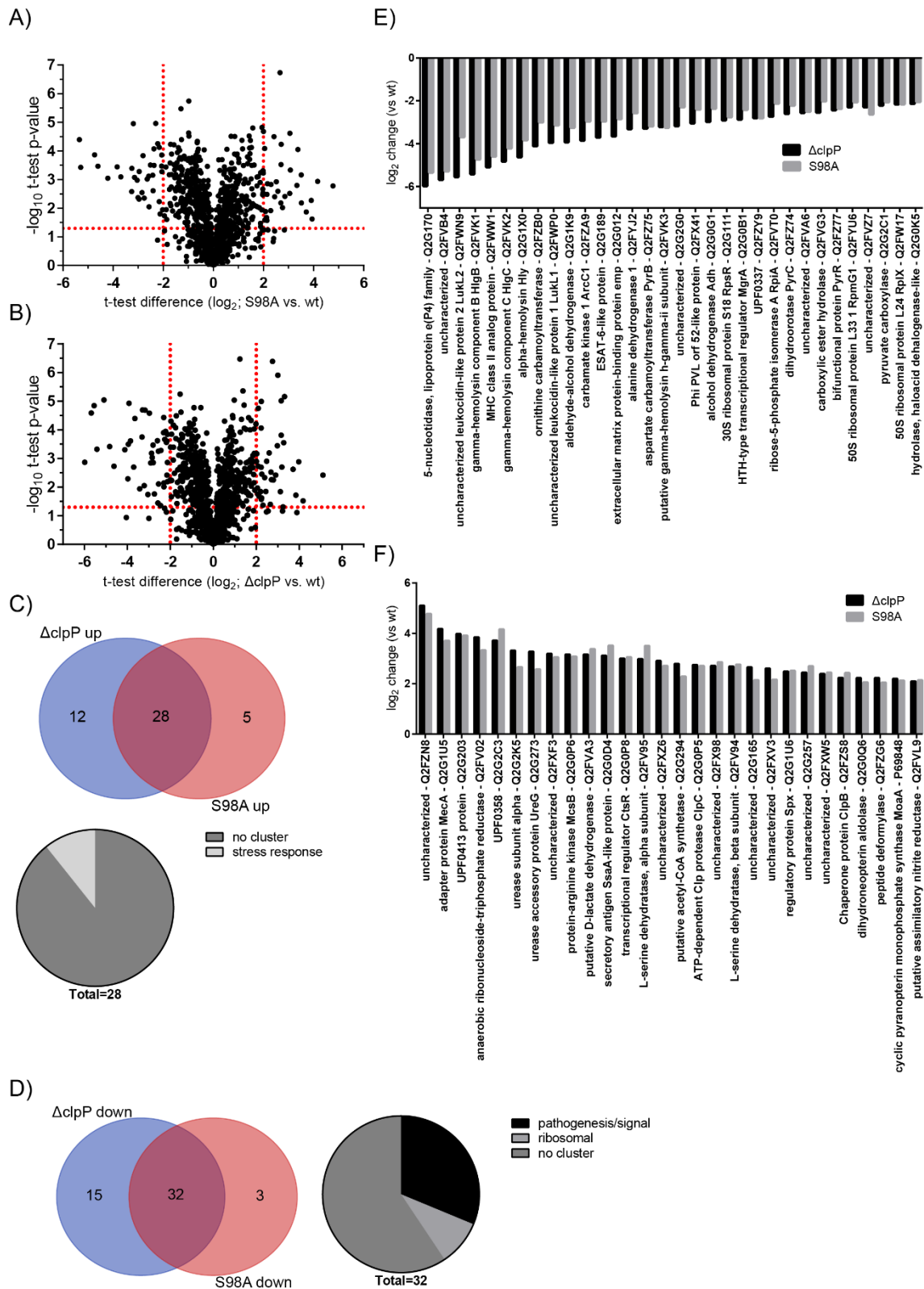
Figure 31 Whole-proteome analysis of *S. aureus* NCTC 8325 *ΔclpP*/S98A compared to wt. A) Volcano plot showing different protein abundances of S98A versus wt. Data results from four experiments. B) Volcano plot showing different protein abundances of *ΔclpP* versus wt. Data results from four experiments. C) Overlap of enriched proteins in *ΔclpP*/S98A samples compared to wt. Proteins with enrichment >2 and a p-value <0.05 (depicted by red dotted lines in A) and B)) were taken for analysis. Cluster analysis performed with DAVID.[162,163] D) Overlap of depleted proteins in *ΔclpP*/S98A samples compared to wt. Proteins with depletion <-2 and a p-value <0.05 (depicted by red dotted lines in A) and B)) were taken for analysis. Cluster analysis performed with DAVID. E) Depleted proteins in

ΔclpP and S98A samples compared to wt. Shown are overlapping proteins with Uniprot IDs. F) Enriched proteins in *ΔclpP* and S98A samples compared to wt. Shown are overlapping proteins with Uniprot IDs.

3. Summary and Outlook

The studies described above show the influence of genetic modifications in the *clpP* gene on the phenotype of *S. aureus*. In order to obtain a *clpP* deletion mutant and two point mutations, S98A and R171A in *S. aureus* NCTC 8325, an elaborate cloning strategy was constructed and executed. A *ΔclpP* shuttle vector for allelic replacement was generated by OE-PCR and transformed into *S. aureus* NCTC 8325 in two steps. For the generation of shuttle vectors containing point mutations of *clpP*, the wt gene was cloned and ligated with the vector followed by site-directed mutagenesis. Following several selection steps, single colonies carrying the desired mutations were acquired. With little difference between the growth rates of three *S. aureus* mutant strains, delayed growth was observed for *ΔclpP* and S98A strains. These two strains reached a higher optical density when reaching stationary phase. In hemolysis assays, *ΔclpP* and S98A strains showed significantly reduced production of hemolysins, whereas R171A mutation led only to minor attenuation of hemolysis. Whole-proteome analysis revealed high similarity of *ΔclpP* and S98A mutants and substantial differences compared to wt *S. aureus*. Reduction of several virulence factors and enrichment of known ClpP substrates substantiate the similarities of a deletion and active site mutant and offer widespread opportunities for future studies. An example would be metabolic profiling of the mutants in comparison to wt in order to decipher the hitherto unknown effects of ClpP on the bacterial metabolism.

Experimental Section

1. Biochemical and Microbiological Procedures

1.1. Media

LB-Medium:

10 g peptone

5 g NaCl

5 g yeast extract

fill to 1 L with ddH$_2$O (pH 7.5)

B-Medium:

10 g peptone

5 g NaCl

5 g yeast extract

1 g K$_2$HPO$_4$

fill to 1 L with ddH$_2$O (pH 7.5)

BHB-Medium:

7.5 g brain infusion

10 g peptone

10 g heart infusion

5 g NaCl

2.5 g Na$_2$HPO$_4$

2 g glucose

fill to 1 L with ddH$_2$O (pH 7.4)

BM-Medium:

10 g soy peptone

5 g yeast extract

5 g NaCl

1 g K$_2$HPO$_4$ × 3 H$_2$O

1 g glucose

fill to 1 L with ddH$_2$O (pH 7.4 – 7.6)

1.2. Overexpression of Recombinant Proteins

1.2.1. Oligonucleotides for Cloning of Expression Vectors

Table 3 Oligonucleotides for overexpression studies used in this thesis for.

Primer	Sequence (5' → 3')
clpX_E183Q_for	GTT TTC AGA TTT ACG TGC AAT TTT ATC AAT CTG ATC TAC ATA AAT AAT ACC TTT TTC GGC TTT
clpX_E183Q_rev	AAA GCC GAA AAA GGT ATT ATT TAT GTA GAT CAG ATT GAT AAA ATT GCA CGT AAA TCT GAA AAC
clpC_for	GGG GAC AAG TTT GTA CAA AAA AGC AGG CTT TAT GTT ATT TGG TAG ATT AAC TGA G
clpC_rev	GGG GAC CAC TTT GTA CAA GAA AGC TGG GTG TTA TGC TTG CGA TGG TGT TTT A
mecA_for	GGG GAC AAG TTT GTA CAA AAA AGC AGG CTA TGA GAA TAG AAC GAG TAG ATG ATA C
mecA_rev	GGG GAC CAC TTT GTA CAA GAA AGC TGG GTG TTA TTC AGT TGT CTC TGG AAA ATA ACG

1.2.2. Expression of ClpP

A C-terminal STREP-II affinity tagged ClpP construct was cloned via GATEWAY technology into the pET301 expression vector.[99] Expression was carried out in *E. coli* BL21 cells overnight at 25 °C after induction at an OD_{600} between 0.5 and 0.6 with IPTG (500 µM final concentration). Cells were harvested by centrifugation (5 min, 6000 g), washed with PBS and lysed by sonication in lysis buffer (100 mM Tris, pH 8.0, 150 mM NaCl, 1 mM EDTA). The lysate was centrifuged (38720 g, 30 min, 4 °C) and ClpP was isolated from the supernatant by STREP-II affinity chromatography. Affinity purified ClpP was either used directly or further purified by size exclusion chromatography on a Superdex 200 16/60 column (GE) using storage buffer (20 mM Hepes, pH 7.0, 100 mM NaCl). Quality control was performed by high-resolution intact-protein mass spectrometry on a LTQ FT Ultra (Thermo).

1.2.3. Expression of GFP-SsrA

eGFP (Uniprot ID C5MKY7) was cloned as a fusion protein with an C-terminal SsrA tag (AANDENYALAA) into vector pDEST007 and was purified as described previously.[124,164] Briefly, *E. coli* KY2266 cells were incubated for 4 h at 37 °C after induction with anhydrotetracycline (0.2 mg/L) at an OD_{600} of 0.4 to 0.6. Cells were harvested by centrifugation (5 min, 6000 g), washed with PBS and lysed by sonication in lysis buffer

(100 mM Tris, pH 8.0, 150 mM NaCl, 1 mM EDTA). The lysate was centrifuged (38720 g, 30 min, 4 °C) and GFP-SsrA was isolated by STREP-II affinity chromatography. After purification, the buffer was exchanged to storage buffer (20 mM Tris, pH 7.0, 100 mM NaCl, 10% glycerol). Quality control was performed by high-resolution intact-protein mass spectrometry on a LTQ FT Ultra (Thermo).

1.2.4. Expression of ClpX

ClpX was cloned as a N-terminal STREP-II construct with a TEV site into vector pDEST007 and as a N-terminal 6xHis-tag construct with TEV site into vector pET300.[124] Expression was performed in *E. coli* BL21 cells for 4 h at 37 °C (25 °C) after induction at an OD_{600} between 0.4 and 0.6 with anhydrotetracycline (0.2 mg/L) or IPTG (500 µM) for pDEST007 or pET300, respectively. Cells were harvested by centrifugation (5 min, 6000 g), washed with PBS and lysed by sonication in lysis buffer (pDEST007: 100 mM Tris, pH 8.0, 150 mM NaCl, 1 mM EDTA, 1 mM DTT; pET300: 25 mM Hepes, pH 7.6, 200 mM KCl, 5 mM $MgCl_2$, 1 mM DTT, 0.5 mM ATP, 5% glycerol). The lysate was centrifuged (38720 g, 30 min, 4 °C) and ClpX was isolated from the supernatant by affinity chromatography. For most assays ClpX was directly used without further processing. For some assays (e.g. analytical SEC) tag-free ClpX was used. Therefore, ClpX was transferred in a buffer containing EDTA (1 mM) but no $MgCl_2$ and incubated with TEV protease (ratio 1:50 to 1:100 w/w) overnight at 10 °C. The sample was then subjected to size exclusion chromatography using a Superdex 200 16/60 column (GE) and ClpX storage buffer (25 mM Hepes, pH 7.6, 200 mM KCl, 5 mM $MgCl_2$, 1 mM DTT, 0.5 mM ATP, 5% glycerol). Quality control was performed by high-resolution intact-protein mass spectrometry on a LTQ FT Ultra (Thermo).

Walker B point mutant generation of SaClpX:

The point mutation (E183Q) in the Walker B motif of SaClpX was constructed using the QuickChange II site-directed mutagenesis protocol (Stratagene). PCR was conducted using the pET300 ClpX expression vector as a template, Phusion polymerase (NEB) and mutagenic primers (Table 3), constructed with the QuickChange Primer Design program. The PCR product was digested with DpnI and transformed into *E. coli* XL1-Blue cells. The plasmids were extracted, retransformed into *E. coli* BL21 and the correct DNA sequence

was verified by Sanger sequencing. Expression was performed under the same conditions as for the pET300 wt expression vector.

1.2.5. Expression of ClpC and MecA

ClpC (Uniprot ID: Q2G0P5) and MecA (Uniprot ID: Q2G1U5) were cloned as N-terminal 6xHis tagged constructs with TEV sites first into pDONR201 (Invitrogen) and finally in the pET300 expression vector using GATEWAY technology and the primers listed in Table 3.[96] Expression was carried out in *E. coli* BL21 cells for 15 h at 25 °C after induction at an OD_{600} between 0.5 and 0.6 with IPTG (250 µM final concentration). Cells were harvested (5 min, 6000 g), washed with PBS, reconstituted in binding buffer (25 mM Hepes, pH 7.6, 200 mM KCl, 5 mM $MgCl_2$, 5% glycerol, 1 mM DTT, 0.5 mM ATP) and lysed by sonication. The lysate was centrifuged (38720 g, 30 min, 4 °C) and the proteins were isolated from the respective supernatants by affinity chromatography. Fractions containing protein were pooled and EDTA was added (1 mM final concentration). The proteins were incubated with TEV protease (ratio 1:50, w/w) overnight at 4 °C and subjected to size exclusion chromatography (25 mM Hepes, pH 7.6, 200 mM KCl, 5 mM $MgCl_2$, 5% glycerol, 1 mM DTT, 0.5 mM ATP). Quality control was performed by high-resolution intact-protein mass spectrometry on a LTQ FT Ultra (Thermo).

1.3. High-Throughput Screen

A library consisting of 40,480 small molecule compounds was screened using the ClpXP GFP degradation assay. On every 384-well plate 352 compounds, as well as 16 wells containing negative controls and 16 wells containing positive controls were measured. 25 µL of ClpXP-master mix (25 mM Hepes, pH 7.6, 200 mM KCl, 5 mM $MgCl_2$, 1 mM DTT, 10% glycerol, 4 mM ATP, 16 mM creatine phosphate, 20 U/mL creatine phosphokinase (Roche), 0.3 µM $ClpP_{14}$, 0.6 µM $ClpX_6$; final assay concentrations) or negative control (same composition as above, except without ClpXP) were dispensed in a black 384-well plate (Corning, #3573) and 0.3 µL of compound (in DMSO) or DMSO was added to each well (10 µM final compound concentration). The plate was shaken for 15 s at 2000 rpm, centrifuged to collect sample at bottom and incubated at r.t. for 15 min. Then, the GFP-SsrA substrate (1.5 µM in H_2O; 5 µL per well) was added and the plate was again shaken and centrifuged. Kinetic fluorescence measurements were performed in a Tecan Safire^2

microplate reader (2 min interval, 10 cycles, λ_{ex} = 465 nm, λ_{em} = 535 nm, 20 nm bandwidth). The overall Z' factor was calculated to be 0.69 ± 0.087.

The 332 best modulating (z-score > 3) primary hit compounds were cherry picked and subsequently analyzed for dose-dependent inhibition (or activation). This was done by double measurements in twofold dilution series with nine different concentrations each, starting at 50 µM.

1.4. Biochemical Assays

1.4.1. In vitro Creatine Kinase Assay

To account for inhibitors of the ATP regeneration system a counter-screen against creatine kinase was performed using Kinase-Glo assay (Promega). Assays were performed in PZ buffer (25 mM Hepes, pH 7.6, 200 mM KCl, 5 mM $MgCl_2$, 1 mM DTT, 10% glycerol) in a white flat-bottom 96-well plate (Brand) with 50 µL reaction volume at r.t. 0.5 µL of compound stock (100x, 50 µM final concentration) or DMSO were mixed with 47 µL of master mix (creatine kinase in PZ buffer, 52 µg/mL final concentration). After incubation for 10 min at r.t. 3 µL of substrate mix (20 µM ADP, 20 µM creatine phosphate; final concentrations) were added and incubated for another 10 min at r.t. 50 µL of Kinase-Glo reagent were added and luminescence was recorded after 10 min incubation at r.t. using an Infinite M200 Pro (Tecan). DMSO-treated samples were normalized to 100% activity and samples without creatine kinase were used as a negative control.

1.4.2. In vitro ClpXP/ClpCP Protease Assay

The ClpXP protease activity was monitored using a fluorescent GFP substrate, which was tagged with a SsrA degradation tag.[133,134] Assays were performed in PZ buffer (25 mM Hepes, pH 7.6, 200 mM KCl, 5 mM $MgCl_2$, 1 mM DTT, 10% glycerol) with 60 µL reaction volume at 30 °C. GFP fluorescence was monitored in white, flat-bottom well plates (Brand) using an Infinite M200 Pro (Tecan; λ_{ex} = 465 nm, λ_{em} = 535 nm). Degradation reactions contained 0.6 µM $ClpX_6$, 0.3 µM $ClpP_{14}$, 0.25 µM GFP-SsrA and an ATP regeneration system (4 mM ATP, 16 mM creatine phosphate, 20 U/mL creatine phosphokinase). In case of ClpCP protease assays 1.0 µM $ClpC_6$, 0.3 µM $ClpP_{14}$ and 2.5 µM MecA were used. 0.6 µL of inhibitor (in DMSO) were added to the wells followed

by all other reaction partners (in 50 µL) except the substrate. After pre-incubation for 15 min at 30 °C, the substrate (10 µL) was added and fluorescence was monitored. Unless stated otherwise all data were collected in duplicates and in three independent experiments. The slope of the curves in the linear region was determined via linear regression using GraphPad Prism. DMSO-treated samples were normalized to 100% activity and samples without ClpX were used as a negative control.

1.4.3. In vitro ClpP Peptidase Assay

Activity of SaClpP was measured using a fluorogenic peptide substrate (Suc-Leu-Tyr-AMC, Bachem) in duplicates.[126] 1 µL of DMSO or compound stock was pipetted to a black flat-bottom 96-well plate (Greiner) and 88 µL of assay-buffer (100 mM Hepes, pH 7.0, 100 mM NaCl) containing 1 µM ClpP (final concentration) were added. After incubation for 15 min at 32 °C, the reaction was started by addition of 10 µL substrate (0.2 mM final concentration) and fluorescence was recorded for 60 min in an infinite M200 pro plate reader (Tecan; λ_{ex} = 380 nm, λ_{em} = 440 nm). Data was analyzed by calculating the initial slope (GraphPad Prism) and normalizing DMSO-treated samples to 100% activity.

1.4.4. In vitro ClpX ATPase Assay (Malachite Green)

Activity of ClpX was measured by detection of free phosphate, which is formed by hydrolysis of ATP using the malachite green assay. The dye solution (0.045% malachite green in H_2O:4.2% ammonium molybdate in 4 N HCl:1% Triton X-100 in H_2O / 36:12:1) was always freshly prepared and filtered (0.45 µM) after incubation for 1 h at r.t. In a reaction tube 4 µM ClpX in PZ buffer (200 µL reaction volume) were incubated with 2 µL of DMSO/compound stock for 10 min at r.t. and then ATP (2 mM final concentration) was added to start the reaction. After defined time points (e.g. 2, 6 and 14 min) 50 µL of the sample were pipetted into a plastic cuvette filled with 800 µL dye solution and 50 µL PZ buffer. The cuvette was sealed and inverted. After 60 s 100 µL of 35% citric acid (in H_2O) were added to the cuvette and absorbance at 650 nm was measured in triplicates after inverting the mixture again. Data was analyzed by calculating the slope (GraphPad Prism) via linear regression and normalizing DMSO-treated samples to 100% activity. Samples without ClpX were used as a negative control to account for potential autohydrolysis of ATP.

62

1.4.5. In vitro ClpX ATPase Assay (Enzyme Coupled)

In a transparent flat-bottom 96-well plate 0.6 µL of DMSO or compound stock were mixed with 54 µL ATPase buffer (100 mM Hepes, pH 7.0, 200 mM KCl, 20 mM MgCl$_2$, 1 mM DTT, 1 mM NADH, 2 mM phosphoenolpyruvate, 50 U/mL lactate dehydrogenase, 50 U/mL pyruvate kinase, 5% (v/v) glycerol) containing ClpX (4 µM final concentration). After incubation for 10 min at 37 °C, 6 µL 200 mM ATP (in H$_2$O) were added to start the assay. The amount of NADH/H$^+$ was monitored by absorbance measurement (λ = 340 nm) using a Tecan M200Pro.

1.4.6. Plasma Stability Assay

Prior to measurements mouse plasma (biowest) was diluted 1:2 with potassium phosphate buffer (0.1 M, pH 7.4) and pre-incubated at 37 °C for at least 30 min. Test compounds and controls (positive control: procaine; negative control: procainamide) were added at 100 µM and incubated at 37 °C at 600 rpm in a shaker. 25 µL aliquots were taken after several time points and pipetted into 30 µL acetonitrile. The mixture was vortexed, cooled down (-20 °C) and centrifuged (10 min, 17000 g). The supernatant was transferred into vials and analyzed using a Dionex Ultimate 3000 HPLC system (XBridge™ BEH130 C18 5 µm, 4.6 × 100 mm) coupled to a Thermo LTQ-FT Ultra mass spectrometer with an APCI ionization source (vaporizer temperature 400 °C, sheath gas 60 arb, aux gas 20 arb, source voltage 6 kV, capillary voltage 4 V, tube lens 45 V). Data was collected in positive mode using full scans (R = 12500) from m/z = 100 to m/z = 500 and SIM scans (R = 12500) for each compound. Xcalibur 2.2 Quan Browser was used for calculation of peak areas (SIM scans) and quantification.

1.5. Analytical Size Exclusion Chromatography

Analytical size exclusion chromatography experiments were performed using a Superdex 200 10/300 gL (GE) or a Superose 6 Increase 10/300 gL (GE) column at 4 °C. For most experiments PZ buffer (with 0.5 mM ATP) was used. Samples (200 µL) were mixed, incubated 10 min at 37 °C and loaded into a 500 µL loop. Elution was monitored at 280 nm. Runs were referenced against the salt peak of the conductivity trace and normalized to the highest peak for easier comparison.

1.6. UV Stability of Chemical Compounds

Compounds were diluted in PZ buffer to 1 µM and transferred to a transparent 96-well plate. After UV irradiation at 365 nm (Philips TL-D BLB 18W) for 10 min on ice, samples were transferred into vials. Measurement was performed on a Dionex Ultimate 3000 HPLC system coupled to a Thermo LCQ-Fleet mass spectrometer with electrospray ionization.

1.7. Extracellular Proteolytic and Hemolytic Activity

Extracellular proteolytic activity was tested on LB agar plates containing 1% skimmed milk. Hemolytic activity was tested on Columbia Sheep Blood Agar plates (PB5039A, Thermo Scientific). Sterile filter paper disks (5 mM diameter) were placed on agar plates and 3 µL DMSO/compound stock and 3 µL of stationary *S. aureus* diluted with B-Medium (1:100) were added. The agar plates were incubated for 20 h at 37 °C and photos were taken using a LAS4000 scanner (GE Healthcare).

For the analysis of hemolytic activity of *S. aureus* supernatants, the DMSO-/compound-treated cells were centrifuged (5 min, 6000 g) and the sterile filtered supernatant (0.22 µm filters) directly added on blood agar plates (20-50 µL) following incubation at 37 °C.

1.8. Thermal Shift Assay

To each well of a white 96-well PCR plate, 50 µL of a 10 µM ClpX (pr ClpP) solution in PZ-buffer (or PBS) containing Sypro Orange (1:2000, Sigma-Aldrich) were added. To this solution 0.5 µL of DMSO or 100× compound stock was added and fluorescence intensity was measured while heating from 20 °C to 89.6 °C (0.3 K steps) in a CFX96 Real-Time System (BioRad). Data was analyzed using Bio-Rad CFX Manager 3.0.

1.9. Intact Protein Mass Spectrometry

A solution of 3 µM ClpX wt or ClpX E183Q (or 1 µM ClpP) in PZ-Buffer (containing 0.5 mM ATP) was incubated (60 min at 30 °C) with up to 100 µM of inhibitor (1% DMSO final concentration). Measurements were performed on a Dionex Ultimate 3000 HPLC system coupled to a Thermo LTQ-FT Ultra mass spectrometer with an electrospray ionization source (spray voltage 4.2 kV, tube lens 110 V, capillary voltage 48 V, sheath gas 60 arb,

aux gas 10 arb). 5 μL of reaction mixture were on-line desalted using a Massprep desalting cartridge (Waters). The mass spectrometer was operated in positive mode collecting full scans at high-resolution (R = 200,000) from m/z = 600 to m/z = 2000. Collected spectra were deconvoluted using the Thermo Xcalibur Xtract algorithm.

1.10. Western Blot Analysis

For western blot analysis of Hla, 10 μL of bacterial supernatant were subjected to SDS-PAGE using Tris-Glycine gels. Blotting was performed according to manufacturer's instructions at 100 V for 60 min on PVDF membrane using the Tetra Blotting Module (Bio-Rad). Membranes were blocked (TBS containing 5% skimmed milk and 0.1% Tween-20) and incubated with primary anti-Hla antibody (1:4000; anti-*Staphylococcus* alpha hemolysin antibody, polyclonal rabbit; Abcam ab50536) overnight at 4 °C. After extensive washing (3 × 15 min) with blocking buffer the membranes were incubated with secondary antibody (1:10000; goat anti-rabbit ATTO 488 conjugate; Sigma Aldrich 18772) for 60 min at r.t. followed by washing (3 × 15 min blocking buffer; 15 min TBST). Bands were detected by fluorescence scan using a LAS4000 (GE).

1.11. Hemolysis Assay

Fresh B-medium was inoculated 1:100 from an overnight culture of *S. aureus* NCTC 8325 and incubated at 37 °C (200 rpm) until an OD_{600} of 0.4-0.6. The culture was then diluted to 3.4×10^4 CFU/mL and split into aliquots of 1 mL in plastic culture tubes. To each tube either 10 μL DMSO or compound stock were pipetted, the lids tightly closed and incubated for 20 h at 37 °C (200 rpm). Cultures were removed and centrifuged for 10 min (6000 g, r.t.). 100 μL of the clear supernatants were mixed with 50 μL of diluted sheep erythrocyte suspension and absorbance was measured at 595 nm. 100 μL of B-medium was used as a negative control and supernatants of DMSO-treated cells as positive controls.

1.12.   Generation of Genetic Modifications of *S. aureus*

1.12.1. Oligonucleotides used for Genetic clpP Modifications

Table 4 Oligonucleotides for generation of mutations in *S. aureus* used in this thesis.

Primer	Sequence (5' → 3')
pMAD-clpP-for	GGA GGA TCC GCT GCG ATG AAA CAA GTT GAG
pMAD-clpP-rev	GGA GGA TCC CTA AAT CTG GGT GGG AAC AC
pMAD-seq-for	CCC AAT ATA ATC ATT TAT CAA CTC TTT TAC ACT TAA ATT TCC
pMAD-seq-rev	GCA ACG CGG GCA TCC CGA TG
clpP_KO_A	ATA TGG TAC CGA AGT ATT ACG TAT TTA AAA GAA GCG
clpP_KO_B	CAT CTA TAT TTC CTC CTT GTA ATA AC
clpP_KO_C	GTT ATT ACA AGG AGG AAA TAT AGA TGT AAT TCA AAG TAA AGA GTA GAC TAA GC
clpP_KO_D	ATA TGA GCT CCT AAA TCT GGG TGG GAA CAC
pIMAY_MCS_for	TAC ATG TCA AGA ATA AAC TGC CAA AGC
pIMAY_MCS_rev	AAT ACC TGT GAC GGA AGA TCA CTT CG
pIMAY-clpP-for	AAA GGA AAG AGA AAA GCG TCA A
pIMAY-clpP-rev	CAT TCA ATC ATA TTT CCG CTC A
SaClpP-S98A-for	ATT TGT ATC GGT ATG GCT GCA GCA ATG GGA TCA TTC TTA TTA G
SaClpP-S98A-rev	CTA ATA AGA ATG ATC CCA TTG CTG CAG CCA TAC CGA TAC AAA T
SAclpP-R171A-for	GTA TTG AAA AAA TAC AAA AAG ACA CAG ATG CTG ATA ACT TCT TAA CTG CAG AAG A
SAclpP-R171A-rev	TCT TCT GCA GTT AAG AAG TTA TCA GCA TCT GTG TCT TTT TGT ATT TTT TCA ATA C
Clpp_for1_SmaI	GCG CCC CGG GGC TGC GAT GAA ACA AGT TGA G
Clpp_rev1_SacI	GCG CGA GCT CGC TAA ATC TGG GTG GGA ACA C

1.12.2. Construction of ΔclpP Shuttle Vector

Approx. 1000 bp upstream (clpP_KO_A and clpP_KO_B) and 1000 bp downstream (clpP_KO_C and clpP_KO_D) region of clpP were amplified by PCR (56.9 °C annealing, GC buffer, Phusion polymerase, NEB) using isolated *S. aureus* NCTC 8325 DNA as template. The PCR products were purified (Cycle Pure Kit, EZNA, Omega Bio-tek) and fused in a following OE-PCR split into two parts. First both templates without primers were used for 15 cycles, then clpP_KO_A and clpP_KO_D primers were added for additional 24 cycles (58.9 °C annealing; GC buffer, Phusion polymerase, NEB). The approx. 2000 bp PCR product was purified (Cycle Pure Kit, EZNA) and digested with *SacI* and *KpnI* (Promega, standard protocol). pIMAY plasmid was also digested with *SacI* and *KpnI* and dephosphorylated by addition of TSAP (Promega, streamlined restriction digestion protocol) for 20 min. After restriction digest products were purified (MicroElute DNA Clean-Up Kit, EZNA, Omega Bio-tek). Ligation into pIMAY vector was conducted using T4 DNA Ligase (Promega, standard protocol) overnight at 8 °C and a vector:insert ratio of

1:6. The ligation product was chemically transformed into *E. coli* TOP10 cells and plated onto LB agar containing chloramphenicol. Insertion of the desired construct was tested after plasmid extraction (Plasmid Mini Kit I, EZNA, Omega Bio-tek) by analytical restriction digest (*SacI*) and sequencing (pIMAY_MCS_for, pIMAY_MCS_rev, pIMAY-clpP-for and pIMAY-clpP-rev).

In order to change from pIMAY to pMAD the constructed pIMAY *ΔclpP* was used as a template in a PCR reaction (70 °C annealing, HF buffer, Phusion polymerase, NEB) with primers pMAD-clpP-for and pMAD-clpP-rev. The PCR product was purified (Cycle Pure Kit, EZNA, Omega Bio-tek), digested (*BamHI*, NEB, standard protocol), purified (MicroElute DNA Clean-Up Kit, EZNA, Omega Bio-tek) and ligated into digested (*BamHI*, NEB, standard protocol) and dephosphorylated (TSAP, Promega, streamlined restriction digestion protocol) pMAD (T4 DNA Ligase, Promega, 8 °C overnight, vector:insert / 1:6). The ligation product was chemically transformed into *E. coli* SA08B cells and plated onto LB agar containing ampicillin. Insertion of the desired construct was tested after plasmid extraction (Plasmid Mini Kit I, EZNA, Omega Bio-tek) by analytical restriction digest (*BamHI*) and sequencing (pMAD-seq-for and pMAD-seq-rev).

1.12.3. Construction of clpP S98A and clpP R171 Shuttle Vectors

Before point mutations were introduced into *clpP* a wt shuttle plasmid was constructed. For this, *clpP* with approx. 900 bp up- and 900 bp downstream region was amplified by PCR (58 °C annealing, GC buffer, Phusion polymerase, NEB) using primers Clpp_for1_SmaI and ClpP_rev1_SacI and isolated *S. aureus* NCTC 8325 DNA as template. The PCR product was purified (Cycle Pure Kit, EZNA, Omega Bio-tek) and digested with *SmaI* and *SacI* (Promega, standard protocol). pIMAY plasmid was also digested with *SmaI* and *SacI* and dephosphorylated by addition of TSAP (Promega, streamlined restriction digestion protocol) for 15 min. After restriction digest products were purified (MicroElute DNA Clean-Up Kit, EZNA, Omega Bio-tek). Ligation into pIMAY vector was conducted using T4 DNA Ligase (Promega, standard protocol) overnight at 8 °C and a vector:insert ratio of 1:3. The ligation product was chemically transformed into *E. coli* TOP10 cells and plated onto LB agar containing chloramphenicol. Insertion of the desired construct was tested after plasmid extraction (Plasmid Mini Kit I, EZNA, Omega Bio-tek) by analytical restriction digest (*SacI*) and sequencing (pIMAY_MCS_for and pIMAY-clpP-for).

The S98A and R171A point mutations were introduced by site-directed mutagenesis using the constructed pIMAY clpP wt vector as a template. Hence, two PCR reactions (62 °C annealing, GC buffer, 0.166 pmol/µL primer, 4 min elongation, phusion polymerase, NEB) with the mutagenic primers for S98A (SaClpP-S98A-for and SaClpP-S98A-rev) or R171A (SAclpP-R171A-for and SAclpP-R171A-rev), respectively, and the wt clpP vector as template were conducted. 1 µL DpnI (NEB) was added to the finished PCR products and incubated at 37 °C for 1 h. The digested products were chemically transformed into *E. coli* XL1Blue cells and plated onto LB agar containing chloramphenicol. Plasmids were extracted (Plasmid Mini Kit I, EZNA, Omega Bio-tek) and successful mutations validated by sequencing (pIMAY-clpP-for, pIMAY-clpP-rev, pIMAY_MCS_for and pIMAY_MCS_rev).

In order to change from pIMAY to pMAD the constructed pIMAY clpP S98A/R171A vectors were used as templates in PCR reactions (65 °C annealing, HF buffer, Phusion polymerase, NEB) with primers pMAD-clpP-for and pMAD-clpP-rev. The PCR products were purified (Cycle Pure Kit, EZNA, Omega Bio-tek), digested (*BamHI*, NEB, standard protocol), purified (MicroElute DNA Clean-Up Kit, EZNA, Omega Bio-tek) and ligated into digested (*BamHI*, NEB, standard protocol) and dephosphorylated (TSAP, Promega, streamlined restriction digestion protocol) pMAD (T4 DNA Ligase, Promega, 8 °C overnight, vector:insert / 1:6). The ligation product was chemically transformed into *E. coli* SA08B cells and plated onto LB agar containing ampicillin. Insertion of the desired construct was tested after plasmid extraction (Plasmid Mini Kit I, EZNA, Omega Bio-tek) by analytical restriction digest (*BamHI*) and sequencing (pMAD-seq-for and pMAD-seq-rev).

1.12.4. Preparation of Electrocompetent S. aureus

100 mL of BM-medium were inoculated with 1 mL (1:100) from a *S. aureus* overnight culture and incubated at 37 °C until an OD_{600} of 0.5 was reached. Cells were centrifuged (5000 g, 15 min, 4 °C) and washed three times with cold 10% glycerol (sterile): 1) 100 mL; 2) 50 mL; 3) 25 mL. The pellet was resuspended in 400 µL cold 10% glycerol and 75 µL aliquots were frozen in liquid nitrogen and stored at -80 °C.

1.12.5. Transformation into S. aureus NCTC 8325

Transformation of plasmids into *S. aureus* NCTC 8325 was carried out in two steps. First, the plasmid produced by *E. coli* was electroporated into *S. aureus* RN4220. The plasmid was extracted from RN4220 and electroporated into NCTC 8325.

Electroporation

Electrocompetent *S. aureus* was thawed at room temperature and incubated for 10 min with > 1 µg plasmid. The suspension was transferred into a 0.2 cm electroporation cuvette (BioRad) and electroporated (exponential, 25 µF, 2 kV, 100 Ω) using a Gene Pulser Xcell (BioRad). Immediately after the pulse 1 mL pre-warmed BM-medium was added and incubated at 30 °C for 90 min. The cell suspension was streaked onto BM agar containing selective antibiotic + X-gal and incubated until colonies were visible.

Plasmid Extraction from S. aureus cultures

25 mL of *S. aureus* RN4220 (carrying pMAD constructs) cultures in BM-medium containing erythromycin were grown overnight at 30 °C. Plasmid extraction was performed using the Plasmid Plus Midi Kit (Qiagen, high-yield protocol) with some modifications. After addition of 4 mL P1 buffer 50 µL lysostaphin (2 mg/mL) was added and incubated for 30 to 40 min at 37 °C without shaking. After elution with 200 µL H_2O, liquid was removed using a vacuum concentrator and the pellet solubilized in 30 µL H_2O.

1.12.6. Selection Protocol - pMAD

After successful transformation into *S. aureus* NCTC 8325, indicated by blue colonies, single colonies were picked and incubated overnight at 30 °C in the presence of 1 µg/mL erythromycin. 10 mL BM-medium were inoculated 1:1000 from the overnight culture and incubated 2 h at 30 °C and 6 h at 42 °C. 100 µL diluted cultures (10^{-2} to 10^{-6}) were plated onto BM-agar (containing 1 µg/mL erythromycin and 100 µg/mL X-gal) and incubated at 42 °C until colonies with blue coloration were visible (enrichment of single crossover). Ten light blue colonies were picked and incubated (together) in 10 mL BM-medium at 30 °C for 8 h followed by overnight incubation at 42 °C. 10 mL BM-medium were inoculated 1:1000 from this overnight culture and grown for 4 h at 30 °C and additional 4 h at 42 °C. 100 µL of diluted cultures (10^{-2} to 10^{-6}) were plated onto BM-agar containing X-gal and incubated at 42 °C. White colonies were picked and streaked onto

BM-agar containing erythromycin and X-gal and onto BM-agar containing only X-gal. Plates were incubated at 30 °C and erythromycin susceptible colonies further analyzed by colony PCR followed by analytical restriction digest and sequencing. For colony PCR small parts of colonies were resuspended in 50 µL sterile H_2O and 1 µL thereof was used in PCR reactions with an initial denaturation step for 10 min (95 °C).

1.13. Bacterial Growth Curves

Monitoring in 96-well Plates

Overnight cultures were diluted 1:10000 in B-medium and pipetted into 96-well plates (200 µL per well). Surrounding wells were filled with 200 µL B-medium and the lid was closed. Incubation (at 37 °C) and measurement of optical density was performed using a Tecan M200Pro multiplate reader.

Monitoring in Erlenmeyer flasks

Overnight cultures were diluted 1:100 in 50 mL B-medium and incubated in 100 mL Erlenmeyer flasks at 37 °C and 200 rpm. For each time point, 1 mL culture was transferred into cuvettes and optical density was measured using a photometer.

2. Transcriptomics – RNA-seq

2.1. Extraction of Total RNA

5 mL of B-Medium were inoculated with 50 µL (1:100) of an overnight culture of *S. aureus* NCTC 8325 (NRS77). The culture was incubated at 37 °C (220 rpm) until OD = 0.3–0.4, then diluted to 3.4×10^4 CFU/mL and 1 mL aliquots were pipetted into plastic culture tubes. After addition of either 10 µL DMSO or 10 µL **334** stock (1 mM in DMSO, 10 µM final concentration) the lids were closed and incubated for 20 h at 37 °C (220 rpm).

Per sample, 2 mL RNAprotect bacterial reagent (Qiagen) were added, centrifuged (2 min, 10000 g, 4 °C), pellets resuspended in 400 µL lysis buffer (RLT buffer (Qiagen) containing 2% β-mercaptoethanol) and transferred into 0.5 mL ball mill tubes (VK05S, Precellys). Lysis was performed using two runs (5500 rpm, 1×20 s) with a Precellys 24 Dual ball mill system and a 2 min break (cooling on ice) in between. Ball mill tubes were centrifuged (1 min, 10000 g, 4 °C) and 500 µL of supernatant transferred into new 2 mL tubes. To each sample 50 µL NaOAc (3 M, pH 4.0), 500 µL water saturated phenol (pH 4.0) and 100 µL chloroform-isoamyl alcohol-mixture (24:1) were added, vortexed for

10 s and incubated on ice for 15 min. The mixture was centrifuged (20 min, 10000 g, 4 °C) and the upper phase transferred into a new 1.5 mL tube. 300 µL chloroform-isoamyl alcohol-mixture (24:1) were added followed by vigorous mixing for 30 s and centrifugation (3 min, 10000 g, 4 °C). The upper phase was again transferred into a new 1.5 mL tube and the extraction process repeated once more. In a new 2 mL tube 400 µL of the upper phase were combined with 40 µL NaOAc (pH 4.0), 1 mL 96% ethanol and 1 µL glycogen (5 mg/mL) and stored at -20 °C overnight.

Total RNA was pelleted by centrifugation at full speed (30 min, 25155 g, 4 °C). The supernatant was carefully discarded and the pellet washed with 500 µL 70% ethanol. After repeated centrifugation at full speed (10 min, 25155 g, 4 °C) the remaining liquid was completely removed and the pellet air-dried for 5 min. The RNA pellet was resuspended in 50 µL nuclease free H_2O and integrity was checked using agarose gel electrophoresis.

5 µg total RNA were treated with the DNase Turbo kit (ThermoFisher) using the "rigorous DNase treatment" protocol. To limit RNA degradation 1 µL of RiboGuard RNase inhibitor (Biozym) was added prior to DNase treatment. RNA integrity was checked again using agarose gel electrophoresis and concentrations were determined by NanoQuant Plate (Tecan) measurement using a M200Pro reader (Tecan).

2.2. RNA-Sequencing

S. aureus ribosomal RNA was depleted from the extracted total RNA using the RiboZero epidemiology kit (Epicenter) according to the manufacturer's protocol. 1 µg of total RNA was used as input into the RiboZero routine. The depletion efficiency of rRNA depletion was accessed using the Agilent 2100 Bioanalyzer (Agilent Technologies).

The cDNA libraries were prepared using the ScriptSeq v2 RNA-Seq library preparation kit (Epicentre) according to the manufacturer's instructions. Therefore, 50 ng of rRNA-depleted RNA were fragmented 5 minutes at 85 °C and cDNA was generated using random hexamer primer additionally adding a 5'-end tagging sequence. RNA was removed and 3'-tagged cDNA was synthesized via Terminal-Tagging Oligos. The generated di-tagged cDNA was purified using minElute PCR Purification kit (Qiagen) according to the manufacturer's instructions. Adaptor-tagged RNA-Seq libraries were generated by amplification of the di-tagged cDNA utilizing indexing primers for later multiplexing and the addition of Illumina adaptor sequences. Excess PCR primers were

removed via exonuclease I treatment and generated libraries were purified using the minElute PCR Purification kit (Qiagen). The cDNA libraries were size-selected by agarose gel electrophoresis in the range between 180 and 650 bp. Gel extraction was performed using the QIAquick gel extraction kit (Qiagen) to exclude remaining nucleic acid contaminations. Library quality and size-selection were controlled using the Agilent 2100 Bioanalyzer. The cDNA libraries were sequenced on the Illumina HiSeq 2500 platform utilizing the TruSeq S.R. cluster kit, v3-cBot-HS (Illumina), using single-end sequencing (50 bp). Libraries were multiplexed on one lane and sequenced to 58 cycles in one direction to generate roughly 20 million reads per sample.

2.3.   Transcriptome Analysis

Raw sequenced reads were quality filtered and trimmed using fastq-mcf.[165] Remaining reads were aligned to the genome of *S. aureus* strain 8325 using STAR.[166] Sequence matches of 30 nucleotides with a minimal sequence homology of 93.33% (2 mismatches) were included. Mapped reads were collapsed using samtools and counted using HTSeq.[167,168] The transcriptional profiles of **334**-treated and DMSO-treated *S. aureus* were compared using principal component analysis (PCA) within the DESeq2 routine.[169] DESeq2 algorithm was applied to identify genes differentially expressed between **334**-treated and DMSO-treated *S. aureus*. A gene was considered significantly differential expressed between treatments if the Benjamini-Hochberg adjusted *p*-value was ≤ 0.05.

3. Proteomics

3.1. Labeling Reagents for "Click Chemistry"
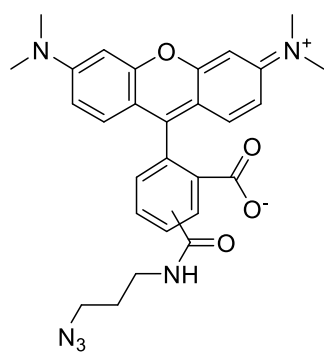
rhodamine azide
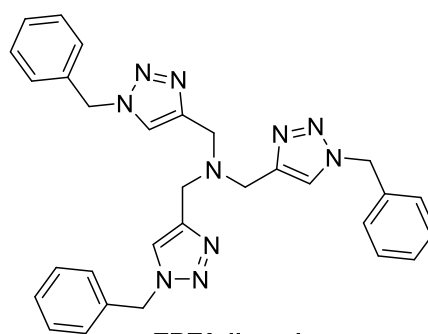
TBTA ligand
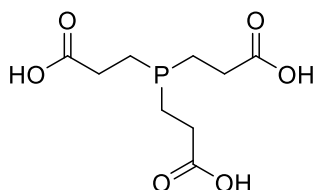
TCEP
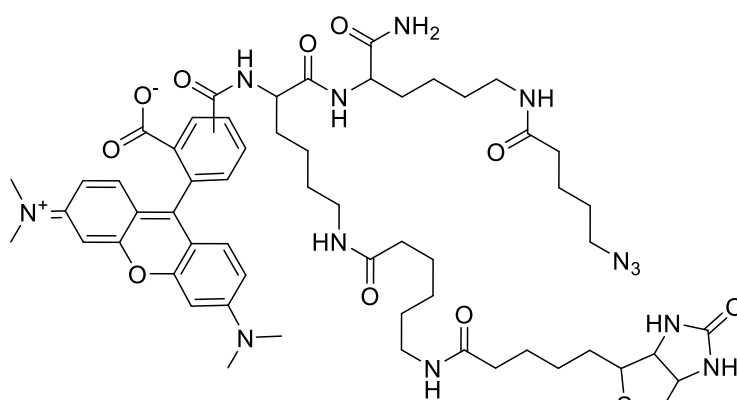
trifunctional linker
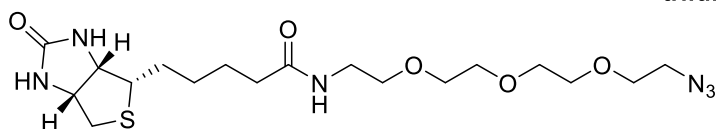
biotin azide

3.2. Analytical AfBPP Labeling of Recombinantly Expressed Proteins

In a transparent 96-well plate SaClpP, SaClpX and/or BSA were diluted into EP buffer (100 mM Hepes, pH 7.0, 100 mM NaCl) or PZA buffer (25 mM Hepes, pH 7.6, 200 mM KCl, 5 mM MgCl$_2$, 1 mM DTT, 10% (v/v) glycerol, 4 mM ATP) and incubated with diluted probe (10 µM final concentration) for 10 min at r.t. The samples were irradiated at 365 nm (Philips TL-D BLB 18 W) for 15 min on ice. Coupling to rhodamine was achieved via "click reaction" by addition of 0.1 µL rhodamine-azide (5 mM in DMSO), 0.1 µL TCEP (52 mM in H$_2$O), 0.3 µL TBTA ligand (1.667 mM in 80% *t*-BuOH and 20% DMSO) and 0.1 µL CuSO$_4$ (50 mM in H$_2$O) and incubation at r.t. for 1 h. The samples were transferred to 1.5 mL tubes, one equivalent 2x Laemmli sample buffer was added and incubated at 95 °C for 10 min. Samples were subsequently analyzed by SDS-PAGE.

3.3.   Quantitative *in situ* AfBPP Labeling of *S. aureus*

100 mL of B-Medium were inoculated 1:100 from an overnight culture of *S. aureus* NCTC 8325 (NRS77) and incubated for 6 h at 37 °C (220 rpm). 45 mL of the culture were transferred in 50 mL tubes and centrifuged for 5 min at 6000 g (4 °C). The pellet was washed with 30 mL PBS, centrifuged again (5 min, 6000 g, 4 °C) and resuspended in the appropriate volume of PBS to reach an OD_{600} of 40. For each state, 1 mL aliquots of culture in 2 mL tubes was mixed with either 20 μL DMSO (control), 10 μL DMSO followed by 10 μL 0.3 mM **376** (enrichment) or 10 μL 3 mM **334** followed by 10 μL 0.3 mM **376** (competition). Samples were first incubated for 15 min (37 °C, 220 rpm) with DMSO (control and enrichment) or **334** (competition) before addition of either DMSO (control) or photoprobe **376** (enrichment and competition). Followed by another incubation for 45 min (37 °C, 220 rpm), samples were transferred into transparent 6-well plates and irradiated without lid for 15 min on ice (Philips TL-D BLB 18 W). The suspension was transferred back into the 2 mL tubes, centrifuged (5 min, 6000 g, 4 °C), washed with 1 mL PBS and stored at -80 °C.

Pellets were resuspended in 1 mL lysis buffer (1 protease-inhibitor cocktail (Roche), 1% (v/v) Triton 100, 0.5% (w/v) SDS in 10 mL PBS) and transferred in 2 mL ball mill tubes (SK38, Precellys). Cells were lysed using Precellys Homogenizer (5× 5800 rpm for 15 s and 1× 6500 rpm for 20 s) with 2 min cooling breaks between each run. Samples were centrifuged at full speed for 10 min (4 °C) and the supernatants were transferred into new 1.5 mL tubes. Protein concentrations were adjusted using BCA assay (Pierce) to obtain 600 μL for each sample with 700 μg total protein. Samples were "clicked" to trifunctional linker (TFL) by addition of 3.6 μL TFL (10 mM in DMSO), 12 μL TCEP (15 mg/mL in H_2O), 36 μL TBTA ligand (1.667 mM in 80% *t*-BuOH and 20% DMSO) and 12 μL $CuSO_4$ (50 mM in H_2O). After incubation for 1 h at r.t., proteins were precipitated by transferring everything into 15 mL tubes, adding 2.5 mL cold acetone (-80 °C) and storing the samples overnight at -20 °C. The precipitate was centrifuged (15 min, 18000 g) and washed twice with 1 mL cold methanol (-80 °C) with resuspension (5 s ultrasonic bath) and centrifugation steps (10 min, 18000 g) in between.

Washed pellets were resuspended in 500 μL 0.4% (w/v) SDS in PBS using sonication (15 s, 10% intensity) and insolubilized particles removed by centrifugation (10 min, full speed). The supernatants were incubated with 80 μL avidin beads for 2 h at r.t. in low-

bind tubes. Prior to incubation, avidin beads were washed three times with 1 mL 0.4% (w/v) SDS in PBS (centrifugation at 400 g, 2 min). After incubation, beads were centrifuged (400 g, 2 min), washed (3× 0.4% SDS in PBS, 2× 6 M Urea and 3× PBS) and resuspended in 25 µL elution buffer I (50 mM Tris-HCl, pH 8.0, 2 M urea, 1 mM DTT, 5 ng/µL trypsin). Samples were incubated at 25 °C for 30 min (700 rpm) followed by addition of 100 µL elution buffer II (50 mM Tris-HCl, pH 8.0, 2 M urea, 5 mM iodoacetamide) and overnight incubation at 25 °C (700 rpm).

On the next day, the digest was stopped by addition of 20 µL 10% (v/v) formic acid (FA) and the supernatant transferred into a new low-bind tube. Beads were washed with 1 mL 0.1% (v/v) trifluoroacetic acid (TFA) and the supernatants combined. The samples were split, one aliquot treated for dimethyl labeling[170,171] and the other aliquot for label-free quantification (LFQ).[148] Desalting of the samples was conducted on 50 mg SepPak C18 columns (Waters). The columns were equilibrated with 1 mL acetonitrile (ACN), 500 µL elution buffer (80% ACN, 0.5% FA) and 3 mL aqueous 0.1% TFA solution. The acidified samples were loaded by gravity flow, washed twice with 1 mL 0.1% TFA and once with 0.5% FA and then labeled with five times 1 mL of the respective dimethyl labeling agents (light (L): 30 mM $NaBH_3CN$, 0.2 % CH_2O, 45 mM sodium phosphate buffer, pH 7.5; medium (M): 30 mM $NaBH_3CN$, 0.2 % CD_2O, 45 mM sodium phosphate buffer, pH 7.5; heavy (H): 30 mM $NaBD_3CN$, 0.2 % $^{13}CD_2O$, 45 mM sodium phosphate buffer, pH 7.5). Labels were switched throughout the replicates. Column bound peptides were washed two more times with 1 mL 0.5% FA and then eluted with two times 250 µL elution buffer. 900 µL of each sample were combined in a 15 mL tube, frozen in liquid nitrogen and lyophilized. Samples, which were analyzed by LFQ, were eluted directly after the washing step and lyophilized individually. Prior to LC-MS/MS measurement the samples were dissolved in 30 µL 1% FA (for LFQ: 20 µL) and filtered with 0.22 µm ultrafree centrifugal filters (Merck) equilibrated with 300 µL 1% FA. The filtrates were transferred into MS vials and queued for LC-MS/MS measurement on Q Exactive Plus (for method see 3.5.6).

3.4.   Affinity Pull-Down Experiments

100 mL of B-Medium were inoculated 1:2000 from an overnight culture of *S. aureus* NCTC 8325 (NRS77) and incubated for 20 h at 37 °C (220 rpm). The culture was transferred to three 50 mL tubes, centrifuged for 5 min at 6000 g (4 °C) and washed with

20 mL PBS. The pellets were resuspended in a total of 10 mL lysis buffer (1 protease-inhibitor cocktail (Roche), 5% (w/v) glycerol in 10 mL PBS) and transferred into four 2 mL ball mill tubes (SK38, Precellys). Cells were lysed using Precellys Homogenizer (3× 6500 rpm for 20 s) with 2 min cooling breaks between each run. Samples were centrifuged at full speed for 10 min (4 °C) and the supernatants were sterile filtered (0.22 μm) and combined. For each state 500 μL lysate was pipetted into 1.5 mL tubes and mixed with DMSO/**371** or **334/371** (**334**: 100 μM final concentration; **371**: 10/30 μM final concentration). Samples were incubated for 1 h at 4 °C (rotation), then 50 μL avidin agarose beads were added and again incubated for 1 h. Avidin agarose was washed three times with 500 μL PBS prior to incubation. Beads were washed with five times 500 μL PBS and resuspended in X-buffer (20 mM Hepes, pH 7.5, 7 M urea, 2 M thiourea). Samples were further processed for LC-MS/MS using the dimethyl labeling protocol (light and heavy labels) according to chapter 3.5.3. For SDS-PAGE analysis, beads were directly resuspended in Laemmli buffer, incubated at 95 °C for 5 min and the supernatant loaded on polyacrylamide gels.

3.5.   Whole Proteome Analysis (Chapter I)

The following whole proteome analyses were performed using different quantification methods and LC-MS/MS devices. Table 5 gives detailed information about the setup used for each experiment. The mass spectrometry proteomics data have been deposited to the ProteomeXchange Consortium via the PRIDE[172] partner repository with the dataset identifier PXD007259.

Table 5 Experimental layout for whole proteome LC-MS/MS analyses. Quantification was either achieved by dimethyl labeling (DML) or label-free quantification (LFQ).

Strains	Experiment	Quantification Method	MS instrument
S. aureus NCTC 8325/USA300 wt	Intracellular proteome/Secretome at 10 μM **334**	DML	Orbitrap Fusion (Thermo Fisher)
S. aureus NCTC 8325 wt	Secretome titration	LFQ	LTQ Orbitrap XL (Thermo Fisher)
S. aureus NCTC 8325-4 wt/*ΔclpX*[93]	Intracellular proteome at 10 μM **334**	LFQ	Q Exactive Plus (Thermo Fisher)

5 mL of B-Medium were inoculated 1:100 from an overnight culture of *S. aureus* NCTC 8325 (NRS77), *S. aureus* USA300 (BAA-1556), *S. aureus* NCTC 8325-4[93] or *S. aureus* NCTC 8325-4 *ΔclpX*[93] and incubated (37 °C, 200 rpm) until OD$_{600}$ = 0.3 - 0.5. The culture was

then diluted to $3×10^4$ CFU/mL with fresh B-Medium and split into 1.5 mL (for NCTC 8325-4: 3 mL) aliquots in 14 mL PP plastic tubes (17×100 mM, VWR). 15 μL (for NCTC 8325-4: 30 μL) of DMSO or compound stocks were added to the aliquots following incubation for 19-20 h at 37 °C and 200 rpm. On the next day the cultures were transferred to 2 mL tubes (for NCTC 8325-4: 15 mL tubes) and centrifuged (10 min, 6000 g).

3.5.1. Secretome Analysis

The supernatant was removed and sterile filtered (0.22 μm) into a 50 mL Falcon tube and 12 mL cold acetone (-80 °C) were added. Proteins were allowed to precipitate overnight at -80 °C. The precipitate was centrifuged (15 min, 18000 g) and washed twice with 1 mL cold methanol (-80 °C) with resuspension (5 s ultrasonic bath) and centrifugation steps (10 min, 18000 g) in between. The washed pellet was dissolved in 200 μL X-buffer (20 mM Hepes, pH 7.5, 7 M urea, 2 M thiourea) and transferred in low-bind Eppendorf tubes for further analysis.

3.5.2. Intracellular Proteome Analysis

Cell pellets were washed twice with cold PBS (10 min, 6000 g), resuspended in 400 μL PBS and transferred into 0.5 mL ball mill tubes (VK05S, Precellys). Lysis was performed using two runs (5500 rpm, 1×20 s; 5800 rpm, 6×15 s) with a Precellys 24 Dual ball mill system and a 2 min break (cooling on ice) in between. The tubes were centrifuged (5 min, 6000 g) and the supernatant transferred in a low-bind Eppendorf tube. The protein concentration was adjusted to 2.5 mg/mL (for 8325-4: 380 μg/mL) using BCA assay and 200 μL (for 8325-4: 350 μL) were subjected to new low-bind tubes for further analysis.

3.5.3. Sample Preparation

Proteins were reduced by addition of 0.2 μL dithiothreitol (DTT, 1 M) and incubation for 45 min at r.t. and 450 rpm). Alkylation was performed by adding 2 μL iodoacetamide (IAA, 550 mM) and incubation for 30 min at r.t. in the dark with subsequent quenching of the reaction with 0.5 μL DTT (1 M) for 30 min. The samples were pre-digested by addition of 1 μL LysC (0.5 mg/mL) and incubation at r.t. for 4 h. After diluting with 600 μL triethylammonium bicarbonate buffer (TEAB, 50 mM) 1.5 μL trypsin (0.5 mg/mL in 50 mM acetic acid) was added followed by overnight incubation at 37 °C. Digestion was

stopped by addition of 8 µL formic acid (FA). Desalting of the samples was conducted on 50 mg SepPak C18 columns (Waters). The columns were equilibrated with 1 mL acetonitrile (ACN), 1 mL elution buffer (80% ACN, 0.5% FA) and 3 mL aqueous 0.5% FA solution. The acidified samples were loaded by gravity flow, washed five times with 1 mL 0.5% FA and then labeled with five times 1 mL of the respective dimethyl labeling agents (light (L): 30 mM NaBH$_3$CN, 0.2 % CH$_2$O, 45 mM sodium phosphate buffer, pH 7.5; medium (M): 30 mM NaBH$_3$CN, 0.2 % CD$_2$O, 45 mM sodium phosphate buffer, pH 7.5; heavy (H): 30 mM NaBD$_3$CN, 0.2 % ^{13}CD$_2$O, 45 mM sodium phosphate buffer, pH 7.5). Labels were switched throughout the replicates. Column bound peptides were washed two more times with 1 mL 0.5% FA and then eluted with two times 250 µL elution buffer. 900 µL of each sample were combined in a 15 mL tube, frozen in liquid nitrogen and lyophilized. Samples, which were analyzed by label-free quantification (LFQ)[148], were eluted directly after the washing step and lyophilized individually. Prior to LC-MS/MS measurement the samples were dissolved in 40 µL 1% FA (for 8325-4: 30 µL) and filtered with 0.22 µm ultrafree centrifugal filters (Merck) equilibrated with 300 µL 1% FA. The filtrates were transferred into MS vials and queued for LC-MS/MS measurement.

3.5.4. Measurement on LTQ Orbitrap XL

Samples were analyzed with an UltiMate 3000 nano HPLC system (Dionex) using Acclaim C18 PepMap100 75 µm IDx2 cm trap and Acclaim C18 PepMap RSLC, 75 µm ID x 15 cm separation columns (buffer A: 95% H$_2$O, 5% DMSO, 0.1% FA, buffer B: 95% MeCN, 5% DMSO, 0.1% FA, flow 200 nL/min, gradient 4 to 35% buffer B in 112 min, then to 80% buffer B in 4 min and hold 80% buffer B for 4 min, then to 4% buffer B in 2 min and hold 4% buffer B for 20 min) coupled to a LTQ Orbitrap XL (Thermo Fisher). The mass spectrometer was operated in data dependent mode using the following settings: Measurement of precursors in the orbitrap at R = 60000; ion target of 1e6 in a scan range from 350 to 1400 m/z; enabled preview mode for FTMS master scans; dynamic exclusion settings (repeat count 1, repeat duration 30 s, exclusion duration 120 s, exclusion mass width relative to low mass 10 ppm, exclusion mass width relative to high mass 10 ppm); fragmentation settings (Charge states > 1, minimum signal threshold 1000 counts). Five most intensive precursors were fragmented using collision-induced dissociation (CID) with the normalized collision energy of 35%. Fragments were measured in the ion trap with an ion target of 1e4.

3.5.5. Measurement on Orbitrap Fusion

Samples were analyzed with an UltiMate 3000 nano HPLC system (Dionex) using Acclaim C18 PepMap100 75 μm ID x 2 cm trap and Acclaim Pepmap RSLC C18 (75 μm ID x 50 cm) separation columns in an EASY-spray setting coupled to an Orbitrap Fusion (Thermo Fisher). LC-MS/MS methods were adapted from a previous publication.[96]

Experiments with strain NCTC 8325:

Samples were loaded on the trap and washed with 0.1% TFA, then transferred to the analytical column (buffer A: H_2O with 0.1% FA, buffer B: MeCN with 0.1% FA, flow 200 nL/min, gradient 3 to 25% buffer B in 120 min, then to 40% buffer B in 5 min, then to 90% buffer B in 0.1 min and hold 90% buffer B for 4.9 min, then to 3% buffer B in 0.1 min and hold 3% buffer B for 9.9 min). Orbitrap Fusion was operated in a 3 s top speed data dependent mode. Full scan acquisition was performed in the orbitrap at a resolution of 120000 and an AGC target of 4e5 in a scan range of 300 – 1700 m/z. Monoisotopic precursor selection as well as dynamic exclusion (exclusion duration: 60 s, exclusion mass width relative to low mass: 10 ppm, exclusion mass width relative to high mass: 10 ppm) was enabled. Precursors with charge states of 2 – 7 and intensities greater than 5e3 were selected for fragmentation. Isolation was performed in the quadrupole using a window of 1.6 m/z. Precursors were collected to an AGC target of 3e3 for a maximum injection time of 250 ms with "inject ions for all available parallelizable time" set to true. Fragments were generated using higher-energy collisional dissociation (HCD, normalized collision energy: 27%) and detected in the ion trap at a rapid scan rate. Internal calibration was performed using the ion signal of fluoranthene cations (EASY-IC).

Experiments with strain USA300:

Samples were loaded on the trap and washed with 0.1% TFA, then transferred to the analytical column (buffer A: H_2O with 0.1% FA, buffer B: MeCN with 0.1% FA, flow 300 nL/min, gradient 5 to 22% buffer B in 115 min, then to 32% buffer B in 10 min, then to 90% buffer B in 10 min and hold 90% buffer B for 10 min, then to 5% buffer B in 0.1 min and hold 5% buffer B for 9.9 min). Orbitrap Fusion was operated in a 3 s top speed data dependent mode. Full scan acquisition was performed in the orbitrap at a resolution of 120000 and an AGC target of 2e5 in a scan range of 300 – 1500 m/z.

Monoisotopic precursor selection as well as dynamic exclusion (exclusion duration: 60 s, exclusion mass width relative to low mass: 10 ppm, exclusion mass width relative to high mass: 10 ppm) was enabled. Precursors with charge states of 2 – 7 and intensities greater than 5e3 were selected for fragmentation. Isolation was performed in the quadrupole using a window of 1.6 m/z. Precursors were collected to an AGC target of 1e4 for a maximum injection time of 35 ms with "inject ions for all available parallelizable time" set to true. Fragments were generated using higher-energy collisional dissociation (HCD, normalized collision energy: 30%) and detected in the ion trap at a rapid scan rate. Internal calibration was performed using the ion signal of fluoranthene cations (EASY-IC).

3.5.6. Measurement on Q Exactive Plus

Samples were analyzed with an UltiMate 3000 nano HPLC system (Dionex) using Acclaim C18 PepMap100 75 µm ID x 2 cm trap and Acclaim Pepmap RSLC C18 (75 µm ID x 50 cm) separation columns in an EASY-spray setting coupled to a Q Exactive Plus (Thermo Fisher). Samples were loaded on the trap and washed with 0.1% TFA, then transferred to the analytical column (buffer A: H_2O with 0.1% FA, buffer B: MeCN with 0.1% FA, flow 300 nL/min, gradient 5 to 22% buffer B in 115 min, then to 32% buffer B in 10 min, then to 90% buffer B in 10 min and hold 90% buffer B for 10 min, then to 5% buffer B in 0.1 min and hold 5% buffer B for 9.9 min). Q Exactive Plus was operated in a TOP12 data dependent mode. Full scan acquisition was performed in the orbitrap at a resolution of 70000 and an AGC target of 3e6 in a scan range of 300 – 1500 m/z. Monoisotopic precursor selection as well as dynamic exclusion (exclusion duration: 60 s) was enabled. Precursors with charge states of > 1 and intensities greater than 1e5 were selected for fragmentation. Isolation was performed in the quadrupole using a window of 1.6 m/z. Precursors were collected to an AGC target of 5e4 for a maximum injection time of 50 ms. Fragments were generated using higher-energy collisional dissociation (HCD, normalized collision energy: 27%) and detected in the orbitrap.

3.5.7. MS Data Analysis

MS raw data were analyzed with MaxQuant[173] software (1.5.3.8) using largely default settings. Peptide searches were performed against the Uniprot databases for *S. aureus* NCTC 8325 (taxon identifier: 93061) or USA300 (taxon identifier: 367830). For dimethyl

labeling quantification, the corresponding labels ("DimethLysX" and "DimethNterX"; "Max. labeled AAs" 4) were set appropriately and the "requantify" option was enabled. For label-free quantification the "LFQ" option (LFQ min. ratio count 1) as well as the "Match between runs" option were enabled.

Statistical analyses were performed with Perseus software. Rows were filtered (potential contaminant, reverse, only identified by site) and normalized ratios (DML) or LFQ intensities (LFQ) were $\log_2$ transformed. DML ratios were z-score normalized and a one-sample t-test was performed. Missing LFQ intensities were replaced by imputation from normal distribution and a two-sample t-test was performed (Benjamini-Hochberg FDR 0.05).

3.6. Whole Proteome Analysis (Chapter III)

50 mL B-medium (100 mL Erlenmeyer flasks) were inoculated 1:100 from overnight cultures of *S. aureus* NCTC 8325 wt, *ΔclpP* or clpP S98A and incubated for 16 h, 21 h or 20 h, at 37 °C (200 rpm), respectively. Different incubation times resulted in similar post exponential growth phases of all three strains. Cells were centrifuged (6000 g, 5 min, 4 °C), washed with PBS and pellets corresponding to 20 mL culture were prepared and stored at -80 °C until further use. Pellets were resuspended in PBS and transferred in 2 mL ball mill tubes (SK38, Precellys). Lysis was performed using three runs (5500 rpm, 3×20 s) with a Precellys 24 Dual ball mill system and 2 min breaks (cooling on ice) in between. The tubes were centrifuged (6000 g, 5 min, 4 °C) and the supernatant transferred in low-bind Eppendorf tubes. The protein concentration was adjusted to 1 mg/mL using BCA assay and 200 μL were subjected to new low-bind tubes for further analysis. Samples were reduced, alkylated, desalted and labeled (dimethyl labeling; including label switch throughout replicates) according to section 3.5.3. After lyophilization samples were resuspended in 600 μL 1% formic acid and filtered using equilibrated nylon filters (2×500 μL H_2O, 500 μL 0.05 N NaOH and 2 × 500 μL 1% formic acid). Samples were measured at Orbitrap Fusion (Thermo) with an injection volume of 2 μL with the method mentioned in section 3.5.5 "*Experiments with strain NCTC 8325*".

4. Synthesis

General Remarks

All reactions were carried out under argon in oven-dried glassware. All chemicals were of reagent grade or better and used without further purification. Chemicals and solvents were purchased from Sigma Aldrich. Solvents for chromatography and workup purposes were generally of reagent grade. ^{1}H NMR and ^{13}C spectra of small molecules were recorded on Bruker instruments (400 MHz or 500 MHz) and referenced to the residual proton signal of the deuterated solvent. HR-MS-ESI spectra were recorded with a Thermo Scientific LTQ FT Ultra.

Isolation of single **320** enantiomers was achieved by using chiral high-performance liquid chromatography using a Daicel Chiralpak AD-H column (250×4.6mm). Compounds **327** and **332** (both Enamine) were commercially available.

N-(2-(2-azidoethoxy)ethyl)-5-((3a*S*,4*S*,6a*R*)-2-oxohexahydro-1*H*-thieno[3,4-*d*]imidazol-4-yl)pentanamide – Biotin-PEG8-Azide
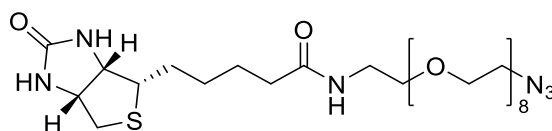
A solution of biotin (418 mg, 1.70 mmol, 1.5 eq.), HOBt (185 mg, 1.40 mmol, 1.2 eq.), DIPEA (221 mg, 1.70 mmol, 1.5 eq.) and amino-PEG8-azide (500 mg, 1.10 mmol) in a mixture of CH_2Cl_2 (32 mL) and DMF (5 mL) was stirred and HCTU (566 mg, 1.40 mmol, 1.2 eq.) was added. The reaction was stirred overnight at r.t. followed by removal of solvent *in vacuo*. Column chromatography (CH_2Cl_2 : MeOH = 10 : 1 to 10 : 1.5) yielded 504 mg (69%) of the desired product. – ^{1}H NMR (400 MHz, *MeOD-d$_4$*): 4.50 (dd, *J* = 7.9, 4.9 Hz, 1H), 4.31 (dd, *J* = 7.9, 4.4 Hz, 1H), 3.74 – 3.60 (m, 28H), 3.54 (t, *J* = 5.4 Hz, 2H), 3.37 (q, *J* = 5.5 Hz, 4H), 3.26 – 3.15 (m, 1H), 2.93 (dd, *J* = 12.8, 5.0 Hz, 1H), 2.71 (d, *J* = 12.7 Hz, 1H), 2.22 (t, *J* = 7.4 Hz, 2H), 1.84 – 1.52 (m, 4H), 1.52 – 1.26 (m, 4H). – ^{13}C NMR (125 MHz, *MeOD-d$_4$*): 174.72, 164.69, 126.87, 125.83, 119.59, 110.05, 109.24, 69.85, 69.74, 69.20, 61.96, 60.21, 55.63, 54.43, 50.37, 39.66, 38.96, 35.33, 28.39, 28.12, 25.47. – HRMS (ESI) calcd. for $C_{28}H_{53}N_6O_{10}S$ [M+H]$^+$ 665.3538, found 665.3534.

11-(3-hydroxyphenyl)-12-oxo-*N*-((1-(28-oxo-32-((3a*S*,4*S*,6a*R*)-2-oxohexahydro-1*H*-thieno[3,4-*d*]imidazol-4-yl)-3,6,9,12,15,18,21,24-octaoxa-27-azadotriacontyl)-1*H*-1,2,3-triazol-4-yl)methyl)-11,12-dihydro-5*H*-benzo[*b*]indeno[1,2-*e*][1,4]thiazepine-2-carboxamide - 371
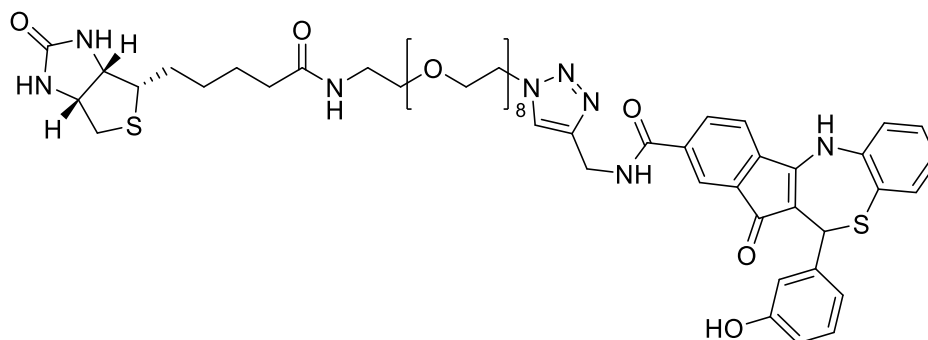
A solution of Biotin-PEG8-Azide (45.1 mg, 47.8 µmol, 1.7 eq.), 400 µL 100 mM **369** DMSO stock (17.5 mg, 40.0 µmol), CuSO$_4$ pentahydrate (6.50 mg, 26.0 µmol, 0.7 eq.) and sodium ascorbate (43.0 mg, 0.22 mmol, 5.4 eq.) in MeOH (4.5 mL) was stirred overnight at r.t. MeOH was removed *in vacuo* and DMSO by lyophilization with H$_2$O as co-solvent. Column chromatography (CH$_2$Cl$_2$: MeOH = 10 : 1.5) yielded 29.0 mg (66%) of the desired product. – ^{1}H NMR (500 MHz, *MeOD-d$_4$*): 8.39 (d, *J* = 1.4 Hz, 1H), 8.05 (s, 1H), 7.88 (dd, *J* = 7.5, 1.3 Hz, 1H), 7.54 – 7.44 (m, 2H), 7.29 (ddd, *J* = 8.3, 7.3, 1.6 Hz, 1H), 7.06 (dd, *J* = 7.7, 1.5 Hz, 1H), 6.93 (td, *J* = 7.5, 1.2 Hz, 1H), 6.85 (t, *J* = 8.1 Hz, 1H), 6.55 – 6.49 (m, 2H), 6.46 – 6.39 (m, 1H), 5.40 (s, 1H), 4.71 (d, *J* = 2.8 Hz, 2H), 4.59 (t, *J* = 4.9 Hz, 2H), 4.47 (dd, *J* = 7.8, 4.8 Hz, 1H), 4.27 (ddd, *J* = 7.9, 4.4, 1.3 Hz, 1H), 3.89 (dd, *J* = 5.5, 4.3 Hz, 2H), 3.63 – 3.47 (m, 28H), 3.35 (s, 5H), 3.23 – 3.12 (m, 1H), 2.90 (ddd, *J* = 12.8, 5.1, 1.1 Hz, 1H), 2.69 (d, *J* = 12.7 Hz, 1H), 2.19 (t, *J* = 7.3 Hz, 2H), 1.78 – 1.49 (m, 4H), 1.48 – 1.36 (m, 2H), 1.36 – 1.26 (m, 2H). – ^{13}C NMR (125 MHz, *MeOD-d$_4$*): 189.42, 174.71, 167.80, 164.68, 157.27, 156.68, 143.22, 143.01, 139.59, 137.59, 136.27, 136.19, 129.30, 128.75, 128.34, 125.15, 124.85, 124.08, 122.89, 120.15, 118.52, 117.69, 114.25, 113.10, 111.21, 69.78, 69.19, 68.96, 61.95, 60.20, 55.61, 50.09, 48.45, 45.91, 39.67, 38.93, 35.33, 35.00, 28.38, 28.10, 25.46.

Appendix

^{1}H- and ^{13}C-NMR spectra of Biotin-PEG8-Azide

^{1}H- and ^{13}C-NMR spectra of **371**

License for Chapter I
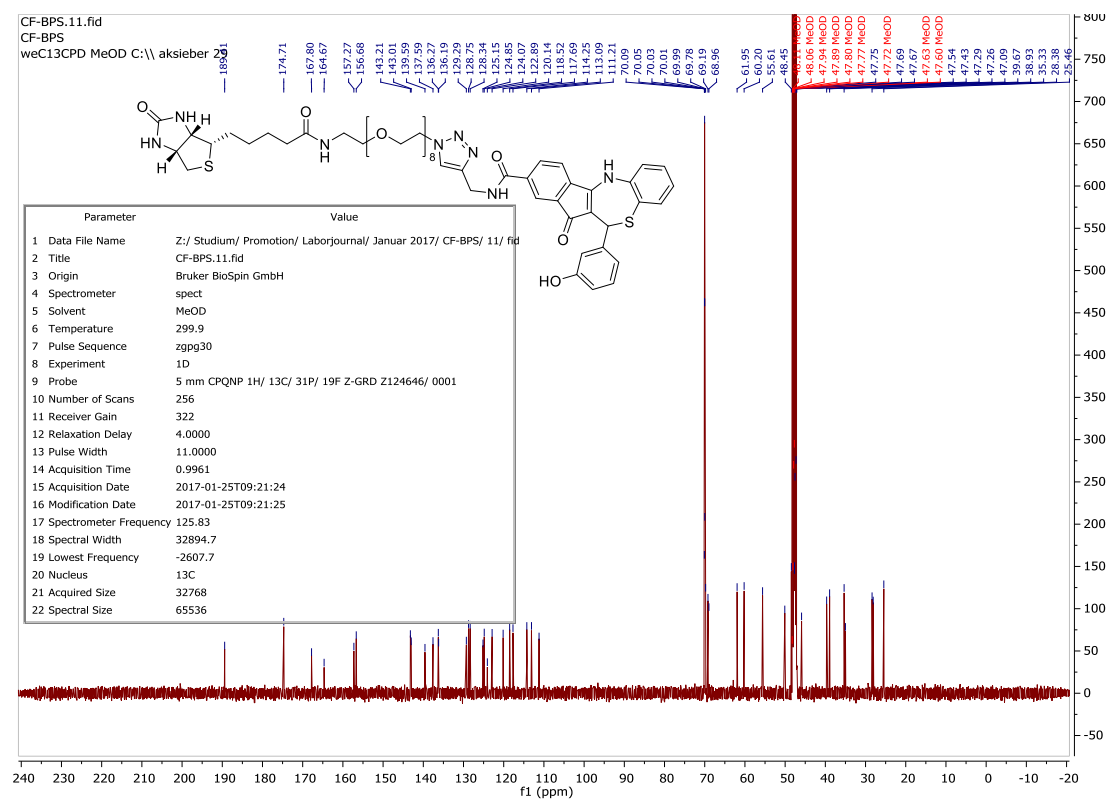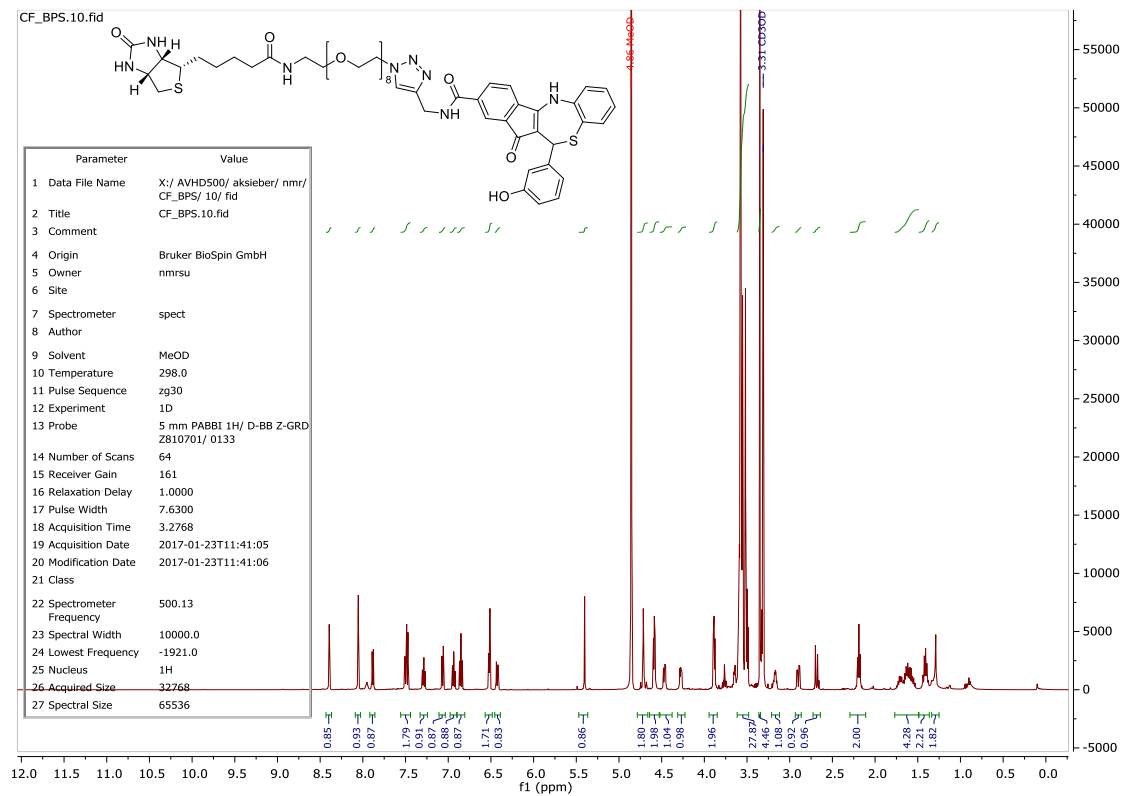
License Number	4216471436939
License date	Oct 26, 2017
Licensed Content Publisher	John Wiley and Sons
Licensed Content Publication	Angewandte Chemie International Edition
Licensed Content Title	A Chemical Disruptor of the ClpX Chaperone Complex Attenuates the Virulence of Multidrug-Resistant Staphylococcus aureus
Licensed Content Author	Christian Fetzer,Vadim S. Korotkov,Robert Thänert,Kyu Myung Lee,Martin Neuenschwander,Jens Peter von Kries,Eva Medina,Stephan A. Sieber
Licensed Content Date	Oct 12, 2017
Licensed Content Pages	1
Type of use	Dissertation/Thesis
Requestor type	Author of this Wiley article
Format	Print and electronic
Portion	Full article
Will you be translating?	No
Title of your thesis / dissertation	Virulence Attenuation through Chemical and Genetic Manipulation of the Staphylococcus aureus ClpXP Protease
Expected completion date	Nov 2017
Expected size (number of pages)	120
Requestor Location	TU München Lichtenbergstrasse 4

Bibliography

[1] A. Fleming, "On the antibacterial action of cultures of a penicillium, with special reference to their use in the isolation of B. influenzae. 1929.", *Br. J. Exp. Pathol.* **1929**, *10*, 226–236.

[2] M. Lobanovska, G. Pilla, "Penicillin's Discovery and Antibiotic Resistance: Lessons for the Future?", *Yale J. Biol. Med.* **2017**, *90*, 135–145.

[3] "The Nobel Prize in Physiology or Medicine 1945", "The Nobel Prize in Physiology or Medicine 1945," can be found under https://www.nobelprize.org/nobel_prizes/medicine/laureates/1945/, accesssed on 2017-09-26.

[4] L. L. Silver, "Challenges of Antibacterial Discovery", *Clin. Microbiol. Rev.* **2011**, *24*, 71–109.

[5] B. G. Spratt, K. D. Cromie, "Penicillin-binding proteins of gram-negative bacteria.", *Rev. Infect. Dis.* **1988**, *10*, 699–711.

[6] N. H. Georgopapadakou, F. Y. Liu, "Penicillin-binding proteins in bacteria.", *Antimicrob. Agents Chemother.* **1980**, *18*, 148–157.

[7] J. F. Fisher, S. O. Meroueh, S. Mobashery, "Bacterial Resistance to β-Lactam Antibiotics: Compelling Opportunism, Compelling Opportunity", *Chem. Rev.* **2005**, *105*, 395–424.

[8] W. P. Hammes, F. C. Neuhaus, "On the mechanism of action of vancomycin: inhibition of peptidoglycan synthesis in Gaffkya homari.", *Antimicrob. Agents Chemother.* **1974**, *6*, 722–8.

[9] P. Canepari, M. Boaretti, M. M. Lleó, G. Satta, "Lipoteichoic acid as a new target for activity of antibiotics: mode of action of daptomycin (LY146032).", *Antimicrob. Agents Chemother.* **1990**, *34*, 1220–6.

[10] W. E. Alborn, N. E. Allen, D. A. Preston, "Daptomycin disrupts membrane potential in growing Staphylococcus aureus.", *Antimicrob. Agents Chemother.* **1991**, *35*, 2282–2287.

[11] M. Boaretti, P. Canepari, M. M. Lleò, G. Satta, "The activity of daptomycin on Enterococcus faecium protoplasts: indirect evidence supporting a novel mode of action on lipoteichoic acid synthesis.", *J. Antimicrob. Chemother.* **1993**, *31*, 227–35.

[12] E. A. Groisman, J. Kayser, F. C. Soncini, "Regulation of polymyxin resistance and adaptation to low-Mg2+ environments", *J. Bacteriol.* **1997**, *179*, 7040–7045.

[13] D. Landman, C. Georgescu, D. A. Martin, J. Quale, "Polymyxins revisited.", *Clin. Microbiol. Rev.* **2008**, *21*, 449–65.

[14] K. Lewis, "Platforms for antibiotic discovery", *Nat. Rev. Drug Discovery* **2013**, *12*, 371–387.

[15] I. Chopra, P. M. Hawkey, M. Hinton, "Tetracyclines, molecular and clinical

aspects", *J. Antimicrob. Chemother.* **1992**, *29*, 245–277.

[16]   B. D. Davis, "Mechanism of bactericidal action of aminoglycosides.", *Microbiol. Rev.* **1987**, *51*, 341–50.

[17]   T. Tenson, M. Lovmar, M. Ehrenberg, "The mechanism of action of macrolides, lincosamides and streptogramin B reveals the nascent peptide exit path in the ribosome.", *J. Mol. Biol.* **2003**, *330*, 1005–14.

[18]   P. Vannuffel, C. Cocito, "Mechanism of action of streptogramins and macrolides.", *Drugs* **1996**, *51 Suppl 1*, 20–30.

[19]   R. T. Marconi, J. S. Lodmell, W. E. Hill, "Identification of a rRNA/chloramphenicol interaction site within the peptidyltransferase center of the 50 S subunit of the Escherichia coli ribosome.", *J. Biol. Chem.* **1990**, *265*, 7894–9.

[20]   S. M. Swaney, H. Aoki, M. C. Ganoza, D. L. Shinabarger, "The oxazolidinone linezolid inhibits initiation of protein synthesis in bacteria.", *Antimicrob. Agents Chemother.* **1998**, *42*, 3251–5.

[21]   E. A. Campbell, N. Korzheva, A. Mustaev, K. Murakami, S. Nair, A. Goldfarb, S. A. Darst, "Structural Mechanism for Rifampicin Inhibition of Bacterial RNA Polymerase", *Cell* **2001**, *104*, 901–912.

[22]   D. I. Edwards, "Nitroimidazole drugs-action and resistance mechanisms I. Mechanism of action", *J. Antimicrob. Chemother.* **1993**, *31*, 9–20.

[23]   D. I. Edwards, J. H. Tocher, L. D. Dale, D. Widdick, N. Virk, "Effects on DNA of Bioreducible Nitroimidazole and Benzotriazine Drugs", in *Sel. Act. Drugs by Redox Process.* (Eds.: G.E. Adams, A. Breccia, E.M. Fielden, P. Wardman), Springer US, Boston, MA, **1990**, pp. 275–283.

[24]   K. Drlica, X. Zhao, "DNA gyrase, topoisomerase IV, and the 4-quinolones.", *Microbiol. Mol. Biol. Rev. MMBR* **1997**, *61*, 377–392.

[25]   A. Banerjee, E. Dubnau, A. Quemard, V. Balasubramanian, K. Um, T. Wilson, D. Collins, G. de Lisle, W. Jacobs, "inhA, a gene encoding a target for isoniazid and ethionamide in Mycobacterium tuberculosis", *Science* **1994**, *263*, 227–230.

[26]   G. S. Timmins, S. Master, F. Rusnak, V. Deretic, "Nitric Oxide Generated from Isoniazid Activation by KatG: Source of Nitric Oxide and Activity against Mycobacterium tuberculosis", *Antimicrob. Agents Chemother.* **2004**, *48*, 3006–3009.

[27]   G. M. Brown, "The biosynthesis of folic acid", *J. Biol. Chem.* **1962**, *237*, 536–40.

[28]   P. Huovinen, L. Sundstrom, G. Swedberg, O. Skold, "Trimethoprim and sulfonamide resistance", *Antimicrob. Agents Chemother.* **1995**, *39*, 279–289.

[29]   E. P. Abraham, E. Chain, "An Enzyme from Bacteria able to Destroy Penicillin", *Nature* **1940**, *146*, 837–837.

[30]   R. I. Aminov, "A Brief History of the Antibiotic Era: Lessons Learned and Challenges for the Future", *Front. Microbiol.* **2010**, *1*, 1–7.

[31]   I. Chopra, L. Hesse, A. O'Neill, "Discovery and development of new anti-bacterial

drugs", in *Elsevier Sci.*, Elsevier, **2002**, pp. 213–225.

[32] A. Coates, Y. Hu, R. Bax, C. Page, "The future challenges facing the development of new antimicrobial drugs", *Nat. Rev. Drug Discovery* **2002**, *1*, 895–910.

[33] D. L. Paterson, R. A. Bonomo, "Extended-Spectrum beta-Lactamases : a Clinical Update", *Clin. Microbiol. Rev.* **2005**, *18*, 657–686.

[34] D. M. Livermore, "Interplay of impermeability and chromosomal beta-lactamase activity in imipenem-resistant Pseudomonas aeruginosa.", *Antimicrob. Agents Chemother.* **1992**, *36*, 2046–8.

[35] H. I. Zgurskaya, H. Nikaido, "Multidrug resistance mechanisms: drug efflux across two membranes", *Mol. Microbiol.* **2000**, *37*, 219–225.

[36] World Health Organization, "Worldwide country situation analysis: response to antimicrobial resistance", **2015**.

[37] World Health Organization, "Prioritization of Pathogens To Guide Discovery, Research and Development of New Antibiotics for Drug-Resistant Bacterial Infections, Including Tuberculosis", **2017**.

[38] L. M. Weiner, A. K. Webb, B. Limbago, M. A. Dudeck, J. Patel, A. J. Kallen, J. R. Edwards, D. M. Sievert, "Antimicrobial-Resistant Pathogens Associated With Healthcare-Associated Infections: Summary of Data Reported to the National Healthcare Safety Network at the Centers for Disease Control and Prevention, 2011–2014", *Infect. Control Hosp. Epidemiol.* **2016**, *37*, 1288–1301.

[39] World Health Organization, "WHO | Antibacterial Agents in Clinical Development", **2017**.

[40] T. Kostyanev, M. J. M. Bonten, S. O'Brien, H. Steel, S. Ross, B. François, E. Tacconelli, M. Winterhalter, R. A. Stavenger, A. Karlén, et al., "The Innovative Medicines Initiative's New Drugs for Bad Bugs programme: European public–private partnerships for the development of new strategies to tackle antibiotic resistance", *J. Antimicrob. Chemother.* **2016**, *71*, 290–295.

[41] M. F. Chellat, L. Raguž, R. Riedl, "Targeting Antibiotic Resistance", *Angew. Chem. Int. Ed.* **2016**, *55*, 6600–6626.

[42] W. Fast, L. D. Sutton, "Metallo-β-lactamase: inhibitors and reporter substrates.", *Biochim. Biophys. Acta* **2013**, *1834*, 1648–59.

[43] D. Brown, "Antibiotic resistance breakers: can repurposed drugs fill the antibiotic discovery void?", *Nat. Rev. Drug Discovery* **2015**, *14*, 821–832.

[44] M. Stavri, L. J. V. Piddock, S. Gibbons, "Bacterial efflux pump inhibitors from natural sources", *J. Antimicrob. Chemother.* **2007**, *59*, 1247–1260.

[45] D. A. Rasko, V. Sperandio, "Anti-virulence strategies to combat bacteria-mediated disease", *Nat. Rev. Drug Discovery* **2010**, *9*, 117–128.

[46] S. W. Dickey, G. Y. C. Cheung, M. Otto, "Different drugs for bad bugs: antivirulence strategies in the age of antibiotic resistance", *Nat. Rev. Drug Discovery* **2017**, *16*, 457–471.

[47]   S. M. Drawz, K. M. Papp-Wallace, R. A. Bonomo, "New β-lactamase inhibitors: a therapeutic renaissance in an MDR world.", *Antimicrob. Agents Chemother.* **2014**, *58*, 1835–46.

[48]   A. Ogston, "Report upon Micro-Organisms in Surgical Diseases.", *Br. Med. J.* **1881**, *1*, 369–375.

[49]   L. Thomer, O. Schneewind, D. Missiakas, "Pathogenesis of Staphylococcus aureus Bloodstream Infections", *Annu. Rev. Pathol.: Mech. Dis.* **2016**, *11*, 343–364.

[50]   A. Ogston, "Micrococcus Poisoning.", *J. Anat. Physiol.* **1882**, *17*, 24–58.

[51]   F. J. Rosenbach, "Mikro-Organismen bei den Wund-Infections-Krankheiten des Menschen", Bergmann, Wiesbaden, **1884**.

[52]   G. Y. Liu, A. Essex, J. T. Buchanan, V. Datta, H. M. Hoffman, J. F. Bastian, J. Fierer, V. Nizet, "Staphylococcus aureus golden pigment impairs neutrophil killing and promotes virulence through its antioxidant activity", *J. Exp. Med.* **2005**, *202*, 209–215.

[53]   A. Clauditz, A. Resch, K. P. Wieland, A. Peschel, F. Götz, "Staphyloxanthin plays a role in the fitness of Staphylococcus aureus and its ability to cope with oxidative stress", *Infect. Immun.* **2006**, *74*, 4950–4953.

[54]   A. Zecconi, F. Scali, "Staphylococcus aureus virulence factors in evasion from innate immune defenses in human and animal diseases", *Immunol. Lett.* **2013**, *150*, 12–22.

[55]   T. J. Foster, "Immune evasion by staphylococci", *Nat. Rev. Microbiol.* **2005**, *3*, 948–958.

[56]   M. Otto, "Staphylococcus aureus toxins", *Curr. Opin. Microbiol.* **2014**, *17*, 32–37.

[57]   N. Balaban, A. Rasooly, "Staphylococcal enterotoxins", *Int. J. Food Microbiol.* **2000**, *61*, 1–10.

[58]   D. J. Fast, P. M. Schlievert, R. D. Nelson, "Toxic shock syndrome-associated staphylococcal and streptococcal pyrogenic toxins are potent inducers of tumor necrosis factor production", *Infect. Immun.* **1989**, *57*, 291–4.

[59]   M. Jusko, J. Potempa, T. Kantyka, E. Bielecka, H. K. Miller, M. Kalinska, G. Dubin, P. Garred, L. N. Shaw, A. M. Blom, "Staphylococcal proteases aid in evasion of the human complement system", *J. Innate Immun.* **2014**, *6*, 31–46.

[60]   M. Bukowski, B. Wladyka, G. Dubin, "Exfoliative toxins of Staphylococcus aureus", *Toxins* **2010**, *2*, 1148–1165.

[61]   T. Jin, M. Bokarewa, T. Foster, J. Mitchell, J. Higgins, A. Tarkowski, "Staphylococcus aureus resists human defensins by production of staphylokinase, a novel bacterial evasion mechanism", *J. Immunol.* **2004**, *172*, 1169–1176.

[62]   L. Thomer, O. Schneewind, D. Missiakas, "Multiple ligands of von willebrand factor-binding protein (vWbp) promote Staphylococcus aureus clot formation in human plasma", *J. Biol. Chem.* **2013**, *288*, 28283–28292.

[63]   A. G. Cheng, M. McAdow, H. K. Kim, T. Bae, D. M. Missiakas, O. Schneewind,

"Contribution of Coagulases towards Staphylococcus aureus Disease and Protective Immunity", *PLoS Pathog.* **2010**, *6*, e1001036.

[64]   J. Deisenhofer, "Crystallographic Refinement and Atomic Models of a Human Fc Fragment and Its Complex with Fragment B of Protein A from Staphylococcus aureus at 2.9- and 2.8-Å Resolution", *Biochemistry* **1981**, *20*, 2361–2370.

[65]   N. Palmqvist, T. Foster, A. Tarkowski, E. Josefsson, "Protein A is a virulence factor in Staphylococcus aureus arthritis and septic death", *Microb. Pathog.* **2002**, *33*, 239–249.

[66]   D. Mcdevitt, T. Nanavaty, K. House-Pompeo, E. Bell, N. Turner, L. Mcintire, T. Foster, M. HooK, "Characterization of the Interaction Between the Staphylococcus Aureus Clumping Factor (ClfA) and Fibrinogen", *Eur. J. Biochem.* **1997**, *247*, 416–424.

[67]   J. Higgins, A. Loughman, K. P. M. Van Kessel, J. A. G. Van Strijp, T. J. Foster, "Clumping factor A of Staphylococcus aureus inhibits phagocytosis by human polymorphonuclear leucocytes", *FEMS Microbiol. Lett.* **2006**, *258*, 290–296.

[68]   H. F. Wertheim, D. C. Melles, M. C. Vos, W. van Leeuwen, A. van Belkum, H. a Verbrugh, J. L. Nouwen, "The role of nasal carriage in Staphylococcus aureus infections", *Lancet Infect. Dis.* **2005**, *5*, 751–762.

[69]   S. Y. C. Tong, J. S. Davis, E. Eichenberger, T. L. Holland, V. G. Fowler, "Staphylococcus aureus Infections: Epidemiology, Pathophysiology, Clinical Manifestations, and Management", *Clin. Microbiol. Rev.* **2015**, *28*, 603–661.

[70]   F. D. Lowy, "*Staphylococcus aureus* Infections", *N. Engl. J. Med.* **1998**, *339*, 520–532.

[71]   S. J. van Hal, S. O. Jensen, V. L. Vaska, B. A. Espedido, D. L. Paterson, I. B. Gosbell, "Predictors of Mortality in Staphylococcus aureus Bacteremia", *Clin. Microbiol. Rev.* **2012**, *25*, 362–386.

[72]   C. R. Arciola, D. Campoccia, P. Speziale, L. Montanaro, J. W. Costerton, "Biofilm formation in Staphylococcus implant infections. A review of molecular mechanisms and implications for biofilm-resistant materials", *Biomaterials* **2012**, *33*, 5967–5982.

[73]   P. S. Stewart, J. William Costerton, "Antibiotic resistance of bacteria in biofilms", *The Lancet* **2001**, *358*, 135–138.

[74]   C. Rağbetli, M. Parlak, Y. Bayram, H. Guducuoglu, N. Ceylan, "Evaluation of Antimicrobial Resistance in Staphylococcus aureus Isolates by Years", *Interdiscip. Perspect. Infect. Dis.* **2016**, *2016*, 1–4.

[75]   European Centre for Disease Prevention and Control, "Antimicrobial resistance surveillance in Europe 2015. Annual Report of the European Antimicrobial Resistance Surveillance Network (EARS-Net)", Stockholm, **2017**.

[76]   J. B. Locke, D. E. Zuill, C. R. Scharn, J. Deane, D. F. Sahm, G. A. Denys, R. V. Goering, K. J. Shawa, "Linezolid-resistant Staphylococcus aureus strain 1128105, the first known clinical isolate possessing the cfr multidrug resistance gene", *Antimicrob.*

Agents Chemother. **2014**, *58*, 6592–6598.

[77] A. S. Bayer, T. Schneider, H.-G. Sahl, "Mechanisms of daptomycin resistance in Staphylococcus aureus: role of the cell membrane and cell wall", *Ann. N. Y. Acad. Sci.* **2013**, *1277*, 139–158.

[78] K. Hiramatsu, H. Hanaki, T. Ino, K. Yabuta, T. Oguri, F. C. Tenover, "Methicillin-resistant Staphylococcus aureus clinical strain with reduced vancomycin susceptibility", *J. Antimicrob. Chemother.* **1997**, *40*, 135–136.

[79] S. Mühlen, P. Dersch, "Anti-virulence Strategies to Target Bacterial Infections", *Curr. Top. Microbiol. Immunol.* **2016**, *398*, 147–183.

[80] A. E. Clatworthy, E. Pierson, D. T. Hung, "Targeting virulence: a new paradigm for antimicrobial therapy.", *Nat. Chem. Biol.* **2007**, *3*, 541–548.

[81] R. C. Allen, R. Popat, S. P. Diggle, S. P. Brown, "Targeting virulence: can we make evolution-proof drugs?", *Nat. Rev. Microbiol.* **2014**, *12*, 300–308.

[82] Behring, "Die Blutserumtherapie bei Diphtherie und Tetanus", *Zeitschrift für Hyg. und Infect.* **1892**, *12*, 1–9.

[83] V. Oganesyan, L. Peng, M. M. Damschroder, L. Cheng, A. Sadowska, C. Tkaczyk, B. R. Sellman, H. Wu, W. F. Dall'Acqua, "Mechanisms of Neutralization of a Human Anti-α-toxin Antibody", *J. Biol. Chem.* **2014**, *289*, 29874–29880.

[84] H. Rouha, A. Badarau, Z. C. Visram, M. B. Battles, B. Prinz, Z. Magyarics, G. Nagy, I. Mirkina, L. Stulik, M. Zerbs, et al., "Five birds, one stone: Neutralization of α-hemolysin and 4 bi-component leukocidins of Staphylococcus aureus with a single human monoclonal antibody", *mAbs* **2015**, *7*, 243–254.

[85] A. Badarau, H. Rouha, S. Malafa, M. B. Battles, L. Walker, N. Nielson, I. Dolezilkova, A. Teubenbacher, S. Banerjee, B. Maierhofer, et al., "Context matters: The importance of dimerization-induced conformation of the LukGH leukocidin of Staphylococcus aureus for the generation of neutralizing antibodies", *mAbs* **2016**, *8*, 1347–1360.

[86] O. Schneewind, P. Model, V. A. Fischetti, "Sorting of protein a to the staphylococcal cell wall", *Cell* **1992**, *70*, 267–281.

[87] S. K. Mazmanian, G. Liu, E. R. Jensen, E. Lenoy, O. Schneewind, "Staphylococcus aureus sortase mutants defective in the display of surface proteins and in the pathogenesis of animal infections", *Proc. Natl. Acad. Sci.* **2000**, *97*, 5510–5515.

[88] J. Zhang, H. Liu, K. Zhu, S. Gong, S. Dramsi, Y.-T. Wang, J. Li, F. Chen, R. Zhang, L. Zhou, et al., "Antiinfective therapy with a small molecule inhibitor of Staphylococcus aureus sortase", *Proc. Natl. Acad. Sci.* **2014**, *111*, 13517–13522.

[89] E. A. George, T. W. Muir, "Molecular mechanisms of agr quorum sensing in virulent staphylococci", *ChemBioChem* **2007**, *8*, 847–855.

[90] B. Wang, T. W. Muir, "Regulation of Virulence in Staphylococcus aureus: Molecular Mechanisms and Remaining Puzzles", *Cell Chem. Biol.* **2016**, *23*, 214–224.

[91]   E. K. Sully, N. Malachowa, B. O. Elmore, S. M. Alexander, J. K. Femling, B. M. Gray, F. R. DeLeo, M. Otto, A. L. Cheung, B. S. Edwards, et al., "Selective Chemical Inhibition of agr Quorum Sensing in Staphylococcus aureus Promotes Host Defense with Minimal Impact on Resistance", *PLoS Pathog.* **2014**, *10*, e1004174.

[92]   D. Frees, K. Sørensen, H. Ingmer, "Global virulence regulation in Staphylococcus aureus: pinpointing the roles of ClpP and ClpX in the sar/agr regulatory network.", *Infect. Immun.* **2005**, *73*, 8100–8108.

[93]   D. Frees, S. N. A. Qazi, P. J. Hill, H. Ingmer, "Alternative roles of ClpX and ClpP in Staphylococcus aureus stress tolerance and virulence", *Mol. Microbiol.* **2003**, *48*, 1565–1578.

[94]   A. Michel, F. Agerer, C. R. Hauck, M. Herrmann, J. Ullrich, J. Hacker, K. Ohlsen, "Global Regulatory Impact of ClpP Protease of Staphylococcus aureus on Regulons Involved in Virulence, Oxidative Stress Response, Autolysis, and DNA Repair", *J. Bacteriol.* **2006**, *188*, 5783–5796.

[95]   F. Weinandy, K. Lorenz-Baath, V. S. Korotkov, T. Böttcher, S. Sethi, T. Chakraborty, S. A. Sieber, "A β-Lactone-Based Antivirulence Drug Ameliorates Staphylococcus aureus Skin Infections in Mice", *ChemMedChem* **2014**, *9*, 710–713.

[96]   J. Krysiak, M. Stahl, J. Vomacka, C. Fetzer, M. Lakemeyer, A. Fux, S. A. Sieber, "Quantitative Map of β-Lactone-Induced Virulence Regulation", *J. Proteome Res.* **2017**, *16*, 1180–1192.

[97]   T. Böttcher, S. A. Sieber, "β-lactones as specific inhibitors of ClpP attenuate the production of extracellular virulence factors of Staphylococcus aureus", *J. Am. Chem. Soc.* **2008**, *130*, 14400–14401.

[98]   D. Frees, U. Gerth, H. Ingmer, "Clp chaperones and proteases are central in stress survival, virulence and antibiotic resistance of Staphylococcus aureus", *Int. J. Med. Microbiol.* **2014**, *304*, 142–149.

[99]   M. Gersch, A. List, M. Groll, S. A. Sieber, "Insights into structural network responsible for oligomerization and activity of bacterial virulence regulator caseinolytic protease P (ClpP) protein", *J. Biol. Chem.* **2012**, *287*, 9484–9494.

[100] F. Ye, J. Zhang, H. Liu, R. Hilgenfeld, R. Zhang, X. Kong, L. Li, J. Lu, X. Zhang, D. Li, et al., "Helix Unfolding/Refolding Characterizes the Functional Dynamics of Staphylococcus aureus Clp Protease", *J. Biol. Chem.* **2013**, *288*, 17643–17653.

[101] J. Zhang, F. Ye, L. Lan, H. Jiang, C. Luo, C.-G. Yang, "Structural Switching of Staphylococcus aureus Clp Protease", *J. Biol. Chem.* **2011**, *286*, 37590–37601.

[102] S. R. Geiger, T. Böttcher, S. A. Sieber, P. Cramer, "A Conformational Switch Underlies ClpP Protease Function", *Angew. Chem. Int. Ed.* **2011**, *50*, 5749–5752.

[103] R. Sprangers, A. Gribun, P. M. Hwang, W. A. Houry, L. E. Kay, "Quantitative NMR spectroscopy of supramolecular complexes: Dynamic side pores in ClpP are important for product release", *Proc. Natl. Acad. Sci.* **2005**, *102*, 16678–16683.

[104] K. Liu, A. Ologbenla, W. A. Houry, "Dynamics of the ClpP serine protease: A model for self-compartmentalized proteases.", *Crit. Rev. Biochem. Mol. Biol.* **2014**, *9238*,

1–13.

[105] J. Feng, S. Michalik, A. N. Varming, J. H. Andersen, D. Albrecht, L. Jelsbak, S. Krieger, K. Ohlsen, M. Hecker, U. Gerth, et al., "Trapping and proteomic identification of cellular substrates of the ClpP protease in Staphylococcus aureus", *J. Proteome Res.* **2013**, *12*, 547–558.

[106] S. E. Glynn, A. Martin, A. R. Nager, T. A. Baker, R. T. Sauer, "Structures of Asymmetric ClpX Hexamers Reveal Nucleotide-Dependent Motions in a AAA+ Protein-Unfolding Machine", *Cell* **2009**, *139*, 744–756.

[107] G. L. Hersch, R. E. Burton, D. N. Bolon, T. A. Baker, R. T. Sauer, "Asymmetric Interactions of ATP with the AAA+ ClpX6 Unfoldase: Allosteric Control of a Protein Machine", *Cell* **2005**, *121*, 1017–1027.

[108] A. H. Abdelhakim, E. C. Oakes, R. T. Sauer, T. A. Baker, "Unique Contacts Direct High-Priority Recognition of the Tetrameric Mu Transposase-DNA Complex by the AAA+ Unfoldase ClpX", *Mol. Cell* **2008**, *30*, 39–50.

[109] J. L. Camberg, J. R. Hoskins, S. Wickner, "ClpXP protease degrades the cytoskeletal protein, FtsZ, and modulates FtsZ polymer dynamics", *Proc. Natl. Acad. Sci.* **2009**, *106*, 10614–10619.

[110] C. J. LaBreck, S. May, M. G. Viola, J. Conti, J. L. Camberg, "The protein chaperone ClpX targets native and non-native aggregated substrates for remodeling, disassembly and degradation with ClpP", *Front. Mol. Biosci.* **2017**, *4*, 26.

[111] R. T. Sauer, T. A. Baker, "AAA+ Proteases: ATP-Fueled Machines of Protein Destruction", *Annu. Rev. Biochem.* **2011**, *80*, 587–612.

[112] K. C. Keiler, P. R. H. Waller, R. T. Sauer, "Role of a Peptide Tagging System in Degradation of Proteins Synthesized from Damaged Messenger RNA", *Science* **1996**, *271*, 990–993.

[113] S. Gottesman, E. Roche, Y. N. Zhou, R. T. Sauer, "The ClpXP and ClpAP proteases degrade proteins with carboxy-terminal peptide tails added by the SsrA-tagging system", *Genes Dev.* **1998**, *12*, 1338–1347.

[114] T. A. Baker, R. T. Sauer, "ClpXP, an ATP-powered unfolding and protein-degradation machine", *Biochim. Biophys. Acta - Mol. Cell Res.* **2012**, *1823*, 15–28.

[115] A. Martin, T. A. Baker, R. T. Sauer, "Diverse Pore Loops of the AAA+ ClpX Machine Mediate Unassisted and Adaptor-Dependent Recognition of ssrA-Tagged Substrates", *Mol. Cell* **2008**, *29*, 441–450.

[116] O. Iosefson, A. R. Nager, T. A. Baker, R. T. Sauer, "Coordinated gripping of substrate by subunits of a AAA+ proteolytic machine", *Nat. Chem. Biol.* **2015**, *11*, 201–206.

[117] Y. I. Kim, I. Levchenko, K. Fraczkowska, R. V Woodruff, R. T. Sauer, T. A. Baker, "Molecular determinants of complex formation between Clp/Hsp100 ATPases and the ClpP peptidase.", *Nat. Struct. Biol.* **2001**, *8*, 230–3.

[118] A. Martin, T. A. Baker, R. T. Sauer, "Distinct Static and Dynamic Interactions Control ATPase-Peptidase Communication in a AAA+ Protease", *Mol. Cell* **2007**,

27, 41–52.

[119] L. Cheng, T. A. Naumann, A. R. Horswill, S.-J. Hong, B. J. Venters, J. W. Tomsho, S. J. Benkovic, K. C. Keiler, "Discovery of antibacterial cyclic peptides that inhibit the ClpXP protease", *Protein Sci.* **2007**, *16*, 1535–1542.

[120] S. M. McGillivray, D. N. Tran, N. S. Ramadoss, J. N. Alumasa, C. Y. Okumura, G. Sakoulas, M. M. Vaughn, D. X. Zhang, K. C. Keiler, V. Nizet, "Pharmacological inhibition of the ClpXP protease increases bacterial susceptibility to host cathelicidin antimicrobial peptides and cell envelope-active antibiotics", *Antimicrob. Agents Chemother.* **2012**, *56*, 1854–1861.

[121] H. Brötz-Oesterhelt, D. Beyer, H.-P. Kroll, R. Endermann, C. Ladel, W. Schroeder, B. Hinzen, S. Raddatz, H. Paulsen, K. Henninger, et al., "Dysregulation of bacterial proteolytic machinery by a new class of antibiotics", *Nat. Med.* **2005**, *11*, 1082–1087.

[122] J. Kirstein, A. Hoffmann, H. Lilie, R. Schmidt, H. Rübsamen-Waigmann, H. Brötz-Oesterhelt, A. Mogk, K. Turgay, "The antibiotic ADEP reprogrammes ClpP, switching it from a regulated to an uncontrolled protease", *EMBO Mol. Med.* **2009**, *1*, 37–49.

[123] D. H. S. Li, Y. S. Chung, M. Gloyd, E. Joseph, R. Ghirlando, G. D. Wright, Y.-Q. Cheng, M. R. Maurizi, A. Guarné, J. Ortega, "Acyldepsipeptide Antibiotics Induce the Formation of a Structured Axial Channel in ClpP: A Model for the ClpX/ClpA-Bound State of ClpP", *Chem. Biol.* **2010**, *17*, 959–969.

[124] M. Gersch, K. Famulla, M. Dahmen, C. Göbl, I. Malik, K. Richter, V. S. Korotkov, P. Sass, H. Rübsamen-Schaeff, T. Madl, et al., "AAA+ chaperones and acyldepsipeptides activate the ClpP protease via conformational control", *Nat. Commun.* **2015**, *6*, 6320.

[125] A. Szyk, M. R. Maurizi, "Crystal structure at 1.9 Å of E. coli ClpP with a peptide covalently bound at the active site", *J. Struct. Biol.* **2006**, *156*, 165–174.

[126] M. Gersch, R. Kolb, F. Alte, M. Groll, S. A. Sieber, "Disruption of oligomerization and dehydroalanine formation as mechanisms for ClpP protease inhibition", *J. Am. Chem. Soc.* **2014**, *136*, 1360–1366.

[127] M. Gersch, F. Gut, V. S. Korotkov, J. Lehmann, T. Böttcher, M. Rusch, C. Hedberg, H. Waldmann, G. Klebe, S. A. Sieber, "The Mechanism of Caseinolytic Protease (ClpP) Inhibition", *Angew. Chem. Int. Ed.* **2013**, *52*, 3009–3014.

[128] T. Böttcher, S. A. Sieber, "Structurally refined β-lactones as potent inhibitors of devastating bacterial virulence factors", *ChemBioChem* **2009**, *10*, 663–666.

[129] E. Zeiler, V. S. Korotkov, K. Lorenz-Baath, T. Böttcher, S. A. Sieber, "Development and characterization of improved β-lactone-based anti-virulence drugs targeting ClpP", *Bioorganic Med. Chem.* **2012**, *20*, 583–591.

[130] T. Böttcher, S. A. Sieber, "β-Lactones as Privileged Structures for the Active-Site Labeling of Versatile Bacterial Enzyme Classes", *Angew. Chem. Int. Ed.* **2008**, *47*, 4600–4603.

[131] M. W. Hackl, M. Lakemeyer, M. Dahmen, M. Glaser, A. Pahl, K. Lorenz-Baath, T. Menzel, S. Sievers, T. Böttcher, I. Antes, et al., "Phenyl Esters Are Potent Inhibitors of Caseinolytic Protease P and Reveal a Stereogenic Switch for Deoligomerization", *J. Am. Chem. Soc.* **2015**, *137*, 8475–8483.

[132] A. Pahl, M. Lakemeyer, M.-T. Vielberg, M. W. Hackl, J. Vomacka, V. S. Korotkov, M. L. Stein, C. Fetzer, K. Lorenz-Baath, K. Richter, et al., "Reversible Inhibitors Arrest ClpP in a Defined Conformational State that Can Be Revoked by ClpX Association", *Angew. Chem. Int. Ed.* **2015**, *54*, 15892–15896.

[133] Y. I. Kim, R. E. Burton, B. M. Burton, R. T. Sauer, T. A. Baker, "Dynamics of substrate denaturation and translocation by the ClpXP degradation machine.", *Mol. Cell* **2000**, *5*, 639–648.

[134] G. L. Hersch, T. A. Baker, R. T. Sauer, "SspB delivery of substrates for ClpXP proteolysis probed by the design of improved degradation tags", *Proc. Natl. Acad. Sci.* **2004**, *101*, 12136–12141.

[135] E. K. Schmitt, M. Riwanto, V. Sambandamurthy, S. Roggo, C. Miault, C. Zwingelstein, P. Krastel, C. Noble, D. Beer, S. P. S. Rao, et al., "The natural product cyclomarin kills mycobacterium tuberculosis by targeting the ClpC1 subunit of the caseinolytic protease", *Angew. Chem. Int. Ed.* **2011**, *50*, 5889–5891.

[136] E. Gavrish, C. S. Sit, S. Cao, O. Kandror, A. Spoering, A. Peoples, L. Ling, A. Fetterman, D. Hughes, A. Bissell, et al., "Lassomycin, a ribosomally synthesized cyclic peptide, kills mycobacterium tuberculosis by targeting the ATP-dependent protease ClpC1P1P2", *Chem. Biol.* **2014**, *21*, 509–518.

[137] M. J. Evans, B. F. Cravatt, "Mechanism-based profiling of enzyme families", *Chem. Rev.* **2006**, *106*, 3279–3301.

[138] P. P. Geurink, L. M. Prely, G. A. Van Der Marel, R. Bischoff, H. S. Overkleeft, "Photoaffinity labeling in activity-based protein profiling", *Top. Curr. Chem.* **2012**, *324*, 85–113.

[139] D. Greenbaum, A. Baruch, L. Hayrapetian, Z. Darula, A. Burlingame, K. F. Medzihradszky, M. Bogyo, "Chemical Approaches for Functionally Probing the Proteome", *Mol. Cell. Proteomics* **2002**, *1*, 60–68.

[140] Z. Li, P. Hao, L. Li, C. Y. J. Tan, X. Cheng, G. Y. J. Chen, S. K. Sze, H. M. Shen, S. Q. Yao, "Design and synthesis of minimalist terminal alkyne-containing diazirine photo-crosslinkers and their incorporation into kinase inhibitors for cell- and tissue-based proteome profiling", *Angew. Chem. Int. Ed.* **2013**, *52*, 8551–8556.

[141] R. Huisgen, "Proceedings of the Chemical Society. October 1961", *Proc. Chem. Soc.* **1961**, 357.

[142] V. V Rostovtsev, L. G. Green, V. V Fokin, K. B. Sharpless, "A Stepwise Huisgen Cycloaddition Process: Copper(I)-Catalyzed Regioselective "Ligation" of Azides and Terminal Alkynes", *Angew. Chem. Int. Ed.* **2002**, *41*, 2596–2599.

[143] C. W. Tornøe, C. Christensen, M. Meldal, "Peptidotriazoles on Solid Phase: [1,2,3]-Triazoles by Regiospecific Copper(I)-Catalyzed 1,3-Dipolar Cycloadditions of

Terminal Alkynes to Azides", *J. Org. Chem.* **2002**, *67*, 3057–3064.

[144] P. Kleiner, W. Heydenreuter, M. Stahl, V. S. Korotkov, S. A. Sieber, "A Whole Proteome Inventory of Background Photocrosslinker Binding", *Angew. Chem. Int. Ed.* **2017**, *56*, 1396–1401.

[145] S. Sato, A. Murata, T. Shirakawa, M. Uesugi, "Biochemical Target Isolation for Novices: Affinity-Based Strategies", *Chem. Biol.* **2010**, *17*, 616–623.

[146] B. Lomenick, R. W. Olsen, J. Huang, "Identification of Direct Protein Targets of Small Molecules", *ACS Chem. Biol.* **2011**, *6*, 34–46.

[147] M. Kawatani, H. Osada, "Affinity-based target identification for bioactive small molecules", *MedChemComm* **2014**, *5*, 277.

[148] J. Cox, M. Y. Hein, C. A. Luber, I. Paron, N. Nagaraj, M. Mann, "Accurate Proteome-wide Label-free Quantification by Delayed Normalization and Maximal Peptide Ratio Extraction, Termed MaxLFQ", *Mol. Cell. Proteomics* **2014**, *13*, 2513–2526.

[149] M. Arnaud, A. Chastanet, M. Débarbouillé, "New vector for efficient allelic replacement in naturally nontransformable, low-GC-content, gram-positive bacteria.", *Appl. Environ. Microbiol.* **2004**, *70*, 6887–91.

[150] J. Valle, A. Toledo-Arana, C. Berasain, J.-M. Ghigo, B. Amorena, J. R. Penadés, I. Lasa, "SarA and not σB is essential for biofilm development by Staphylococcus aureus", *Mol. Microbiol.* **2003**, *48*, 1075–1087.

[151] J. Y. Park, B. Y. Moon, J. W. Park, J. A. Thornton, Y. H. Park, K. S. Seo, "Genetic engineering of a temperate phage-based delivery system for CRISPR/Cas9 antimicrobials against Staphylococcus aureus", *Sci. Reports* **2017**, *7*, 44929.

[152] I. R. Monk, I. M. Shah, M. Xu, M.-W. Tan, T. J. Foster, "Transforming the untransformable: application of direct transformation to manipulate genetically Staphylococcus aureus and Staphylococcus epidermidis.", *mBio* **2012**, *3*, DOI 10.1128/mBio.00277-11.

[153] I. R. Monk, T. J. Foster, "Genetic manipulation of Staphylococci—breaking through the barrier", *Front. Cell. Infect. Microbiol.* **2012**, *2*, 1–9.

[154] I. R. Monk, J. J. Tree, B. P. Howden, T. P. Stinear, T. J. Foster, "Complete Bypass of Restriction Systems for Major Staphylococcus aureus Lineages.", *mBio* **2015**, *6*, e00308-15.

[155] R. Higuchi, B. Krummel, R. K. Saiki, "A general method of in vitro preparation and specific mutagenesis of DNA fragments: study of protein and DNA interactions", *Nucleic Acids Res.* **1988**, *16*, 7351–7367.

[156] M. R. Sadykov, "Restriction-Modification Systems as a Barrier for Genetic Manipulation of Staphylococcus aureus.", *Methods Mol. Biol. (Clifton, N.J.)* **2016**, *1373*, 9–23.

[157] M. J. Jones, N. P. Donegan, I. V. Mikheyeva, A. L. Cheung, "Improving transformation of Staphylococcus aureus belonging to the CC1, CC5 and CC8 clonal complexes", *PLoS One* **2015**, *10*, 1–14.

[158] B. N. Kreiswirth, S. Löfdahl, M. J. Betley, M. O'Reilly, P. M. Schlievert, M. S. Bergdoll, R. P. Novick, "The toxic shock syndrome exotoxin structural gene is not detectably transmitted by a prophage.", *Nature* **1983**, *305*, 709–12.

[159] E. Krüger, D. Zühlke, E. Witt, H. Ludwig, M. Hecker, "Clp-mediated proteolysis in Gram-positive bacteria is autoregulated by the stability of a repressor", *EMBO J.* **2001**, *20*, 852–863.

[160] S. J. Pamp, D. Frees, S. Engelmann, M. Hecker, H. Ingmer, "Spx Is a Global Effector Impacting Stress Tolerance and Biofilm Formation in Staphylococcus aureus", *J. Bacteriol.* **2006**, *188*, 4861–4870.

[161] Z. Mei, F. Wang, Y. Qi, Z. Zhou, Q. Hu, H. Li, J. Wu, Y. Shi, "Molecular determinants of MecA as a degradation tag for the ClpCP protease", *J. Biol. Chem.* **2009**, *284*, 34366–34375.

[162] D. W. Huang, B. T. Sherman, R. A. Lempicki, "Systematic and integrative analysis of large gene lists using DAVID bioinformatics resources.", *Nat. Protoc.* **2009**, *4*, 44–57.

[163] D. W. Huang, B. T. Sherman, R. A. Lempicki, "Bioinformatics enrichment tools: paths toward the comprehensive functional analysis of large gene lists", *Nucleic Acids Res.* **2009**, *37*, 1–13.

[164] M. Ober, H. Müller, C. Pieck, J. Gierlich, T. Carell, "Base pairing and replicative processing of the formamidopyrimidine-dG DNA lesion", *J. Am. Chem. Soc.* **2005**, *127*, 18143–18149.

[165] E. Aronesty, "ea-utils : Command-line tools for processing biological sequencing data", *Expr. Anal. Durham* **2011**, 2.

[166] A. Dobin, C. A. Davis, F. Schlesinger, J. Drenkow, C. Zaleski, S. Jha, P. Batut, M. Chaisson, T. R. Gingeras, "STAR: Ultrafast universal RNA-seq aligner", *Bioinformatics* **2013**, *29*, 15–21.

[167] H. Li, B. Handsaker, A. Wysoker, T. Fennell, J. Ruan, N. Homer, G. Marth, G. Abecasis, R. Durbin, "The Sequence Alignment/Map format and SAMtools", *Bioinformatics* **2009**, *25*, 2078–2079.

[168] S. Anders, P. T. Pyl, W. Huber, "HTSeq-A Python framework to work with high-throughput sequencing data", *Bioinformatics* **2015**, *31*, 166–169.

[169] M. I. Love, W. Huber, S. Anders, "Moderated estimation of fold change and dispersion for RNA-seq data with DESeq2.", *Genome Biol.* **2014**, *15*, 550.

[170] P. J. Boersema, R. Raijmakers, S. Lemeer, S. Mohammed, A. J. R. Heck, "Multiplex peptide stable isotope dimethyl labeling for quantitative proteomics.", *Nat. Protoc.* **2009**, *4*, 484–494.

[171] P. J. Boersema, T. T. Aye, T. A. B. Van Veen, A. J. R. Heck, S. Mohammed, "Triplex protein quantification based on stable isotope labeling by peptide dimethylation applied to cell and tissue lysates", *Proteomics* **2008**, *8*, 4624–4632.

[172] J. A. Vizcaíno, A. Csordas, N. Del-Toro, J. A. Dianes, J. Griss, I. Lavidas, G. Mayer, Y. Perez-Riverol, F. Reisinger, T. Ternent, et al., "2016 update of the PRIDE database

and its related tools", *Nucleic Acids Res.* **2016**, *44*, D447–D456.

[173] J. Cox, M. Mann, "MaxQuant enables high peptide identification rates, individualized p.p.b.-range mass accuracies and proteome-wide protein quantification", *Nat. Biotechnol.* **2008**, *26*, 1367–1372.

Abbreviations and Acronyms

a.u.	arbitrary units
AAA+	ATPases associated with diverse cellular activities
ACN	acetonitrile
ADEP	acyldepsipeptide
ADP	adenosine diphosphate
AfBPP	affinity-based protein profiling
AGC	automatic gain control
APCI	atmospheric pressure chemical ionization
approx.	approximately
ATP	adenosine triphosphate
BCA	bicinchoninic acid
bp	base pair
BSA	bovine serum albumin
BuLi	butyllithium
c	concentration
calcd.	calculated
cDNA	complementary deoxyribonucleic acid
CFU	colony-forming unit
CID	collision-induced dissociation
CMK	chloromethyl ketone
Da	Dalton
ddH$_2$O	purified water
DIPEA	*N,N*-diisopropylethylamine
DMF	dimethylformamide
DML	dimethyl labeling
DMSO	dimethyl sulfoxide
DNA	deoxyribonucleic acid
DTT	dithiothreitol
e.g.	*exempli gratia* (for example)
EDTA	ethylenediaminetetraacetic acid

102

eq.	equivalents
ESI	electrospray ionization
et al.	*et alii* (and others)
EtOH	ethanol
FA	formic acid
FDR	false discovery rate
FMP	Leibniz-Forschungsinstitut für Molekulare Pharmakologie
g	units of gravity
GFP	green fluorescent protein
HCD	higher-energy collisional dissociation
HCTU	*N,N,N',N'*-Tetramethyl-*O*-(6-chloro-1*H*-benzotriazol-1-yl)uronium hexafluorophosphate
HOAc	acetic acid
HOBt	1-hydroxybenzotriazole
HPLC	high-performance liquid chromatography
HR	high-resolution
HTS	high-throughput screen
Hz	Hertz
IAA	iodoacetamide
IC_{50}	half maximal inhibitory concentration
*i*PrOH	isopropyl alcohol
IPTG	isopropyl β-D-1-thiogalactopyranoside
J	coupling constant in Hz
K	Kelvin
LC	liquid chromatography
LFQ	label-free quantification
MeOH	methanol
MRSA	methicillin-resistant *Staphylococcus aureus*
MS	mass spectrometry
MS/MS	tandem mass spectrometry
MW	molecular weight
NaOAc	sodium acetate

NMR	nuclear magnetic resonance
o.n.	overnight
OD	optical density
OE	overlap extension
PAGE	polyacrylamide gel electrophoresis
PBS	phosphate buffered saline
PCR	polymerase chain reaction
PEG	polyethylene glycol
PP	polypropylene
ppm	parts per million
PVDF	polyvinylidene difluoride
R	resolution
r.t.	room temperature
rel.	relative
RFU	relative fluorescence units
RNA	ribonucleic acid
rpm	rounds per minute
rRNA	ribosomal ribonucleic acid
SAR	structure-activity relationship
SDS	sodium dodecyl sulfate
SEC	size exclusion chromatography
seq	sequencing
SIM	selected ion monitoring
t	time
TBS	tris-buffered saline
TBSCl	*tert*-butyldimethylsilyl chloride
TBST	tris-buffered saline containing Tween
TBTA	tris[(1-benzyl-1*H*-1,2,3-triazol-4-yl)methyl]amine
t-BuOH	*tert*-butyl alcohol
TCEP	tris(2-carboxyethyl)phosphine
TFA	trifluoroacetic acid
TFL	trifunctional linker

THF	tetrahydrofurane
TSAP	thermosensitive alkaline phosphatase
UV	ultraviolet
V	volume
vs.	versus
WHO	world health organization
wt	wild type
X-gal	5-bromo-4-chloro-3-indolyl-β-D-galactopyranoside
λ	wavelength

Curriculum Vitae

Christian Fetzer, born 12th October 1988 in Ulm, Germany

Academic Education	10/2013 – 12/2017	**Doctoral Studies** Supervisor Prof. Dr. Stephan A. Sieber, Chair of Organic Chemistry II, Technische Universität München *"Virulence Attenuation through Chemical and Genetic Manipulation of the Staphylococcus aureus ClpXP Protease"*
	10/2011 – 09/2013	**Master of Science** in Chemistry Technische Universität München **Thesis** Supervisor Prof. Dr. Stephan A. Sieber, Chair of Organic Chemistry II, Technische Universität München *"Target identification of beta-lactone derivatives and analogues by solid phase immobilisation, affinity chromatography and LC-MS"*
	10/2008 – 11/2011	**Bachelor of Science** in Chemistry Technische Universität München **Thesis** Supervisors Prof. Dr. Reinhard Niessner and Prof. Dr. Dietmar Knopp, Chair of Analytical Chemistry and Water Chemistry, Technische Universität München *"Optimization of extraction and immunological determination of Fumonisin B_1 in crops"*

Military Service	07/2007 – 03/2008	**Führungsunterstützungsbataillon Dillingen a. d. Donau** 1./FüUstgBtl 292
Scholar Education	09/1999 – 06/2007	**Albert-Einstein-Gymnasium Ulm-Wiblingen** Higher education entrance qualification (Abitur)
Conferences	06/2017	ASM Microbe 2017, New Orleans, USA
	06/2016	Gordon Research Conference, Bioorganic Chemistry, Boston, USA
	05/2014	European Congress of Clinical Microbiology and Infectious Diseases (ECCMID), Barcelona, Spain